THE HYDROELASTIC VIBRATION OF A HYDRAULIC SWING CHECK VALVE

This thesis is dedicated to my mother

THE HYDROELASTIC VIBRATION OF A HYDRAULIC SWING CHECK VALVE

by

Francis Ajibola Ajiboye Adubi, M.A.Sc.

A Thesis

Submitted to the School of Graduate Studies

in Partial Fulfilment of the Requirements

for the Degree of

Doctor of Philosophy

McMaster University

December 1974

Doctor of Philosophy (1974)
(Mechanical Engineering)

McMaster University
Hamilton, Ontario.

Title: The Hydroelastic Vibration of a Hydraulic Swing Check Valve

Author: Francis Ajibola A. Adubi, B.Sc. (University of Lagos)
M.A.Sc. (University of Waterloo)

Supervisor: Dr. D. S. Weaver

Number of Pages: xii, 170

ABSTRACT

The purpose of this thesis is to discover the mechanism of excitation and methods of alleviation of self-excited vibrations in a swing check valve following rapid pump shut-down. The problem was first encountered when the valve manufacturer incorporated an adjustable spring-damper into the original design to prevent its violent slamming. Tests on the modified design showed that, rather than eliminate the slamming, the valve disc bounced several times on its seat at a well-defined frequency. With increased damping the number of oscillations as well as the amplitude increased while the frequency decreased. For sufficiently high damping a stable limit cycle oscillation is established. This limit cycle oscillation continued until the valve pivot shaft pins failed. These vibrations are clearly hydroelastic in nature, the oscillations being perpetuated through a transfer of energy from the fluid flow.

A two-dimensional geometrically-similar model of the valve was constructed with perspex sides for flow

visualization. A central portion along the base of the model was also laminated with perspex to allow the projection of a collimated sheet of light. Aluminium powder tracer preparation was injected into the flow and cine-photography of the flow during vibration carried out. In addition, dynamic measurements of upstream and downstream pressures, valve angular displacement and the load on the damper arm were synchronized with the films. The data collected in this way for a number of restraining spring rates and initial spring deflection angles allowed a detailed stability map of the valve's dynamic behaviour to be plotted. The essential characteristics of the instability observed in the model are the same as those found in the prototype valve tests although the model was not scaled dynamically. This was necessary in order to guarantee the structural integrity of the model over the long period of tests.

The results of the research show that there is a sudden increase in the hydrodynamic closing load as the valve approaches its seat, primarily as a result of the changing discharge characteristics. Although upstream and downstream waterhammer waves are produced as the valve slams onto its seat, the valve responds only to the pressure difference across it. It remains closed until this pressure difference reduces to the point where it either cracks the valve open or allows the damper spring to pull it open. On the opening part of the vibration cycle the hydrodynamic closing load is substantially lower than the load at the same angle during

closing. This hysteretic effect shows that there is a net energy input from the fluid during each cycle and the motion is perpetuated.

Tests on the model further show that if the damping spring is stiff enough to eliminate the slamming, either the valve will never close or it will exhibit limit cycle oscillations. Clearly, neither alternative is acceptable. Based on the aforementioned results, it was realised that another possible means of alleviating the problem is to alter the discharge characteristics of the valve at small angles of closure by suitable changes in geometry. In the second part of the thesis, a number of such changes were made in the model and the experiments repeated. It was discovered that by making the rate of change of discharge a more gradual function of the valve closure angle, the dynamic instability in the model could be entirely eliminated.

ACKNOWLEDGEMENTS

The author wishes to express his sincere gratitude to his supervisor and friend, Dr. D. S. Weaver, for suggesting the problem and for his advice, assistance and encouragement throughout the course of this work.

The author would also like to thank Dr. N. Kouwen of the University of Waterloo and Professors J. L. Tlusty and M. H. I. Baird of McMaster University for the loan of part of his experimental equipment.

Appreciation is extended to the Canadian Commonwealth Scholarship and Fellowship Committee and to McMaster University for financial assistance.

The encouragement of my family and friends is also gratefully acknowledged.

TABLE OF CONTENTS

LIST OF ILLUSTRATIONS

CHAPTER 1

INTRODUCTION

1.1 Introduction

Fluids may be classified as liquids, gases, or vapours. Each class presents its own handling problems. Moreover, it is sometimes required to transport solids in suspension. This problem of controlling fluids has always taxed man's ingenuity.

The tapered plug appears to have been the earliest method of arresting fluid flow; indeed historians tell us that two galleys of the Emperor Caligula (AD 12-41) were equipped with taper-plug cocks to enable the vessels to be scuttled in the event of imminent capture. This common stop cock retained its form and importance for many centuries while valve design waited for the development of technology in other fields. For example, the screw-down stop valve as we know it today depended on the introduction of the modern screw-cutting lathe about 1790.

Modern conditions of application have become more exacting and valve designs may now be quite complex [1][1]. Simple mechanical principles while still indispensable are

---

1 Numbers in square brackets refer to references given at the end of this thesis.

being supplemented by electric, hydraulic and pneumatic aids, and the modern valve designer has to utilise his knowledge, not only of mechanics and physics but also of new materials. As operating conditions have become more arduous, valve design has changed, inevitably becoming more complex and sophisticated. Today, the greater emphasis on public safety and the environment, the development of more sophisticated sensing devices and the demand for more automatic control, all contribute to influence design. Phenomenal rises in temperatures and pressures, for example, have compelled the abandonment of long-standing designs and techniques; a fundamental example being the replacement of the spring-loaded safety valve method of relieving pressure by the torsion-bar loaded, piston assisted and thermal element types [1].

Valve selection for a particular application is determined by such factors as size of particulate matter in flow, viscosity, velocity, pressure, temperature and whether the fluid's state remains constant throughout the system. The type of service required of the valve is also an important factor in valve selection: for example whether the valve is required for isolating or regulating service, and if shut-off service is needed whether it be quick and bubble tight. Each type of valve has its own characteristics that determine its suitability for particular kinds of service.

Today there are a great number of different types of valves on the market. For reasons of space the applications to which each type of valve can be put will not be enumerated

here. The book by the British Valve Manufacturers Association [2] describes a variety of valves in industrial use. Glickman and Hehn [3] have also written a general paper on this subject. Suffice it to say that the most common types are the globe, check, gate, slide, relief, plug, butterfly, diaphragm, cone, and pinch valves. The subclassifications are also numerous. For example the lubricated plug valve may have a tapered or parallel plug, or it may be a simple gland cock.

1.2 Check Valves

Swing-check and lift-check valves act automatically and are used in systems where flow in one direction only is desired. Selection of the most suitable pattern and size is determined by parameters such as working temperature and pressure, flow velocity and allowable friction losses.

Other types of check valves [2], [3] on the market include the simple flap, tilting disc, multi-door, recoil, V-ring and cone check valves. In essence they are all merely devices which permit flow in only one direction.

In the simplest form, a check valve comprises a casing containing a hinged flap which is sensitive to small differences between upstream and downstream pressure. As long as the downstream pressure is less than the upstream pressure, the valve remains open, the degree of opening depending on the pressure difference. However, any drop in upstream pressure below downstream pressure will cause valve closure

and hence prevent reverse flow.

Various forms of swing-check valves range from the single hinged pattern in pipelines a few inches in diameter, to the large multi-door patterns for large pipe systems several feet in diameter. Lift check valves are normally associated with smaller pipelines up to about twelve inches diameter in high pressure systems.

1.3 Closure of Check Valves

The action of a simple check valve, installed in a centrifugal pumping installation, is basically as follows. The valve door is normally held open by impinging flow. If the reduction in flow velocity (following pump shut-down) is slow - as in the case of a centrifugal pump which continues to rotate for a short time after being shut down - the valve closes slowly.

When the pump is provided with a brake and therefore shuts down very rapidly, the pressure at the pump is suddenly reduced below that of the fluid downstream of the valve, and reverse flow may be established. The resulting pressure on the valve disc slams it heavily onto its seat. This leads to the generation of dangerous pressure surges which can cause damage to pipework and associated equipment or at the very least, cause a loud startling noise which may not be acceptable in commercial application.

1.4 Oscillation or "Hunting" of Valves

Under certain conditions of operation, almost all valves display a tendency to "chatter". Problems of this kind generally occur when the valve is operating partially closed, or more nearly fully closed. They are caused by the slight but rapid movements of the valve element which change the flow area, giving rise to pressure fluctuations. For example, the spring type pressure relief valve is prone to chatter, and here oscillations can build up to such a degree as to cause mechanical failure of the seat. Sluice valves can also produce undesirable pressure fluctuations. In this case the nature of the connection between valve spindle and wedge is generally such as to permit small movements of the wedge which result in changes in flow and pressure. In modern pumping installations the valve most liable to oscillate is the terminal float-operated valve [4]. In this case, wave motion in the tank or reservoir can directly affect the float and cause repeated closing and opening of the valve.

In the case of pressure-reducing valves, oscillations are sometimes inadvertently initiated. Normally, this valve is sensitive to changes in downstream pressure and by automatic adjustment, endeavours to maintain a reasonably constant outlet pressure. A change in the downstream conditions, for example due to reduced draw-off, causes the valve to move in the closing direction. If the valve over-corrects in its attempt to settle at the new required position, "hunting" may be initiated unless sufficient damping is incorporated in the

servo-system.

In all the cases mentioned, if the period of valve vibration falls in phase with the period of the fluid-mass oscillation in the pipe a repeating pressure pattern occurs [8], [9]. Such resonance is usually avoided by introducing damping to the valve arrangements. With float-operated valves, the float is usually arranged to operate within an auxiliary container, thereby shielding it from wave motion.

These examples indicate that valve oscillation can be a very real problem and if engineers and manufacturers are conscious of this fact, they can design and specify the inclusion of appropriate preventive features.

1.5 Background of the Present Problem

The swing check valve detailed in Fig. 1.1 is typical of a variety of valves manufactured and marketed by the Darling Valve and Manufacturing Company of Williamsport, Pa., U.S.A. Under conditions of rapid pump shut-down in service, the disc was found to slam so hard on the seat that it often led to shearing of the pivot pins connecting the swing arm to the pivot shaft. In addition, it created a very real noise-annoyance problem to customers. An external hydraulic oil damper, shown in Fig. 1.2, was then incorporated into the original design, the aim being to reduce the slamming force on the seat. The results of this modification, shown in the form of gross pressure traces (which may be taken to indicate valve displacement), obtained in tests of a 12 inch diameter

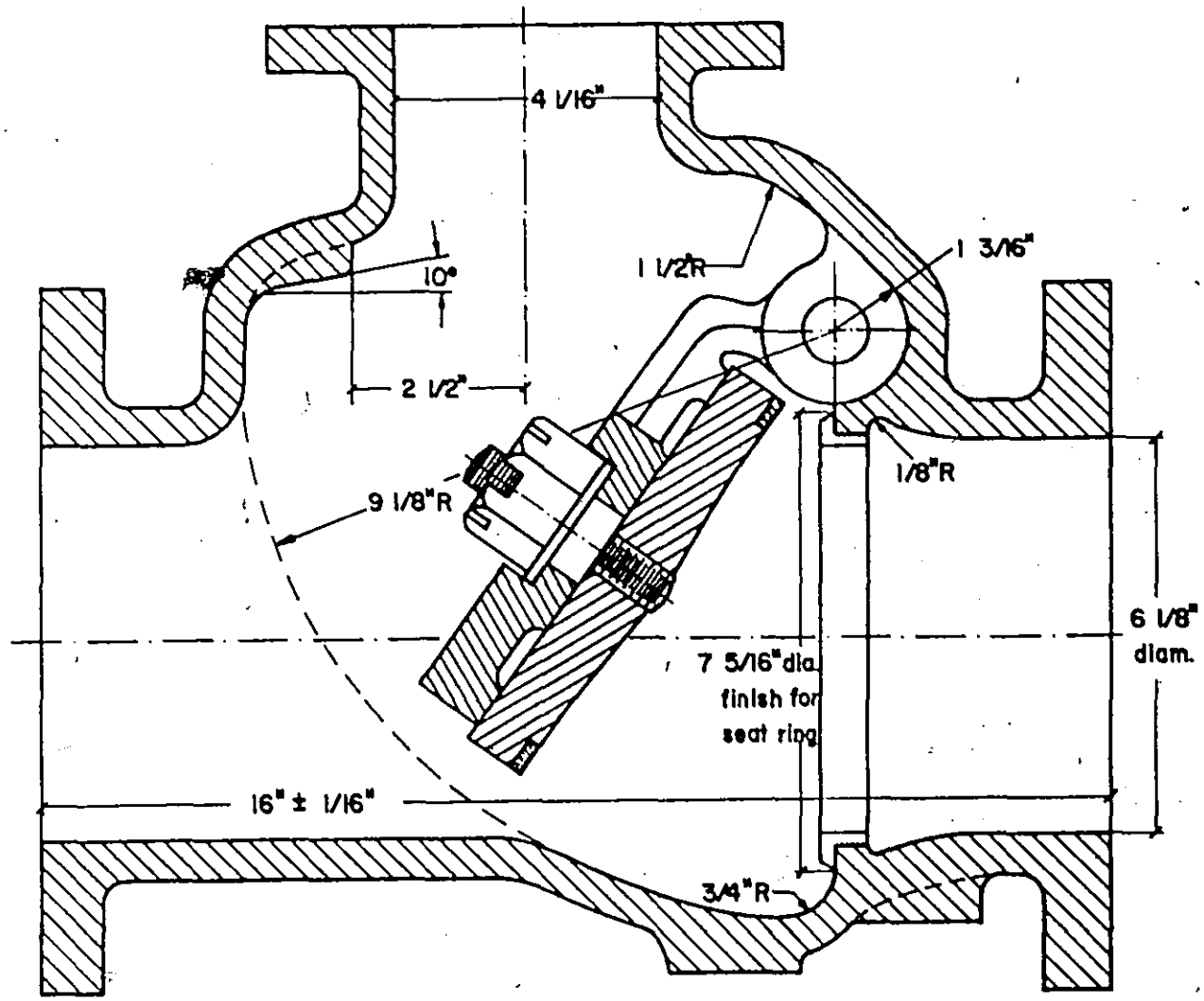

Figure 1.1. Inner Contours of Hydraulic Swing Check Valve.

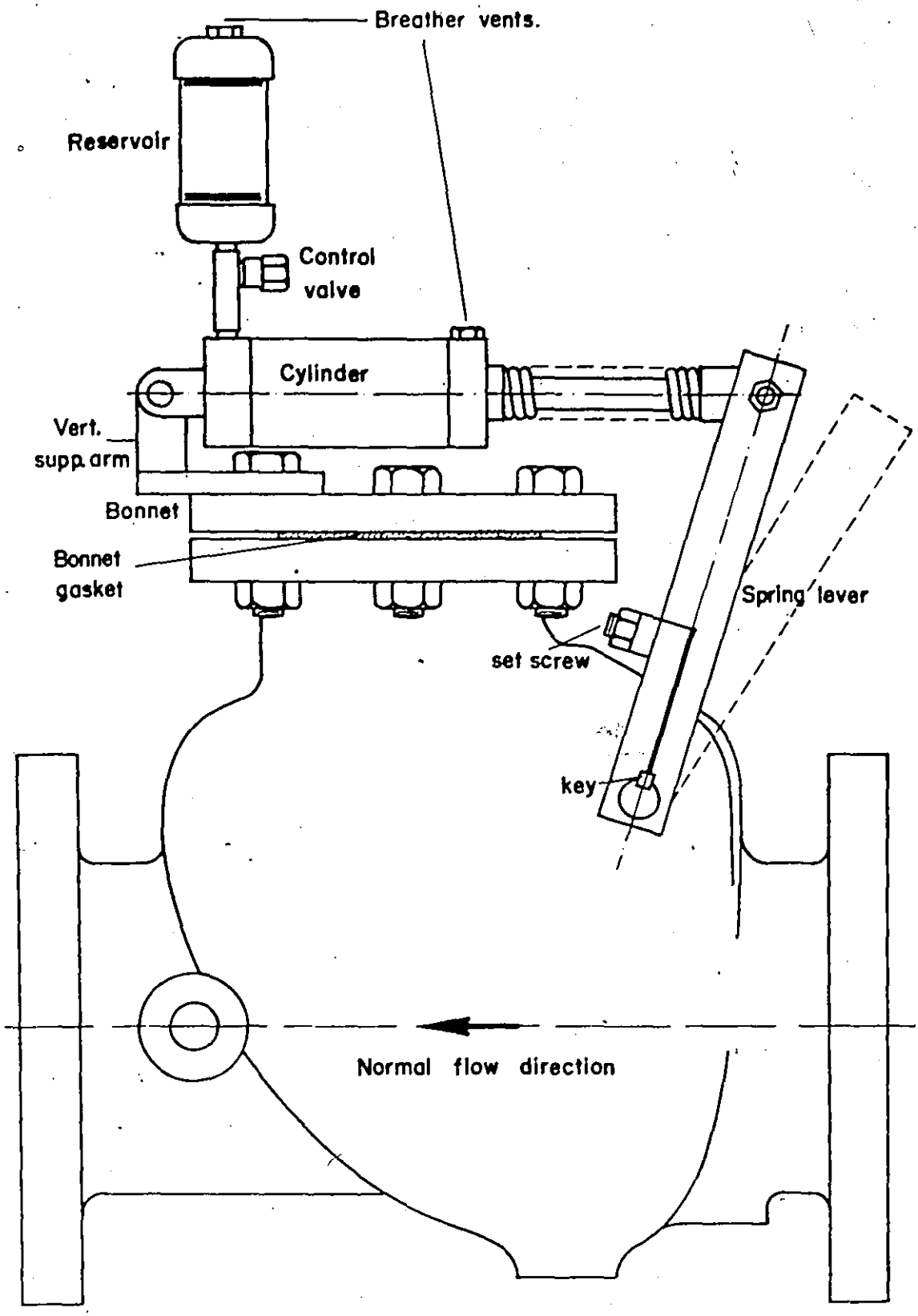

Figure 1.2. Check Valve with Hydraulic Oil Cylinder Arrangement.

prototype valve, were as follows:

With little or no damping, the hydrodynamic load on the valve element was such that closure was followed by several oscillations at a well-defined frequency but reducing amplitude, Fig. 1.3(a).

With an increase in the amount of damping the number of oscillations as well as the amplitude increased while the frequency decreased, Fig. 1.3(b).

With sufficient damping a stable limit cycle oscillation is established, Fig. 1.3(c). This limit cycle oscillation would continue, if permitted, until some mechanical failure occurs.

The problem is fluid-elastic in nature - under certain conditions the elastic and inertia forces of the valve interact with the hydrodynamic forces in such a way that energy is transferred from the flow to perpetuate the motion of the structure.

1.6 Purpose of the Investigation

It is clear from the above that the dynamic behaviour of the valve system was not understood. The proposed method of alleviation of the slamming vibrations actually had the effect of making them much worse. Before the most effective cure can be devised, it seems necessary to develop an understanding of the mechanism involved.

The purpose of this work was therefore two-fold:

(i) to develop an understanding of the phenomenon responsible for the dynamic instability of the valve;

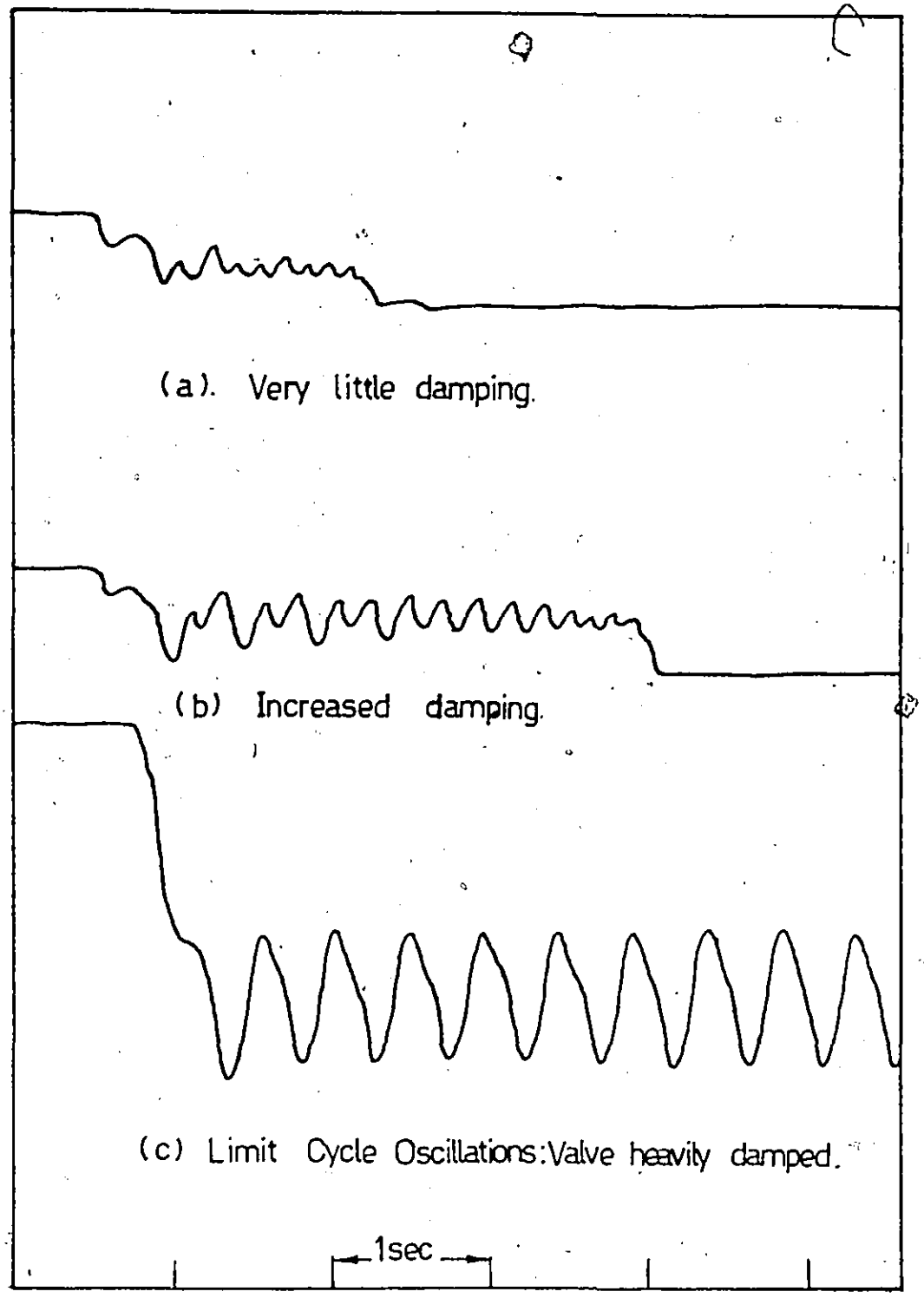

Figure 1.3. Preliminary Test Results on Manufacturer's Modified Design.

(ii) to conduct an exhaustive investigation into the dynamic behaviour of the valve with the object of devising a means of improving its performance.

CHAPTER 2

BASIC CONCEPTS OF FLOW-INDUCED STRUCTURAL VIBRATIONS

2.1 Introduction

The vibration of structural members when exposed to a flow field has long been of interest and concern to the engineer. Even though structural engineers have experienced these phenomena for hundreds of years and have come to recognise their general nature at least since the suspension bridge failures of the 1800's, the methods developed for their study are largely a contribution of the aerodynamicist. The onset of powered flight early in this century brought the aerodynamicist an empirical familiarity with the problems arising from the mutual interaction between aerodynamic and elastic forces. Frequent disastrous consequences of aero-elastic phenomena now known by such names as "flutter", "buffeting", and "divergence" stimulated their analytical study beginning in the 1920's, thus assuring their prominent role in both theoretical and experimental aerodynamics to the present time.

Flutter is defined by the aerodynamicist [10] as the dynamic instability of an elastic body in a fluid stream, the only forces necessary to produce it being those caused by deflections of the elastic structure from its undeformed state. If the system is linear in its response to loading, its

stability to infinitesimal motion provides the complete definition of its flutter properties and the origin of the forces producing this motion becomes unimportant. If, on the other hand, the system is nonlinear such that dynamic stability is dependent on the degree of elastic deformation, it is clear that the origin of the forcing function is of vital importance [11]. When the magnitude of the force increases with the amplitude of the motion it provides, the phenomena are called "self-excited", [12].

Buffeting, as usually defined represents the elastic response of a structure to forces which are little affected by the body motion. These forces may result from the presence of the body in the fluid flow field, such as the alternating forces accompanying the vortex street in the wake of a bluff body, but as long as the forces are not altered by the resulting elastic deflection, the phenomenon is considered as forced vibration, [13], [14].

Following the failure of the Tacoma Narrows bridge in 1940, structural engineers have made significant progress in applying the theories of aerodynamic stability to the analysis of bridge oscillations. But while it is generally accepted that both flutter and buffeting may be involved in these bridge motions, the complex nature of the structural geometry and stiffness of the prototype bridges usually demand model studies of the structural behaviour which leave the true nature of the dynamic excitation unresolved.

In the very recent past, the term hydroelasticity has become increasingly popular in discussions of problems

falling in between hydromechanics and structural mechanics. This word was coined by analogy to aeroelasticity to denote its naval counterpart. By taking advantage of the great attention which has been given to aeroelasticity, it is possible to define, by analogy, hydroelasticity. Heller and Abramson [15] proposed the following definition: "Hydroelasticity is concerned with phenomena involving mutual interactions among inertial, elastic and hydrodynamic forces". This mutual interaction between types of forces is the necessary condition for classifying a problem as one of hydroelasticity. When the effects of inertial forces are so small that they may be neglected, we have a problem of "static hydroelasticity" in which the mutual interaction is between hydrodynamic and elastic forces only. "Dynamic hydroelasticity" is concerned with phenomena involving mutual interaction among inertial, elastic, and hydrodynamic forces, Fig. 2.1.

While there are many similarities between aeroelasticity and hydroelasticity, differences between the two also exist. First, hydroelasticity may include the effect of a free surface, the interface between two fluid media. Such a surface is not present in aeroelastic phenomena. Secondly, the possibility of cavitation exists in hydroelasticity but not in aeroelasticity. Thirdly, the significance of the added mass which is usually negligible in aeroelasticity is of great importance in hydroelastic phenomena.

Interest in flow-induced vibrations arises primarily because of the possibility of damage or disastrous failure [9].

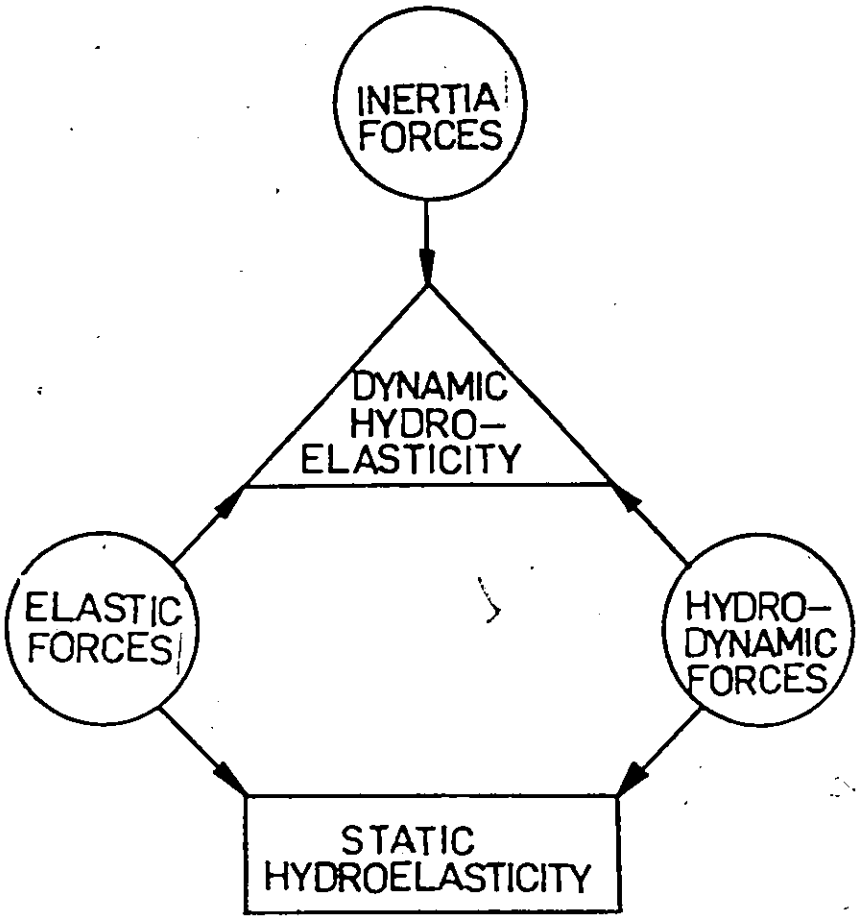

Figure 2.1. A Reduced Hydroelastic Triangle.

An equally important reason in many cases is that undesirable noise levels are sometimes produced. This occurs, for example, in the case of propeller blades which can "sing" in water owing to high-frequency vibrations induced by vortex shedding, [25].

Research efforts in the field of flow-induced structural vibrations have yielded abundant data on specific vibration problems encountered with structures in service and some of the cut and try measures used to improve design, [16], [17], [18], [19]. Other results in the literature illustrate the dynamic behaviour of highly idealized structures, [13], [14], [20], [25]. However, relatively little has been done to synthesize the accumulated information. The multitude of geometric and dynamic parameters as well as the complexity of the phenomena involved seem to have discouraged the search for a common conceptual frame-work.

Relatively few papers have been devoted to developing an understanding of the mechanism of the vibration excitation although there have been a few recent attempts to remedy this situation, [21], [22], [23], [24]. In design-oriented research, the objective has usually been the solution of some immediate and specific problems. But without proper understanding of the basic flow features and mechanisms, a detailed knowledge of specific or idealized vibration problems is of little help to an engineer whose job is to design a structure that will safely withstand flow-induced forces.

2.2 Classifications of Flow-Induced Vibrations

Flow-induced structural vibrations may be classified as one of three types: (a) Forced vibrations induced by turbulence in the flow; (b) Self-controlled vibrations induced by flow periodicity, and (c) Self-excited vibrations induced by a fluid-elastic phenomenon.

Structural motion induced by turbulence in the flow is usually of a random nature and is called "forced" since the motion of the structure usually has no appreciable effect on the fluid forces. This class of problems usually does not represent a source of great concern to designers since the analysis of these problems is relatively straight-forward.

In the case of self-controlled vibrations, some periodicity already exists in the flow field [26]. If this periodicity coincides with one of the natural frequencies of the structure, the amplitude of vibration builds up to the point where the magnitude and frequency of the fluid forces are now controlled by the structural motion. A dynamic feedback mechanism develops. Two possibilities exist for preventing such vibration or severely limiting its amplitude - either the addition of stiffening and damping to the structure, or some geometry change which eliminates the original periodicity in the flow.

In self-excited vibration problems, the motion of the structure creates the periodic forces which amplify the structural motion. These vibrations are different from self-controlled vibrations in that the periodic forces disappear

in the absence of structural motion. For this class of problems, a change in structural geometry may be the only effective means of preventing destructive vibrations.

Both self-controlled and self-excited vibrations are termed fluid-elastic vibrations (aeroelastic or hydro-elastic) since they involve mutual interactions of elastic, inertial and fluid-dynamic forces.

In a recent paper, Naudascher [23], suggested a classification of the complex flow phenomena, and defined the "basic control mechanisms", underlying all flow-induced vibrations arising from shear-layer instabilities. Asserting that "most flow-induced vibrations can be traced to an instability of the flow", he demonstrated that the most common flow instabilities associated with shear layers result in random flow fluctuations when they are combined with random disturbances at higher-than-critical Reynolds numbers. Only when these disturbances (and the fluctuations of velocity and pressure which they generate) become modified by means of control mechanisms can the inevitable trend toward disorder (turbulence) be diminished or delayed. These control mechanisms may be external (periodic finite-amplitude disturbance imposed from outside the flow system) or internal (regular, self-generated disturbance, resulting from the interaction of the flow with its boundaries). Internal control mechanisms represent the important form of control regarding flow-induced excitation. Here, a distinction exists between phenomena involving rigid flow boundaries and those involving

elastic or elastically-restrained flow boundaries. In these cases the control mechanisms are termed fluid-dynamic and fluid-elastic, respectively. Both fluid-dynamic and fluid-elastic control mechanisms are described in terms of feedback mechanisms.

The simplest feedback mechanism is the fluid-dynamic control in which velocity and pressure fluctuations caused by some disturbance are amplified as they are convected downstream; they interact with the rigid boundaries of the flow field, giving rise to new disturbances which, when transmitted back to the origin of the shear layer, will trigger the development of new fluctuations. However, fluid-elastic resonance is significantly more complex: physically, because energy transfer from the flow to the structural motion takes place as well as energy transfer from the basic to the fluctuating components of the flow; analytically, because the dynamic characteristics of the structure are needed in addition to the flow parameters for describing the flow.

In a later paper, Naudascher and Locher [24] showed that the flow past a protruding wall without flow reattachment is highly sensitive to fluid-elastic control. They concluded that flow-induced structural vibrations in this case can only be determined by a detailed study of the complete system including the dynamic characteristics of the structure.

2.3 Use of Mathematical Models

Because the mechanisms of many hydroelastic phenomena are not yet fully understood, difficulties have been

encountered in trying to model them mathematically. The essence of most structural vibrations induced by fluid flow is that structural deformation and fluid-dynamic loading are interdependent. The general mathematical approach to the analysis of the vibrations consists of the determination of the so-called structural operators, inertial operators and fluid-dynamic operators. Weaver [32], [26] has shown that the energy transfer from the fluid to the structure is the result of nonconservative hydrodynamic forces which manifest themselves in the form of non-self-adjoint operators in the differential equation of motion. The solutions to these special class of mathematical problems exhibit two unique characteristics. First, such equations admit complex eigenvalues or, in physical terms, oscillatory types of instability. Secondly, the eigenvectors are generally not the normal modes of free vibration but coupled modes which do not satisfy the usual orthogonality conditions. It is therefore quite clear that, regardless of the specific mechanism of instability involved, hydroelastic problems form a class which is distinct from free and forced vibration, and conservative stability problems.

It is pertinent to add that the mathematics needed to deal with these problems is still being developed [1,1].

2.4 Virtual Mass of Submerged Structures

When a vibrating body is immersed in water, its natural frequency is reduced to a value considerably lower

than that measured in air. The water surrounding the body is in continual motion as energy is imparted to the fluid and a pressure is exerted on the body. Because of the difference in density this energy is much larger in water than it is in air. This effect, well-known in accelerated motion problems in hydrodynamics [27], can be accounted for by an addition to the mass of the body referred to as "added" or "hydrodynamic" mass:

$$F = (M + M_1) \frac{d^2x}{dt^2}$$

where M_1, the added mass, may sometimes be much greater than the actual mass M of the body.

The virtual mass effect is only present in the case of accelerated motions, which of course include vibrations. If we write in general

$$M_1 = K \times \text{(mass of fluid displaced by the body)}$$

K is a coefficient which depends upon the shape of the body, its relative confinement and its degree of submergence. Lamb [27] called these "hydrodynamic inertia coefficients" and other writers have used expressions such as virtual inertia or virtual mass coefficients.

The effect of the surrounding fluid can be thought of in two ways - either the fluid causes a resistance to motion of $M_1 \frac{d^2x}{dt^2}$, or it causes a virtual increase in the mass of the body, which behaves as if it has the mass $(M + M_1)$ instead of M. The mass $(M + M_1)$ may be called the virtual mass,

while M_1 is the "added virtual mass".

A considerable amount of experimental work has been carried out on the added mass of beams vibrating in water, [27], [28], [29], [30]. Moullin et al. [28] carried out exhaustive experiments over a period of years on the vibration of beams in water. They found that the added mass was not dependent to any great extent upon the mode of vibration or the frequency. This finding has recently been confirmed by Blake [29]. However Todd [30] has shown that flexural mode shapes may be affected by three-dimensional flow around the ends of relatively short beam-like bodies because of the subsequent redistribution of effective mass. For more difficult geometries it may be necessary to determine the added mass experimentally.

Todd [30] discusses in his book an extensive review of research on added mass effects, especially results concerning amplitude, frequency, submergence, and relative confinement. When a ship moves from deep to shallow water her vibration characteristics change, the natural frequencies being lowered. If a natural frequency in deep water is just above that of some periodic disturbing force in engines, propeller or auxiliaries, resonant vibrations may result when she moves over shallow water. This reduction in natural frequency is due to an increase in the added virtual mass in the presence of restricting boundaries.

When the confining surfaces are within about two characteristic dimensions of the vibrating body, the added

mass increases considerably and values from five to ten or more are not unusual. The importance of this in lowering the natural frequency is demonstrated by the problems encountered in trying to reduce the vibrations of hollow-cone valves [31]. An attempt to stiffen the valve by increasing the number of vanes from four to six resulted in an increase in confinement of the fluid between the vanes which more than offset the increase in stiffness. The natural frequency was lowered rather than increased, and the vibration amplitude was increased.

For ship hull vibrations, the added mass does not depend to any great extent on the mode of vibration or the frequency. This result appears to be generally applicable as long as the amplitudes are small - of the order of about five percent of a characteristic dimension of the structure. As the amplitude is increased, the added mass becomes both amplitude and frequency dependent [32]. It is still not clear, however, that added mass always increases with frequency at large amplitudes.

2.5 Vibrations of Hydraulic Gates and Valves

The physical situations in which flow-induced vibrations arise are so diverse that it is impossible to cover all known cases in the course of a brief survey. In fact, in the last two years, two different symposia have been organized solely on flow-induced structural vibrations, [33], [34]. The purpose of this section is to briefly review current knowledge

related to vibrations of flow-control structures such as hydraulic gates and valves by critically evaluating the existing literature.

Violent chattering of household taps when nearly fully closed has been experienced by most people occasionally. Such self-excited vibrations have also been encountered with sink and bathtub plugs of particular designs when operating nearly fully closed. Although these phenomena have been experienced for many years, to the author's knowledge only one paper, that of Weaver, Kouwen and Mansour [50], has given a lead towards developing an adequate explanation of the mechanism of excitation of these vibrations. While the vibrations subside on full opening of these devices or closing them completely, and failure very rarely occurs, the unpleasant noise generated is a source of nuisance.

Various papers have reported on vibration problems encountered with hydraulic structures in service and the cut and try methods by which partial or complete solutions to these problems have been attained, [16], [18], [53], [54], [55], [56]. In none of these papers has a clearly defined mechanism of the vibration excitation emerged. However, in the last two years a few papers have appeared in the literature attempting to foster a better understanding of the various phenomena.

Abelev and Dolnikov [52] classified the self-excited vibrations of hydraulic gates into two basic categories. The first category involves vertical vibrations due to the kind of unstable flow reattachment when vortex formation in the

wake past the gate is synchronized with and controlled by the gate motion. This they called the "eddy mechanism of excitation".

The second category involves self-excitation which may result from high velocities of the jet-flow directed along the vertical face of the gate. This they termed the "jet-flow mechanism of excitation". This simplified classification is useful only in so far as it may serve as a background against which various problems reported in the literature may be examined.

Among the flow features which play a significant part in the excitation of structural vibrations are those involving flow separation and reattachment. Whenever flow separates from a boundary, a free shear layer is produced. At certain critical values of the Reynolds number, any lateral perturbation of the unstable shear layer causes the layer to roll up into vortices which grow in size as they move downstream. When the lateral perturbations result from vibration of the solid boundary on which the separation point is located, a regular two-dimensional vortex train with a frequency of formation equal to that of the solid boundary is produced. Naudascher and Locher [24] discussed three possible cases of flow separation from a protruding boundary, such as a gate; (i) the case of no subsequent reattachment of the free shear layer, (ii) the case of an unstable reattachment and (iii) the case of a stable reattachment.

In the case of no reattachment, increased excitation results from gate vibration. The frequency of vortex formation

becomes "locked in" with the frequency of the gate motion, thus reinforcing the excitation. Such vibrations are self-controlled and will occur over a wide-range of gate openings. This is undoubtedly the nature of the gate vibrations described by both Campbell [18] and Schmidgall [16] although their description of the excitation as "pressure fluctuations resulting from Von Karman vortex trails" appears to be a technical misnomer.

Unstable flow reattachment occurs in the case of intermediate gate widths and results in strong periodicity in the excitation due to vortex shedding. Catastrophic vibrations may result from gate operation at certain heads and openings. The recent work of Hardwick [51] falls into this category. Extending the ideas of Naudascher and Locher, Hardwick studied specifically the excitation and elastic response of a vertical-lift gate with a flat bottom which is free to vibrate vertically. Based on his flow visualization experiments, Hardwick found that eddies resulting from the breakdown of the free shear layer lying close to the bottom of the gate induce time-dependent reattachment of the mainstream to the gate bottom, thereby generating an exciting force. Oscillatory motion of the separation point reinforces the excitation and synchronizes it with gate motion. He also gave a semi-quantitative consideration of the gate's vibrational response, attributing the instability to the presence of a negative damping coefficient in the equation of motion. His entire work was based on the crucial assumption that the mean velocity of flow under the

gate during the vibration remains virtually unchanged and that the motion is simple harmonic. However, during operation at very small gate openings, vibrations lead to repeated opening and closing of the gate. In such cases the flow is very unsteady, the fluid velocity being zero during a fraction of the cycle of vibration. Thus Hardwick's explanation is not valid for the case where closure occurs during the cycle.

Stable flow reattachment will occur for large gate widths. This case is of little interest because the massiveness of such a structure will likely make it immune from fluctuating forces. All the cases so far discussed may be put into the classification "eddy mechanism of excitation" as defined by Abelev and Dolnikov [52].

These writers' classification "jet-flow mechanism of excitation" was used to describe conditions when water flows over a partially open gate which is provided with a skimmer wall. Flow between the gate and its skimmer wall occurs as a high velocity jet which lowers the pressure in the gap so that the gate is drawn towards the wall. This reduces the discharge through the gap, setting up inertia pressures which force the gate away from the wall. The resulting horizontal gate vibrations are thus clearly self-excited. The seal problems reported by Schmidgall [16] and by Chepajkin and Lyssenko [22] as well as the "chattering" of valves and sink stoppers discussed earlier are phenomenologically similar and are related to the "jet-flow mechanism".

In a recent paper, Chepajkin and Lyssenko [22] attempted a positive identification of the physical mechanism

of self-excited oscillations of gate seals. However, they neglected the large variations in mean fluid velocities in the gap between seal and sill during the vibration cycle. Large variations do occur in the discharge coefficient as the gap is alternately closed and opened during the vibration. This fact was demonstrated in the paper by Weaver et al. [50]. Thus, the larger proportion of the energy transferred from the flow to the vibrating structure may in fact result from the hysteretic effect of the different flow velocities during closing and opening as well as inertia pressures generated from acceleration and deceleration of the flow past the closure device (whether it be seal, gate or valve). Hence Chepajkin and Lyssenko's theoretical development based on small simple harmonic motions and negative damping appears incapable of accounting for the flow phenomenon which must occur during a cycle which involves closure.

Abelev and Dolnikov [52] in their mathematical model for the jet-flow mechanism assumed a simple linear variation in discharge which again reduces to a negatively damped simple harmonic oscillator. Such a model is reasonable as long as the amplitudes are small and no closure occurs which causes a rapid reduction in discharge. It seems quite clear that the problem being considered in this thesis is most closely related to this phenomenon.

The only paper appearing in the literature which seems to appreciate the importance of the large variation in discharge is that of Weaver, Kouwen and Mansour [50].

However, the discussion presented is qualitative only, being based on preliminary experiments to determine the static discharge characteristics. It remains to establish through dynamic experiments and flow visualization the exact nature of these phenomena when oscillations involve closure.

CHAPTER 3

EXPERIMENTAL APPARATUS

3.1 Introduction

In many problems of applied fluid dynamics there are situations in which it is difficult to picture the exact nature of the flow field. In the planning for this research programme the need for flow visualization was recognized early. For studying complicated time-dependent flows, investigators have employed visual methods to observe the general qualitative features of complex flow patterns, and to determine the limits of flow regimes. Among the earliest examples are the work of Osborne Reynolds (1883), [36] on transition to turbulent flows, and the studies of L. Prandtl and co-workers (1926), [37] on production of vortices downstream of a stationary cylinder.

In order to observe the flow of transparent fluids, the usual procedure is to observe the motion of tracer particles that are placed in the fluid. For successful visualization these tracers should contrast sharply with the background. In addition it is desirable to be able to control both the concentration and the position of the tracers. The method used in this thesis involved suspending tracer particles throughout the fluid medium and illuminating only the region of interest.

This suggested the design and construction of a two-dimensional model of the prototype check valve. As the valve behaviour is dependent on the maximum pressure difference across the valve, some means of pressure control is also necessary. This chapter describes the development of the model and the instrumentation used for the required measurement.

3.2 Experimental Circuit

The main parts of the experimental circuit are shown in Figs. 3.1 and 3.2. The required pressure control could be obtained using the existing constant-head water tank and its associated equipment. This tank provides a head of 11 feet of water and a capacity of about 900 gallons. A six-inch diameter steel pipeline was laid and connected to the constant head reservoir and a gate valve was used to regulate discharge. Water was discharged through the test section into an underground reservoir from where the water was recirculated through the high level tank by a centrifugal pump. The overflow from the constant-head tank was discharged directly into the underground reservoir.

At the entrance into the pipeline from the high level reservoir, a short cruciform, shown inset in Fig. 3.2, was inserted to prevent the development of a vortex and hence the suction of air into the pipeline from the free surface of water in the tank. Also downstream of the gate valve a longer cruciform was inserted into the pipeline to prevent

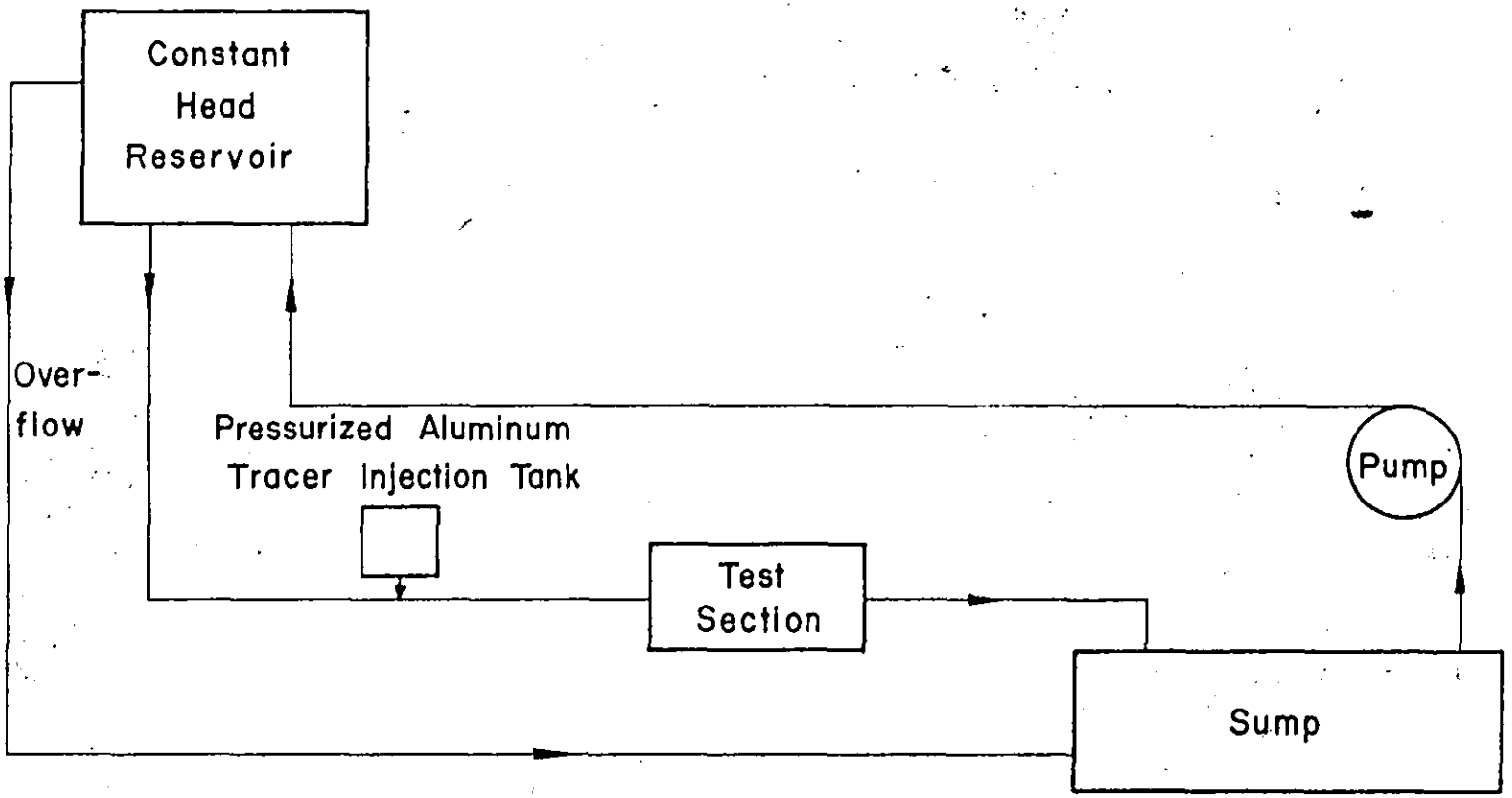

Figure 3.1. Schematic of Closed-Loop Experimental Circuit.

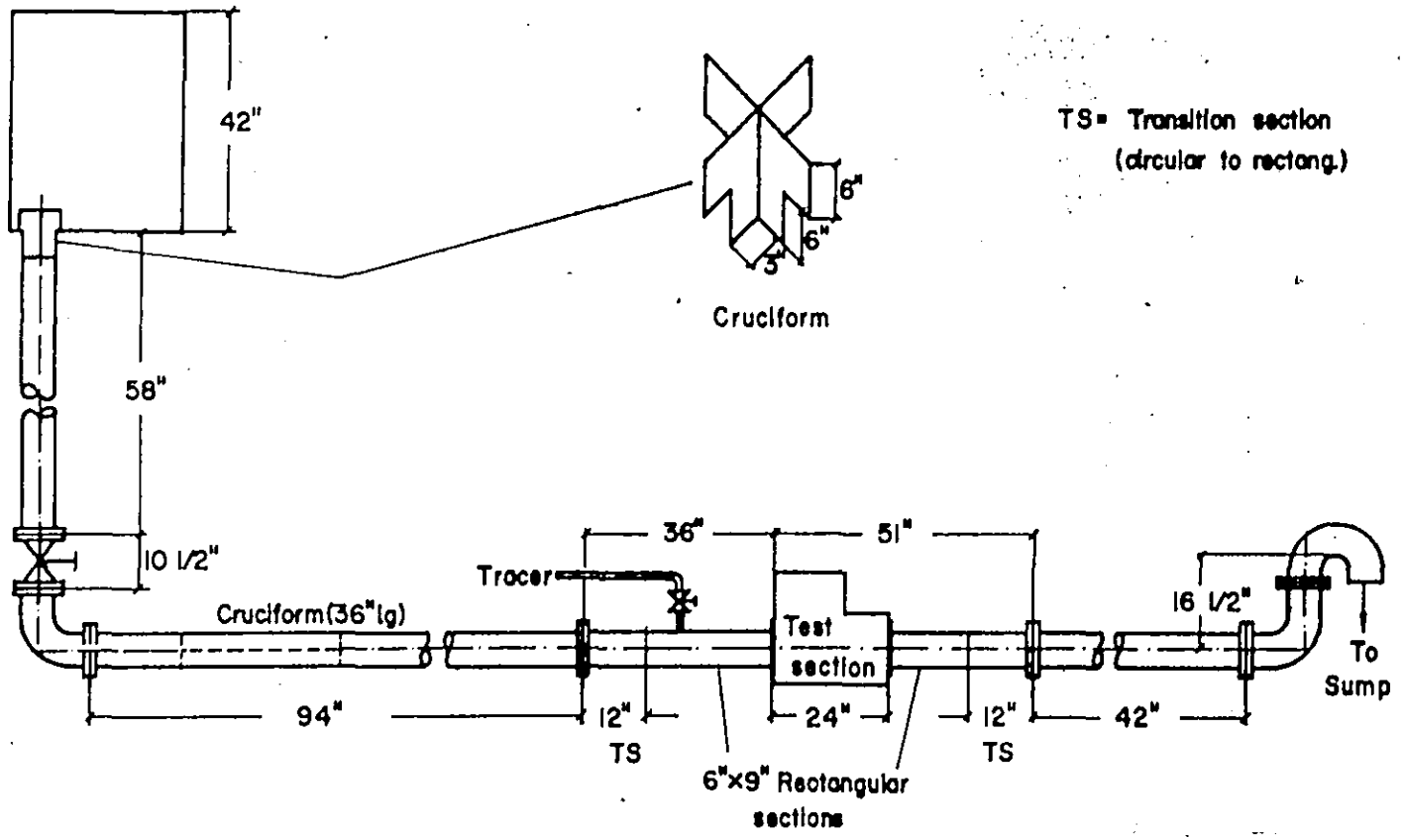

Figure 3.2. General View of Experimental Apparatus.

the development of secondary flows in the pipeline.

Two identical transition sections, shown in plan view in Fig. 3.4 were used to transform the six-inch diameter circular pipeline cross-section into the 6" x 9" rectangular cross-section of the test section. The cross-sectional geometry transformation was effected over a length of 12 inches and the flow was allowed to develop over the remaining 24 inches of rectangular pipeline. This ensured that the flow entering the valve very closely approximated two-dimensional flow and was free of secondary flows. A double-screen filter was installed about 20 inches from the test section inlet to provide a uniform turbulent flow field and also to prevent unwanted foreign bodies from appearing in the test section during filming. This filter could be cleaned and replaced through a cover plate which was screwed to the top of the pipeline.

At the downstream end the pipeline rises a total of 16.5 inches as shown in Fig. 3.2. This was to provide enough reverse hydrostatic head under no-flow conditions to permit expulsion of air from the test section. The entire pipeline was freely supported at a height of 17 inches above the laboratory floor.

For flow visualization the aluminium tracer particles were injected into the pipeline at a point 18 inches upstream of the test-section. A transparent pressurized tank, described elsewhere, was designed for this purpose.

Figure 3.3. Close-Up View of Test Section.

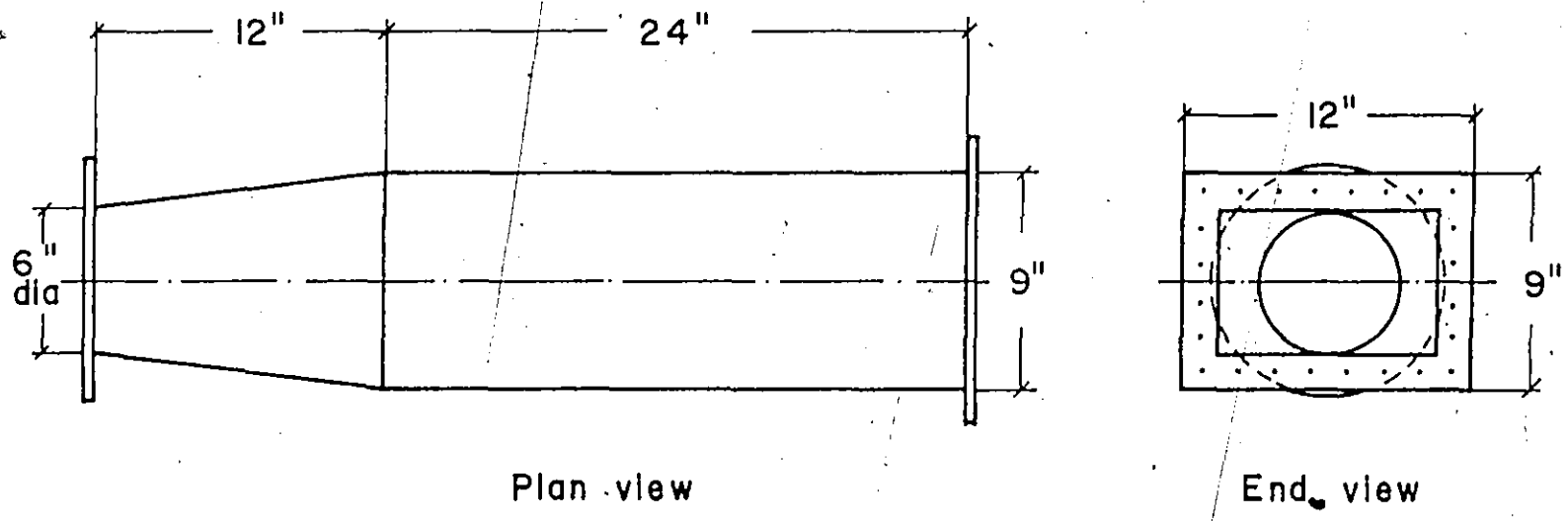

Figure 3.4. Transition Pieces.

3.3 The Valve Model

The purpose of the two-dimensional model was to permit flow visualization. It was felt that the vibration experienced with the prototype was not predominantly dependent on three-dimensional fluid-flow effects. Also, the flow at the vertical longitudinal centreline through the valve should be two dimensional because of symmetry. It follows that the essential character of the dynamic instability will be preserved in a two-dimensional model. This assumption was justified by subsequent experiments in which the essential nature of the vibration observed with the prototype valve was also observed with its geometrically similar two-dimensional model.

It was appreciated from preliminary experiments on the prototype that the relatively large mass of the disc and the high spring rate of its elastic system led to very large hydrodynamic closing loads and slamming forces. To assure model integrity, a low-mass disc model and relatively weak springs were therefore required. The relatively weak springs also meant low frequencies of vibration and large amplitudes.

Practical considerations dictated the choice of the 6 inch diameter valve for the study although the phenomenon had been observed with larger diameter valves of the same design. The model was therefore a two-dimensional geometrical replica of the 6 inch diameter prototype. The scale ratio was 1:1. The test section width was one and a half times the diameter of the valve. The central one sixth was made transparent. The choice of test-section width was based on making the flow

through this central transparent section free from edge effects, so that the flow was truly two-dimensional.

The valve disc was modelled by a one-inch thick perspex plate, nine inches wide by 7 1/8 inches long so that a cross-section through the model was essentially identical to that of the prototype. The pivot shaft diameter was 7/8 inch, the same as in the prototype. The prototype swing arm was used in the model. The model pivot shaft was supported symmetrically in two 3 inch long cylindrical brass bushings. The prototype seat ring was modelled by L-shaped sheet metal pieces screwed to the seat. The pivot shaft was extended 4 1/2 inches at either end. Three inches from one end of this shaft a steel bar 14 inches long, 2 inches wide and 3/4 inch thick was welded to the shaft. Two inches from the free end of the bar, 1 1/4 inch diameter grooves were machined to support an assortment of compression springs. This spring arm and the movable 7 inch long receptacle holding the compression springs are shown in Fig. 3.3. This receptacle is bolted to a one inch thick quadrant-shaped aluminium plate which was itself rigidly bolted to the laboratory floor.

At the other end of the pivot shaft a pointer was attached to the shaft to indicate the displacement of the valve on a protractor attached to the body of the valve. The protractor scale was graduated in degrees.

The front and back of the model were covered with 3/4 inch thick perspex plate. A bleed valve, shown in Fig. 3.3, was fitted to the bonnet to rid the valve of air bubbles which

would otherwise prevent complete liquid filling of the valve.

Reverse flow was simulated by setting the model up in the pipeline such that the flow tended to close the valve.

3.4 Instrumentation for Dynamic Measurements

3.4.1 Introduction

Three basic quantities were chosen for direct measurement, namely the valve displacement, the dynamic pressure fluctuations and an indication of the load on the valve. A fourth quantity, the fluid velocity fluctuations was to be obtained or observed from streak lengths of streamline patterns on the flow visualization films.

3.4.2 The Readout System

A 12 channel Honeywell Visicorder Oscillograph, model 2106 with its galvanometers driven by an Accudata 117 multi-channel direct coupled amplifier was chosen as the readout system. One reason was its facility for the simultaneous recording of many signals. This was very important in giving a total picture of the events taking place simultaneously at the valve during the vibration. Another attractive feature was its ability to automatically draw time-base lines of up to one-hundredths of a second across the signal traces. A third reason was that, because its "pen" is a beam of light reflected from a mirror controlled by a galvanometer, it does not suffer from the disadvantage of poor frequency response due to pen inertia experienced with some conventional pen

recorders. Its very high frequency response (up to 15kHz) guaranteed faithful reproduction of signals as picked up by the various transducers.

3.4.3 Valve Displacement

The design of a system for measuring valve displacement during vibration presented an interesting challenge. These vibrations are of rather large amplitudes and low frequencies. Impact of the valve disc on the seat was involved and there was a substantial fraction of the period of vibration during which the valve remained closed. It was highly desirable to have a clearly defined point of closure of the valve as well as a sharply marked point of departure of the disc from its seat.

A capacitive displacement probe was chosen principally because of its excellent frequency response, its reliability in terms of repeatability of results and its availability. A transducing system for converting purely angular rotation of the pivot shaft into straight line motion of a detector rod, was designed as shown in Fig. 3.5. An eccentric collar was rigidly attached to the pivot shaft by a number of set-screws. A spring-loaded detector rod picked up the rotation of this eccentric collar and converted it into straight line axial motion. Contact between detector rod and eccentric collar was maintained through a steel ball bearing.

The MC1 capacitive probe was used to monitor the motion of the detector rod. The signal was amplified using a Wayne Kerr Vibration/Distance meter, model B731B, filtered and fed into the Visicorder. This vibration meter is a

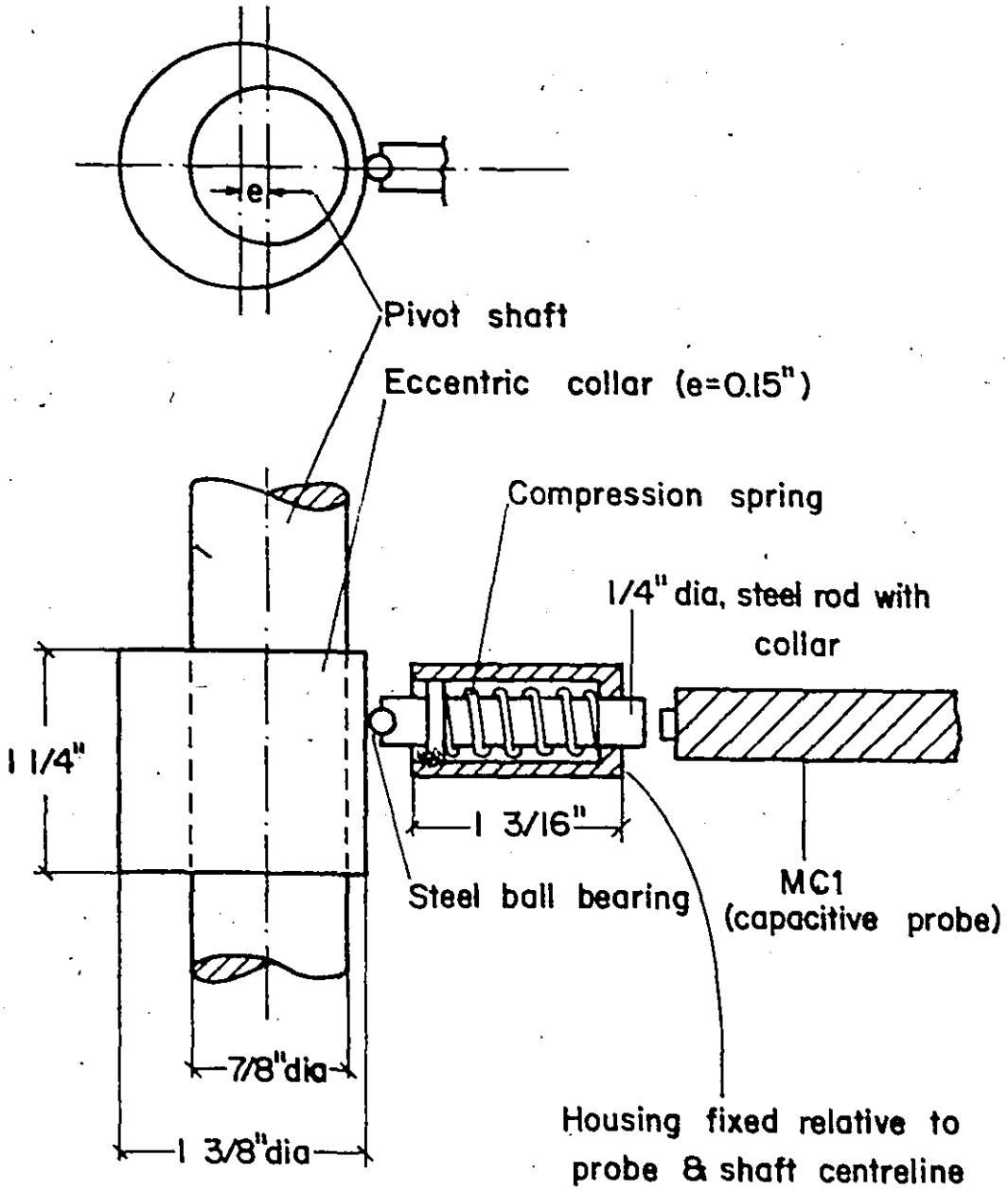

Figure 3.5. Transducing System for Measuring Valve Displacement During Vibration.

portable instrument for the accurate measurement of distance and vibration amplitude from 50 micro inches to 100 thousandths of an inch over the frequency range 1 Hz to 10 kHz. This system is shown in parts in Figs. 3.3, 3.5 and 3.6. The low pass filter (Wayne-Kerr model F731A) had a cut-off frequency of 100 kHz. Its purpose was to remove ripple voltage resulting from higher order harmonics of the modulated 50 kHz signal which was the output from the distance socket of the amplifier.

This transducer was calibrated by noting the pen deflection on the Visicorder oscillograph for angular displacements measured on the protractor. It was found that detector rod displacement varied linearly with angular displacement of the valve.

3.4.4 Hydrodynamic Torque

An indication of the variation of the hydrodynamic load on the valve was obtained by using a piezo-electric load cell to detect the variation in the compressive force in the springs. The load cell is a force transducer, its purpose being to convert a mechanical force into an electrostatic charge signal which can be transformed in a charge amplifier to an electric output voltage and transmitted to a recording device. A Kistler quartz load cell Type 903A having a resonant frequency of 60 kHz was used for the experiments. It was installed in a groove machined into the spring supports.

Its sensitivity having been matched to the charge amplifier, it was calibrated by applying accurately known loads

Figure 3.6. View Showing Remainder of Experimental Equipment.

on the transducer and measuring the pen deflection on the Visicorder corresponding to these loads. The calibration curve is shown in Fig. 3.7.

3.4.5 Pressure

It was desired to measure the upstream and downstream pressures in order to determine the effective pressure difference across the valve at any instant during the vibration. Two "home-made" strain-gauge type diaphragm pressure transducers using a Hewlett-Packard Carrier Preamplifier model 8805A for bridge-excitation and signal-modulation were available at the beginning of the experiments. Almost immediately, problems were encountered over the presence in the modulated signal, of 60 Hz line frequency noise. Although the ideal filter to use in such cases is a narrow band-reject filter, the prohibitive cost of such a unit led to the decision to use a low-pass filter (cut-off frequency, 60 Hz) of cheap construction. Pressure wave shape was preserved in each case but four undesirable effects were noticed during analysis of the results. First, there was a distortion of signal rise time; secondly, a frequency-dependent phase shift made results computed for instantaneous values of pressure difference across the valve from the two different transducers inaccurate. Thirdly, the signals were severely attenuated and finally, there was the inevitable suppression of components of the signal of frequencies higher than about 15 Hz. The difficulties led to the search for a different pressure transducer.

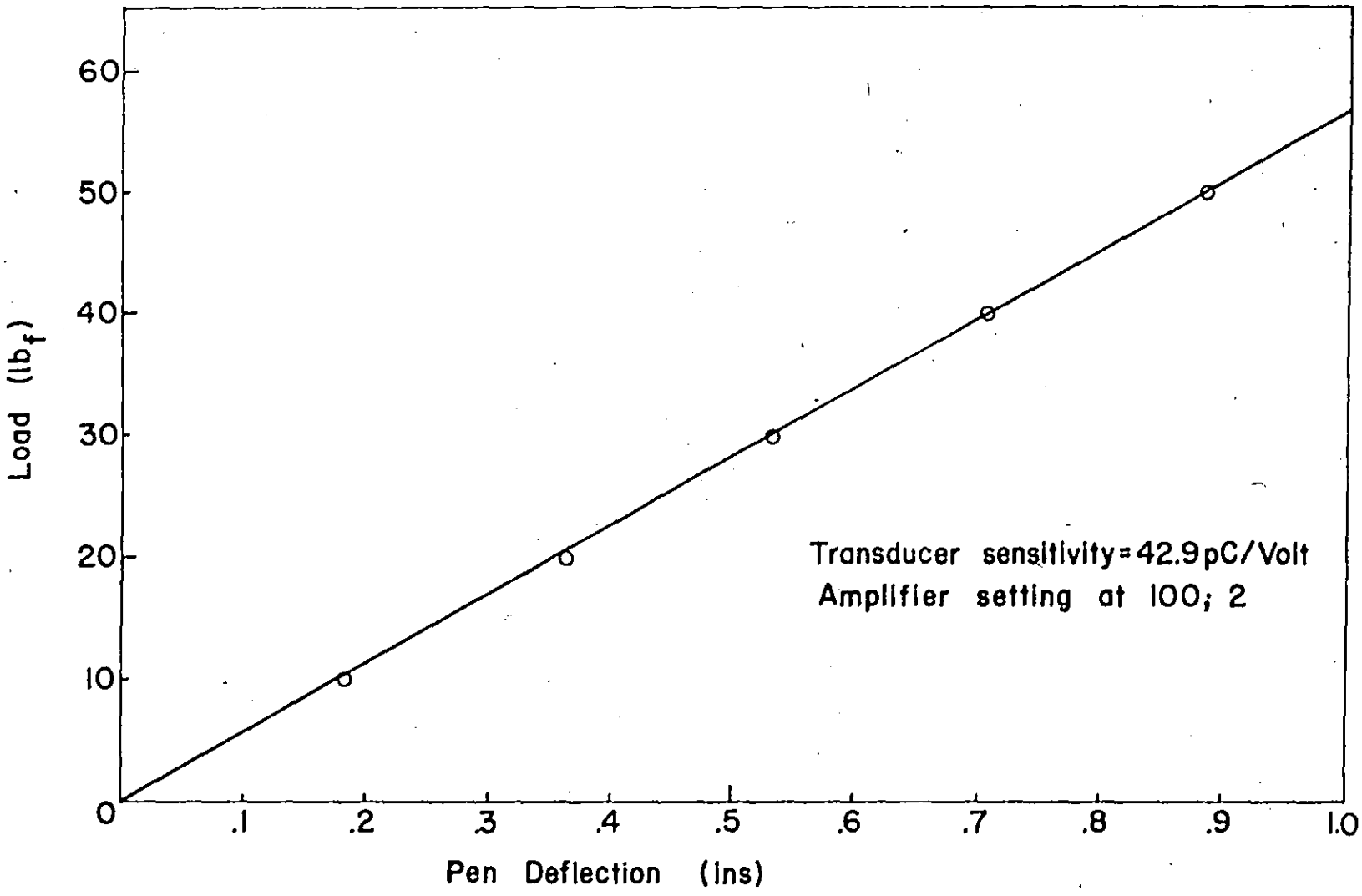

Figure 3.7. Load Cell Calibration.

The pressure transducer used for the final results was a variable reluctance pressure transducer made by Whittaker Corporation, model P7. It was operated with the PACE model CD25 meter readout type carrier system. The response of this transducer indicator was flat to 1000 Hz, and the natural frequency of the stainless steel diaphragm was 14 kHz. It was found that there was no need to filter the output signal because the excitation frequency was quite high, of the order of 1000 Hz to 3000 Hz.

This transducer was used both as a single pressure transducer and as a differential pressure transducer. Measurements were taken very close to the point of valve action thus permitting the use of short connection lines. Excellent results were obtained with this pressure transducer.

The transducer was calibrated by applying known pressures and measuring the signal tracers corresponding to these pressures on the Visicorder oscillograph. The rated transducer linearity was $\pm$ 1/2%.

3.5 Flow Visualization

3.5.1 Flow Visualization in Water: Brief Review of Techniques

Many techniques have been developed for the visualization of water flow. Methods of indicating flow patterns may be broadly classified into two groups: static methods - those applied to boundary surfaces; and kinetic methods - those applied in the fluid itself, either in the stream or in the boundary layer. Static methods illustrate

the pattern of velocity gradient and therefore of shear stress at a solid boundary and may involve the deposition of solids or liquids on the boundary surfaces. Kinetic methods may be used to investigate the flow in either a boundary layer or in the main stream itself, and generally involve injecting tracer material into the fluid. Care is necessary to ensure that neither the tracers nor the injection tubes modify the flow in the boundary layer because interference with the flow pattern may render incorrect, deductions based on it. Injecting tracers into the main stream is less critical.

For quantitative results and those from which time-dependent flow characteristics are to be deduced, kinetic techniques must be used. The oldest of these, applicable to flow in an open channel consists of scattering on the liquid surface a light powder (such as aluminium or lycopodium) and illuminating the particles. Morris and Haythornthwaite [38] used the technique to illustrate two-dimensional flow into a model of a compressor intake and improved a poor pressure distribution there directly as a result of their observations. Difficulties associated with a free surface may be resolved by submerging the model and introducing tracers below the free surface. Highly reflective particles in suspension may be illuminated from an intense light source through a narrow slit approximately parallel to the main flow. The flow may then be examined by viewing the illuminated "slice" along a direction approximately perpendicular to it. Such an aqueous suspension is readily made from small spherical particles of aluminium which have first been wetted with alcohol. Chester, Halliday

and Howes [47] show in their book that aluminium particles show to particular advantage in a channel of rectangular section because the angle of optimum reflection is about 90° to the incoming light. Where the main flow is horizontal and the slit is vertical the particles may be viewed from the side without significant optical distortion of the flow pattern. The method is well suited to photography and accurate results are obtainable if the specific gravity of the tracers is close to unity.

A drawback to the prolonged use of aluminium particles is that they soon become tarnished by an oxide film. Small spheres of polystyrene were successfully used by, among others, McEachern and Bowker [39] and Winter [40]. Winter and a number of other workers also experimented on a limited scale with air bubbles as tracers. It was found that optically, air bubbles are unsatisfactory because they reflect incident light only slightly. The ideal angle of reflection is 90° because tracers may then be viewed in a direction normal to the incident beam and distortion of the flow pattern by optical refraction is eliminated. An even more serious drawback to air bubbles is their low density.

In general the velocity at any point of a two-dimensional flow field can be determined from a photograph of the pattern made by the tracers provided the exposure time is known. In steady two-dimensional flow a qualitative indication of the streamline pattern can be obtained by allowing a fairly long exposure.

For many years injecting streaks of dyes has been a popular method of introducing discrete tracer filaments into a fluid stream. The technique is especially useful in water tunnels where the flow around a model at various depths can be indicated. A critical drawback, however, is the disturbance of the flow caused by the tubes which dispense the dye. The method, moreover, is unsuitable for highly turbulent flow because dye filaments are then rapidly dispersed and broken up. A further drawback to using dye filaments in closed water circuits is that the dye is recirculated and increasingly contaminates the water. In short runs this may not seriously affect the clarity of observation but for longer runs the contamination may be enough to render the new dye filaments indistinguishable from the bulk fluid. Dye filaments cannot be pulsed accurately enough to give direct velocity measurements. The use of dyes is therefore better confined to boundary layer work or steady flows with low turbulence.

The hydrogen bubble technique, apparently first used by Geller [41] to study low-speed water flow through a duct, has been improved upon by a host of other workers, notably Clutter, Smith and Brazier [42]. These workers developed the technique of using a crimped cathode to generate well-defined filaments of bubbles. The bubbles are generated from the whole of the wire but if the apexes are closely spaced the bubbles are swept towards the apexes before being shed into the flow. By pulsing the supply to the cathode they determined the mainstream velocity about an airfoil from photographs showing rows

of bubbles released from the cathode at known intervals of time. With sufficient power input, the hydrogen-bubble technique is not restricted to low velocities. Illumination of the bubbles is fairly critical. They are best seen against a dark background and Clayton and Massey [43] as well as Schraub et al. [44] discovered that a parallel beam of light should be so positioned that the light is deviated through about 65° into the viewing direction.

The principal objection to the method lies in the difference between the densities of bubbles and water. However, the bubbles are usually small enough for their rate of rise to be only a small proportion of the main-stream velocity of the water.

For reasons of space, only the principal methods of flow visualization in water have been briefly discussed here. A discussion of techniques not mentioned here as well as an extensive bibliography, is contained in References [42], [43] and [45].

The purpose of the flow visualization in the present work was to give a clear picture of the nature of the unsteady flow field during the vibration process. It was also desired to obtain a good idea of the fluid and valve disc velocity variations.

Aluminium tracer injection was chosen over all other methods for this work because of a number of outstanding advantages it possesses over the other principal methods, given the aims and conditions of the present experiment. It is

relatively simple to inject enough aluminium tracers into the closed circuit system to keep the quality of the cine-photography reasonably constant from test to test. The aluminium tracers also possess the optimum light reflecting angle of 90^{o}. Moreover it was believed that aluminium tracer injection offered the least expensive and most easily controlled of all the techniques considered. Finally, previous experience by other workers had shown that excellent photography was possible with this method.

3.5.2 The Optical Arrangement

The most successful lighting for photographing flow lines beneath the water surface is a thin slit of intense light that illuminates only the flow region of interest. Financial considerations called for the design of a lighting system which was both simple and inexpensive. The type of lighting required for the photography contemplated had to be a narrow vertical plane beam at least 12 inches long. This called for either a long pencil-thin source of light capable of being focussed with a parabolic reflector, or a series of point sources arranged in a straight line. A survey of the intensity and efficiency of various light sources was carried out before two alternate sources were chosen. The first system was a Westinghouse 1500 Watt, 208 Volt tungsten halogen lamp equipped with a parabolic polished-aluminium reflector. Its filament was 9 inches long and the light intensity could be varied with the operating voltage. The second light source used was a series arrangement of five 300

Watt, 120 Volt Kodak Carousel projector lamps each of which was equipped with its own polished glass reflector. Air cooling of both systems was carried out with a 20 inch fan.

Preliminary experiments were carried out to determine the feasibility of using a cylindrical plano-convex perspex lens to focus the light beam before it reached the transparent portion of the valve apron. Based on the result of several experiments and previous work [46], a plano-convex cylindrical lens was cut out of a 5 inch diameter solid stock of cast acrylic rod, 12 inches long. This lens was carefully polished to high transparency and proved quite adequate. Cooling the lens presented a real problem as the heat from either of the lighting systems could easily cause melting. A special housing for the lens was designed complete with a 1/4 inch thick heat resistant glass plate 12 inches long and 4 inches wide. This cut down the amount of heat radiated to the lens but unfortunately it also reduced the amount of light reaching the lens.

The housing for the lens and heat-resistant glass was made of sheet aluminium and painted flat black to minimize reflection. Two perforated pipes were used to distribute cooling air over the entire length of the lens. The air was tapped from a 20 psi laboratory supply. Even with all these precautions, experience showed that further care was required to prevent the lens from warping under the effect of prolonged heating, even at moderate temperatures. The lights were therefore turned on only when required and even then not for

prolonged periods of time. The optical system is shown in Figs. 3.3 and 3.6.

With these light sources the tracer particles could be photographed at shutter speeds up to 1/1000 second depending on aluminium particle concentration and film rating.

3.5.3 Aluminium Tracer Injection

A pressurized transparent tank was used to inject the aluminium tracer into the system upstream of the test valve. This injection tank was made from 6 inch diameter perspex piping so that the level of the tracer preparation could be visually monitored in the course of an experiment. Its design was based on calculated injection rate and pressure which would eliminate the need for replenishing the preparation during the normal course of shooting about 100 feet of film. Calculation showed that the tank material could safely withstand up to 60 psi without rupturing. However, there was never a need to operate the system above a preset pressure of 15 psi. A Bourdon gauge indicated the injection pressure and a safety-relief valve kept this pressure constant. This tank is shown in Fig. 3.3.

The tracer was injected into the pipeline about 30 inches upstream of the valve seat. A 1/4 inch steel tube was inserted into the centre-top of the rectangular duct, touching the bottom of the duct. A number of 3/32 inch diameter holes were drilled into the bottom three inches of the downstream side of this tube. A valve fitted to the outside

extension of this tube controlled the rate of tracer injection.

The aluminium powder was made into an aqueous suspension by wetting a measured quantity of the powder with methyl alcohol and then vigorously shaking the mixture before transferring it into the injection tank. The tank was then made up to volume by addition of water-alcohol mixture. Experience showed that the make-up of water-alcohol prevented the tracers, once injected into the system, from staining the sides of the transparent plexiglass of the test section.

3.5.4 Photography

Still or movie cameras were mounted on a stand in front of the test section as shown in Figs. 3.3 and 3.6.

Two different cine-cameras were procured for the experiments. The first was a Hycam high-speed camera capable of speeds ranging from 50 to 3000 frames per second full frame. Difficulties were encountered because of the lack of a suitable wide-angle lens to use with this camera. This resulted in the camera having to be moved a considerable distance from the test section to focus the lens. The light reaching the film decreases with the distance of the camera from the object being filmed. Thus to obtain enough light for filming at this relatively far camera position, more concentration of tracer was always required. This resulted in streamlines of the flow around the valve being indistinguishable from one another.

The other camera available was a Bolex H16 Reflex 16mm cine-camera capable of speeds ranging from single frame to 64 frames per second. It was fitted with a 25mm f1.1 wide-

angle lens and it proved excellent for all the cine-photography attempted. This camera was slightly modified by the installation of a microswitch and trigger circuit to synchronize the operation of both the camera and the Visicorder oscillograph. Provision was made for bolting the camera to its stand so that vibration of the camera was eliminated. The camera was also operated with a remote control switch to ensure camera stability.

Still photography was done with an Asahi-Pentax Spotmatic 35mm single lens reflex camera.

Primarily two types of films were used although a third type was briefly experimented with. First, for preliminary experiments, Kodak 4-X Negative film, Type 7224 having a speed rating in sunlight of 400 ASA was used. This was a very fast film but it also had a disadvantage of being rather grainy so that the prints obtained from this film lacked the excellent definition that was desired. For all the permanent movies shot in these experiments, Kodak Plus-X Negative film Type 7231 having a speed rating in sunlight of 64 ASA has been used. For all still photography Kodak Tri-X Ektachrome 35mm black and white film having a speed rating in sunlight of 125 ASA has been used.

Special problems encountered in cine-photography involved the effect of fluid flow velocity and valve disc speed on the quality of picture obtained at different filming speeds. At the higher framing speeds (mainly at 64fps, 1/180 second shutter speed), the film stopped both the flow and the

disc. At low filming speeds a better flow definition was obtained but the disc became blurred during those parts of its oscillation where its velocity was greatest.

3.6 Determination of Spring Stiffnesses

Five different sets of compression springs were assembled for the experiments. All had uncompressed lengths of 4 inches. Differences in spring coil diameter allowed insertion of some into others. In this way eighteen different combinations could be made. The springs were arbitrarily designated as A, B, C, D and E for identification purposes.

Their stiffnesses were accurately determined on an Instron Tester machine by plotting a load-deflection characteristic curve for each spring. The slope of each curve yielded the value of the individual spring stiffnesses. These curves, shown in Fig. 3.8, indicate that all the springs except E exhibit excellent linearity even for large deflections. Under the influence of large loads spring E tended to bend as a beam as well as deflect axially, resulting in larger apparent deflections.

3.7 Experimental Procedure

A typical vibration test was carried out in the following manner. Complete liquid filling of the pipeline was effected by opening the upstream gate valve and bleeding air out of the system by opening the bleed valve on top of the test section. The gate and bleed valves were then closed.

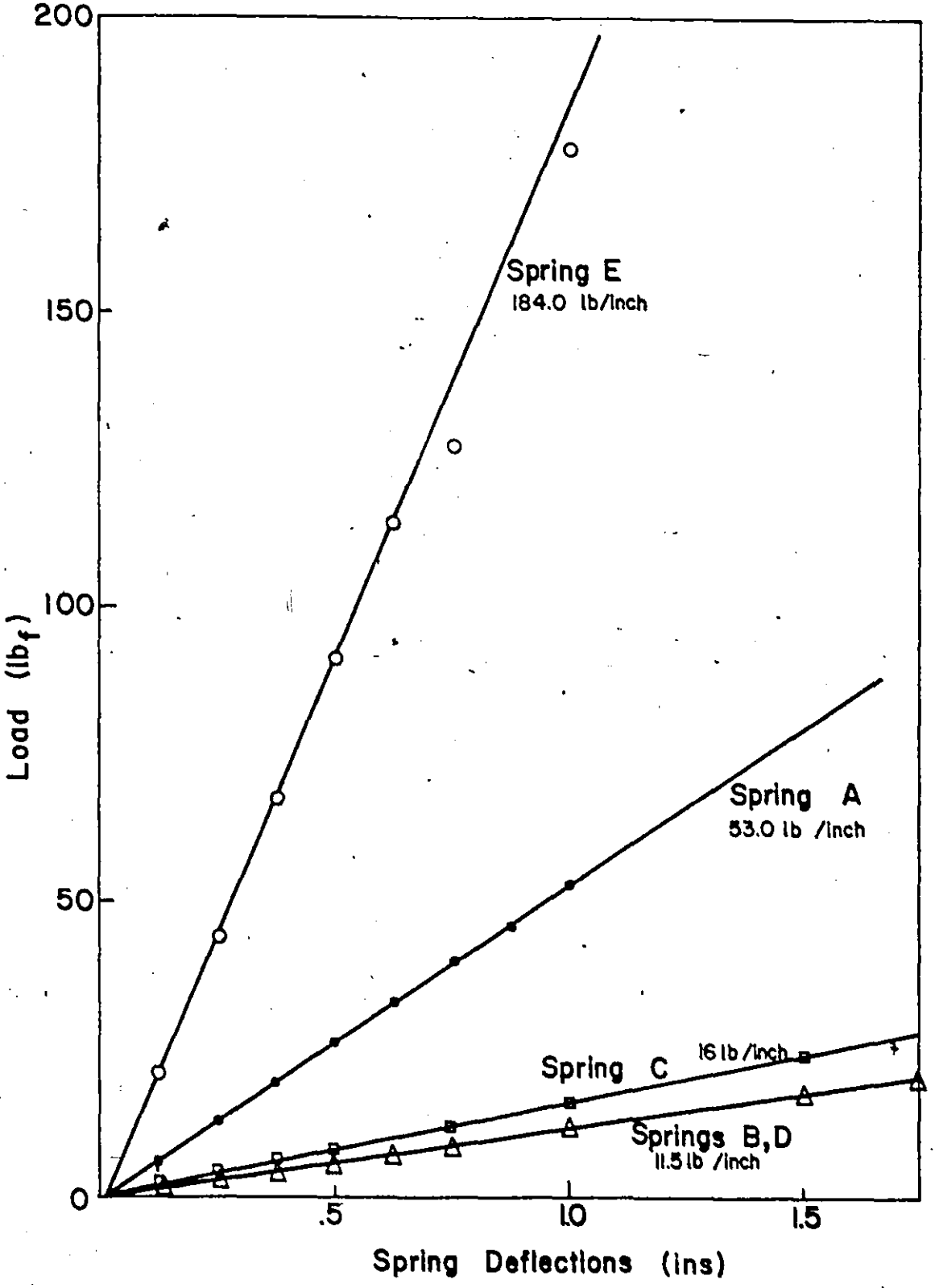

Figure 3.8. Determination of Spring Stiffnesses.

Any tests under no-flow conditions could now be performed.

Next, a spring combination of known total stiffness was inserted into the spring arm and the test valve opened to a predetermined initial angle using the protractor. A record of the displacement, pressure and torque transducer outputs under no-flow conditions was then made. The upstream gate valve was opened completely, and depending on the initial angle and spring stiffness, the valve either closed without vibration, did not close at all, or went into spontaneous vibration. It was found that in some marginal cases vibration could be induced by giving the spring arm a jolt.

Where shooting a film was contemplated the camera light meter reading was taken to determine the exposure time at a desired film speed. At least nine variables must be considered in obtaining the optimum photograph with an available light source:

(i) exposure time
(ii) water velocity
(iii) film type
(iv) developer
(v) developing time
(vi) particle size
(vii) particle type
(viii) particle concentration
(xi) aperture

In order to keep particle concentration constant from test to test enough tracer was injected to obtain a given light meter

reading and then injection was stopped, the camera was synchronized with the visicorder oscillograph and the film was shot.

The film was then developed in the darkroom using Microdol-X developer with an average developing time of 8 1/2 minutes, as specified for average contrast by the film manufacturer.

CHAPTER 4

FREE VIBRATIONS - NO FLOW

4.1 Introduction

In this chapter, the equations governing the small amplitude free vibration of the model valve in air and in quiescent water are derived. These linear differential equations are solved analytically and a computer has been used to obtain numerical data. Experiments to determine the first natural frequency of the system in air and in quiescent water are described. Comparison of the experimental results with the theoretical predictions shows, among other things, that the assumptions made in deriving the theory are fully justified.

4.2 Theoretical Formulation

Fig. 4.1 shows a schematic representation of the valve system.

Consider the system for the purposes of "exact" analysis as a two-degree-of-freedom system, the two masses being the mass of the spring arm and the combined mass of the valve plate and swing arm. The two stiffnesses are the torsional-stiffness K_θ of the pivot shaft and the combined stiffness K_s of the compression springs.

Taking moments about the centre of the pivot shaft,

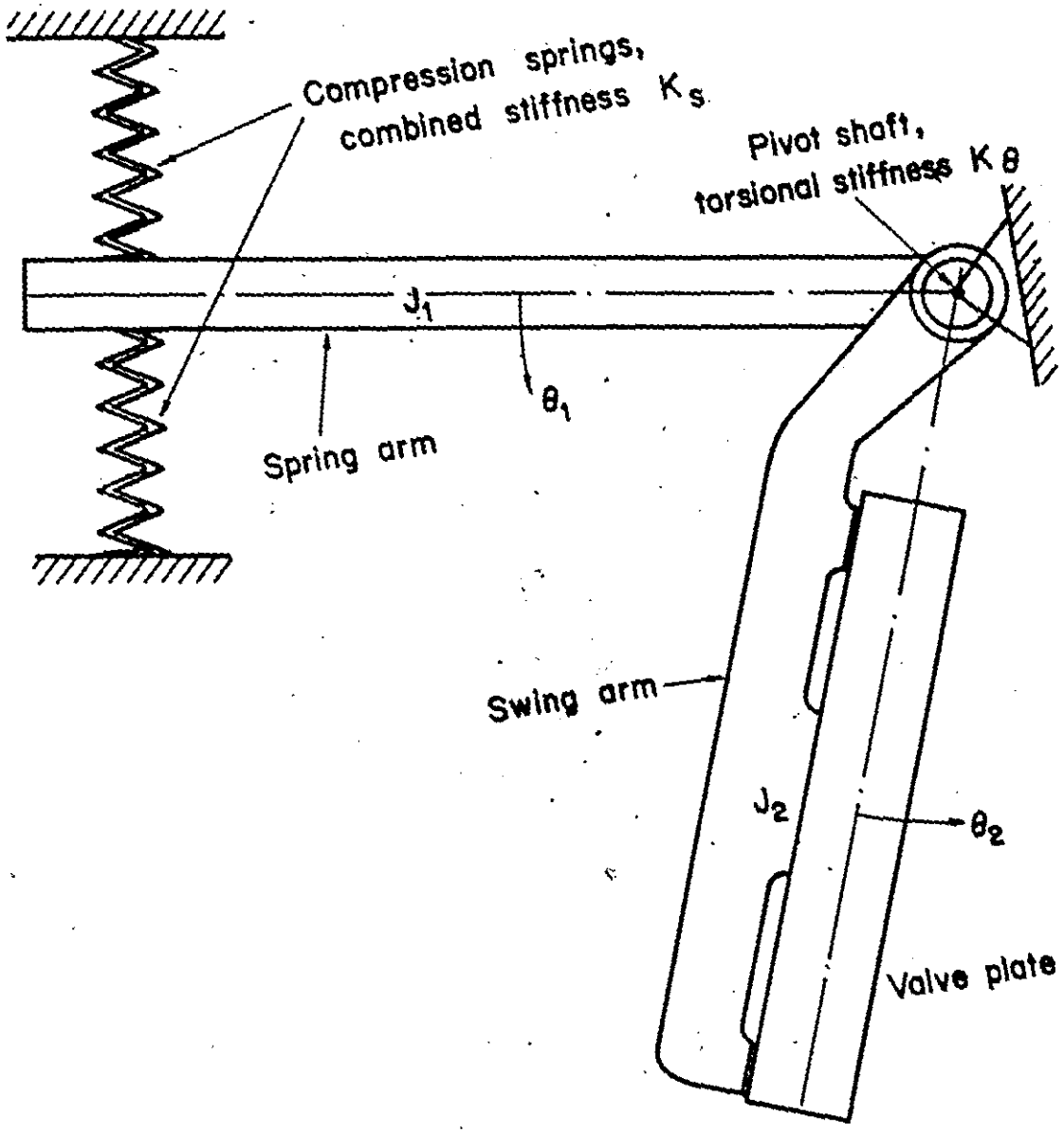

Figure 4.1. Schematic Representation of Valve System.

$$J_1 \ddot{\theta}_1 + K_s L^2 \theta_1 - K_\theta (\theta_2 - \theta_1) = 0 \qquad (4.1a)$$

$$J_2 \ddot{\theta}_2 + K_\theta (\theta_2 - \theta_1) = 0 \qquad (4.1b)$$

where

K_θ is the torsional stiffness of the pivot shaft, 9.6262×10^4 lb_f-in per radian;

K_s is the equivalent stiffness of the combined springs, in lb_f/inch;

J_1 is the mass moment of inertia of the extension arm about the centre of rotation of the system, 1.01 lb_f-in-sec^2;

J_2 is the mass moment of inertia of the swing arm and the valve plate about the centre of rotation of the system, in lb_f-in-sec^2;

θ_1 and θ_2 are the absolute angular rotations of the spring arm and swing arm respectively about the centre of rotation, in radians, and

L is the distance between the spring support and the centre of rotation, 12 inches.

Equations (4.1) are simultaneous linear differential equations with constant coefficients. Assuming a particular solution in the form

$$\theta_1 = \hat{\theta}_1 \sin (\omega t + \alpha)$$

$$\theta_2 = \hat{\theta}_2 \sin (\omega t + \alpha)$$

and substituting, we obtain;

$$\begin{bmatrix} (K_s L^2 + K_\theta - \omega^2 J_1) & -K_\theta \\ -K_\theta & (K_\theta - \omega^2 J_2) \end{bmatrix} \begin{Bmatrix} \hat{\theta}_1 \\ \hat{\theta}_2 \end{Bmatrix} = \{0\} \qquad (4.2)$$

For a non-trivial solution, equation (4.2) yields the frequency equation of the system:

$$J_1 J_2 \omega^4 - [J_1 K_\theta + J_2 (K_s L^2 + K_\theta)]\omega^2 + K_s L^2 K_\theta = 0 \qquad (4.3)$$

The solution of equation (4.3) yields the two natural frequencies of the system:

$$\omega^2 = \frac{[J_1 K_\theta + J_2 (K_s L^2 + K_\theta)] \pm \sqrt{[J_1 K_\theta + J_2 (K_s L^2 + K_\theta)]^2 - 4 J_1 J_2 K_s L^2 K_\theta}}{(2 J_1 J_2)} \qquad (4.4)$$

4.3 Approximate Theory: Reduction to a Single-Degree-of-Freedom System

It is normally desirable to have the torsional stiffness of the shaft K_θ as great as possible. However in order to prevent the slamming of the disc on its seat, K_s may also be rather large, in which case K_θ and $K_s L^2$ may be the same order of magnitude. It is of interest to see for what range of $(K_s L^2 / K_\theta)$, the simple single-degree-of-freedom approximation is good.

If $K_\theta >> K_s L^2$, then

$$\lim_{K_\theta \to \infty} (\theta_2) = \theta_1 \tag{4.5}$$

Substituting equation (4.1b) into equation (4.1a), we obtain

$$J_1 \ddot{\theta}_1 + J_2 \ddot{\theta}_2 + K_s L^2 \theta_1 = 0 \tag{4.6}$$

and using equation (4.5), equation (4.6) reduces to

$$(J_1 + J_2) \ddot{\theta}_1 + K_s L^2 \theta_1 = 0 \tag{4.7}$$

from which

$$\omega_n = \sqrt{\frac{K_s L^2}{(J_1+J_2)}} \tag{4.8}$$

4.4 Experimental Procedure and Typical Results

Free vibration tests in air were performed as follows: The pipeline was completely drained of water and a predetermined spring stiffness was arranged in the spring arm. The spring arm was then suddenly released from a depressed position and the resulting transient vibration recorded in the form of displacement and torque transducer outputs on the visicorder oscillograph. The valve was arranged to execute free vibration about an equilibrium position of 4^o with an initial amplitude of about 2^o. From these records the fundamental frequency of the system was determined for each spring combination. The results are listed below, and plotted in Fig. 4.2.

Stiffness Ratio $(K_s L^2/K_\theta)$	Fundamental Frequency of Valve in Air (Cycles/sec)		
	Determined Experimentally f_a(expt.)	Computed from "exact" theory f_{1a}	Single-degree-of-freedom approx. f_{na}
0.034	8.5	7.86	7.87
0.052	9.86	9.62	9.63
0.058	10.89	10.22	10.24
0.069	11.18	11.10	11.12
0.076	12.10	11.63	11.66
0.096	12.90	13.13	13.17
0.1137	14.28	14.24	14.30
0.1204	14.97	14.66	14.71
0.1309	15.00	15.28	15.34
0.1376	15.28	15.66	15.73
0.1586	16.71	16.80	16.89
0.1758	16.95	17.67	17.78
0.1825	17.88	18.00	18.12
0.1930	18.00	18.51	18.63
0.1997	18.65	18.82	18.95
0.3097	21.28	23.35	23.60
0.3269	22.65	23.97	24.24
0.3336	22.82	24.21	24.49
0.3717	25.25	25.52	25.85

Table 4.1

In equations (4.1) to (4.8), the value of J_2 was not known. Its value was estimated in the following manner:

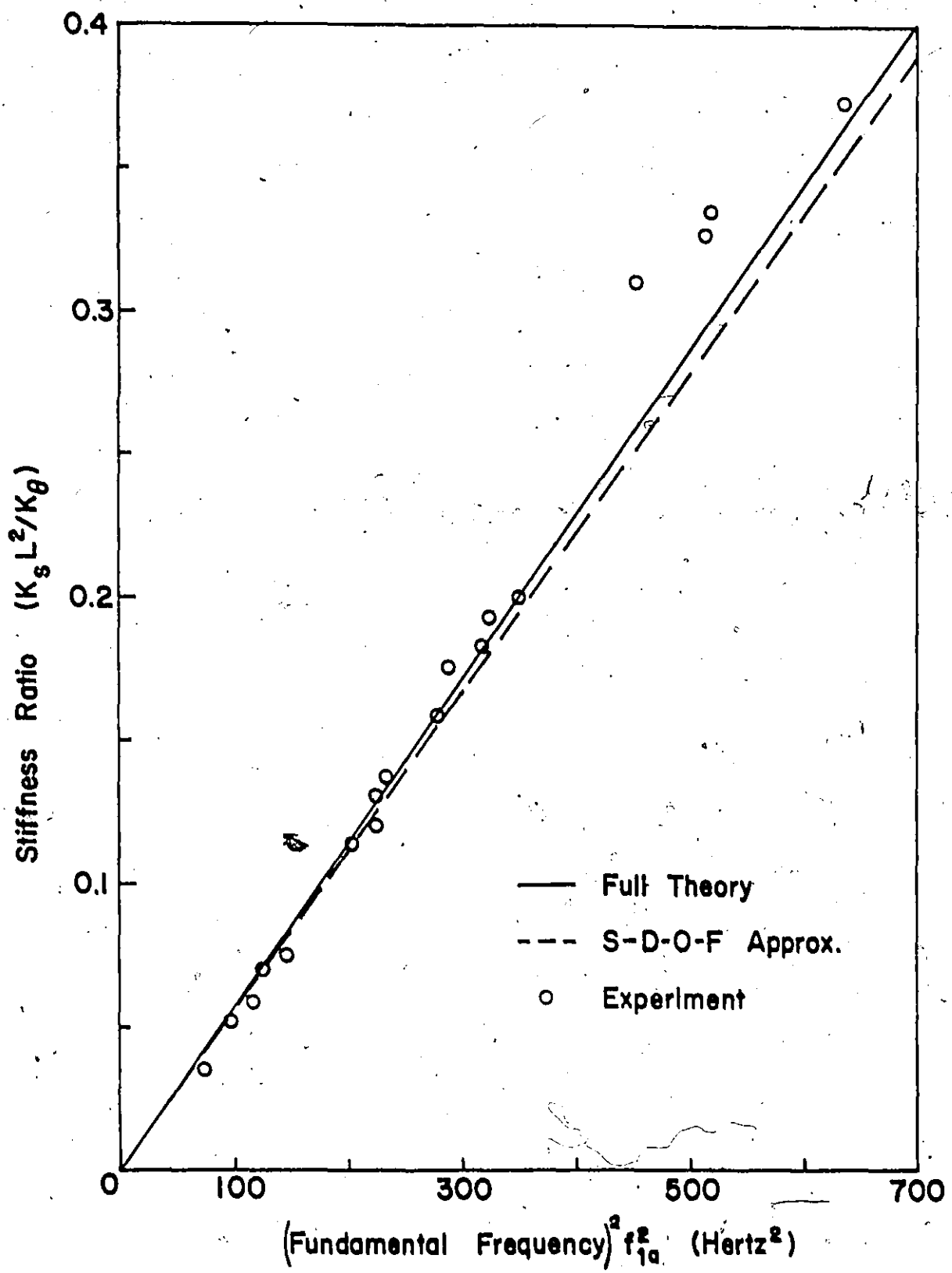

Figure 4.2. Free Vibrations in Air.

From equation (4.3)

$$J_2 = \frac{\omega^2 J_1 K_\theta - K_s L^2 K_\theta}{J_1 \omega^4 - \omega^2 (K_s L^2 + K_\theta)} \qquad (4.9)$$

Using the known values of J_1, K_θ, L, and K_s, and the experimentally measured values of ω for a number of small $(K_s L^2/K_\theta)$, J_2 was calculated and an average taken. This average value of J_2 for free vibration in air is 0.45 lb_f-in-sec^2. Using the average value of J_2 and the appropriate theory the results in columns 3 and 4 of Table 4.1 are calculated.

To determine the fundamental frequency of the system in water, the pipeline was completely filled with water and the upstream gate valve was then shut so that no flow occurred. The spring arm was kept depressed for a few seconds and then released. The valve displacement and spring force were recorded on the visicorder oscillograph. Again the valve was arranged to vibrate freely about an equilibrium position of 4^o with an initial amplitude of approximately 2^o. From the records, the fundamental frequency of the system under this condition was determined for each spring combination. The results are listed below, and plotted in Fig. 4.3

Stiffness Ratio $(K_s L^2/K_\theta)$	Fundamental Frequency of Valve in Quiescent Water (Cps)		
	Determined experimentally f_w(expt.)	Computed from "exact" theory f_{1w}	Single-degree-of freedom approx. f_{nw}
0.034	5.25	4.65	4.69
0.052	5.81	5.67	5.74
0.058	6.36	6.01	6.11
0.069	6.78	6.51	6.63
0.076	7.21	6.81	6.95
0.096	7.66	7.66	7.86
0.1137	8.08	8.27	8.53
0.1204	8.20	8.50	8.78
0.1309	8.39	8.84	9.15
0.1376	8.51	9.04	9.38
0.1586	9.61	9.65	10.07
0.1758	9.68	10.12	10.60
0.1825	9.88	10.29	10.80
0.1930	10.95	10.56	11.11
0.1997	11.20	10.72	11.30
0.3097	12.20	12.98	14.07
0.3269	12.72	13.27	14.46
0.3336	12.73	13.39	14.61

Table 4.2

As in the case of free vibration in air, the value of J_2 for free vibration in water was not known. J_2 was once again evaluated from equation (4.9) using experimentally

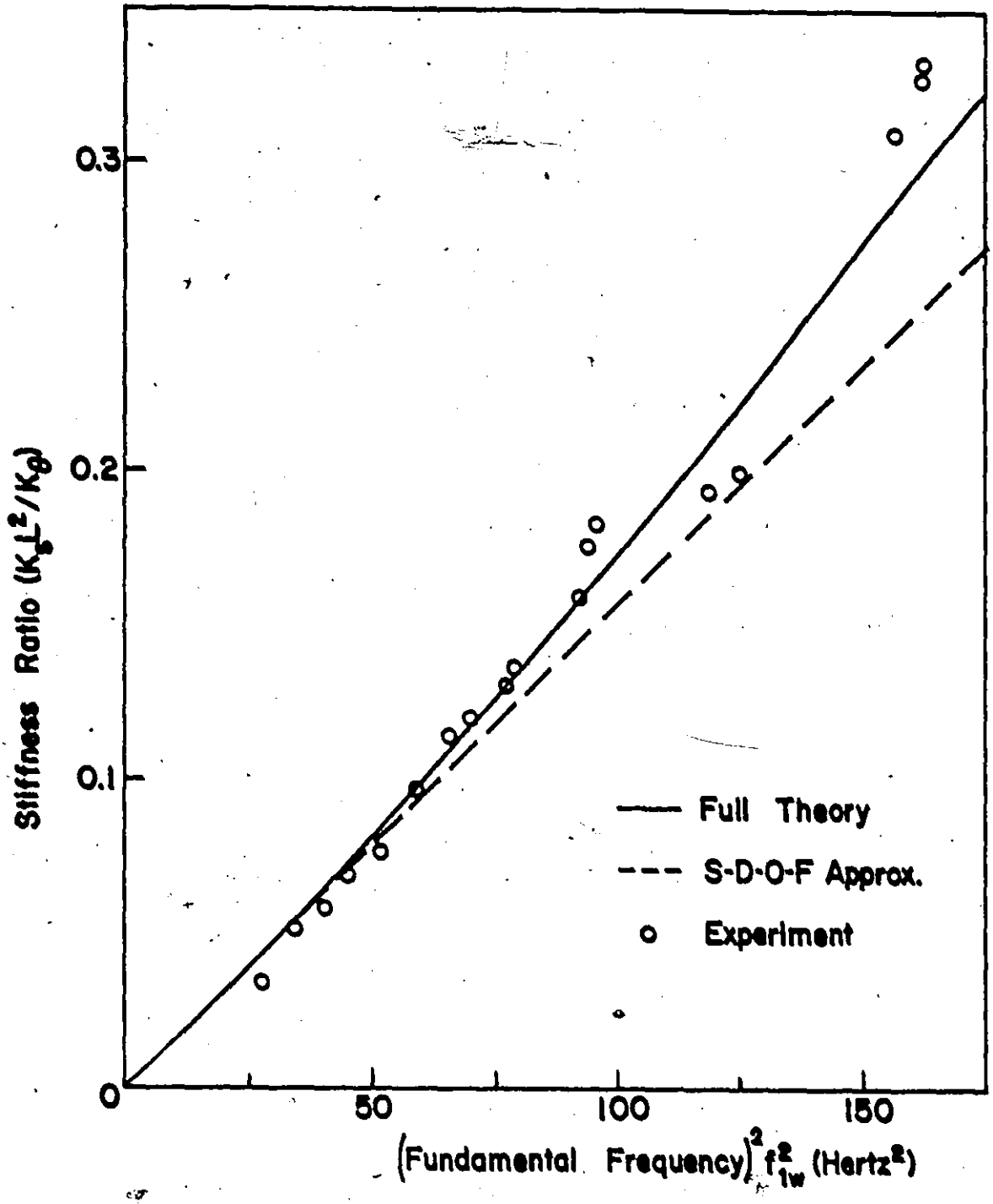

Figure 4.3. Free Vibrations in Water.

measured values of ω for a number of small $(K_s L^2/K_0)$. An average value of J_2 obtained from this procedure (2.802 lb_f-in-sec^2) was then used with the appropriate theory to calculate the results in columns 3 and 4 of Table 4.2.

Values of the damping factor were also determined from the oscillographic records for both free vibration in air and in quiescent water. In the case of free vibration in water, only a few cycles could be recorded for the lower spring stiffness as the vibration decayed very rapidly.

The damping factors were calculated from measured values of the logarithmic decrement of transient vibrations. Substantial variations in the measured values of the damping factor resulted from three sources of error. First, chafing occurred in the coils of the different springs. This problem could not be avoided because spring stiffness was varied by inserting one spring into another. Secondly, the contribution to the damping factor by the sealing compound introduced into the bushings on either side of the pivot shaft could not be estimated. It appears quite clear that this contribution is different for vibration in air and in water. Thirdly, there were errors in measurement which cannot be equalized in every case.

However, in spite of the variations, a clear trend was established in the results. The results show that the damping is substantially greater in water (by a factor of about 2) than it is in air.

4.5 Determination of an Approximate Added Mass

A structure submerged in water exhibits different dynamic characteristics from one which vibrates in air. Theoretical analysis as well as laboratory tests indicate that a system has a longer period of vibration when vibrating in water compared to that in air. For small amplitude vibrations the stiffness of a structure submerged in water does not change appreciably compared to the stiffness in air. Hence the increase in the period of vibration of such a system is only attributable to an increase in the apparent mass of the system due to the participation of the surrounding water in the motion. This apparent additional mass due to the motion of the surrounding water is termed "virtual mass" or "added mass" of the water.

The magnitude of the added mass certainly depends on the geometry of the structure, its relative confinement and the level of submergence. For ship hull vibrations, Todd [30] has shown that the added mass is not dependent to any marked extent on the mode of vibration or frequency. Apparently this result is applicable provided the amplitudes are small - generally not greater than about 5% of a characteristic dimension of the structure. However, Logvinovich and Savchenko [35] have demonstrated that as the amplitude is increased, the added mass becomes both amplitude and frequency dependent. Nevertheless, it has still not been clearly established that the added mass always increases with frequency at large amplitudes. The ratio of the added mass to actual

mass of the structure is known as the "virtual mass factor".

From the results of the experiments,

"Added inertia" due to the presence of fluid

$$= (2.802 - 0.45)\ lb_f\text{-in-sec}^2$$

$$= 2.352\ lb_f\text{-in-sec}^2$$

"Added inertia factor" a is given by

$$a = \frac{J_2(water) - J_2(air)}{J_2(air)} = 5.22$$

Also,

$$\frac{J_2(water)}{J_2(air)} = \frac{2.802}{0.45} = 6.23$$

This means that even for small amplitude free vibration in water the effective mass of the disc increased by a factor of about 6.23.

4.6 Discussion and Conclusions

The small discrepancy between computed and experimental results evident in Figs. 4.2 and 4.3 for stiffness ratios greater than 0.3 are likely due, at least in part, to the error in determining the exact value of the stiffness of spring E reported in Chapter 3. This particular spring was involved in all the combinations used to obtain stiffness ratios above this value.

The following major conclusions may be drawn from the results of the work reported in this chapter:

(i) The added mass of water participating in any vibrations of the valve is much larger than the mass of the disc

and must therefore be taken into account in any vibration analysis of the system.

(ii) Within the range $0 < (K_s L^2/K_\theta) < 0.2$ the valve system may reasonably be approximated by a single-degree-of-freedom system, provided also that $(J_2/J_1) < 1$. In the case of free vibration in water $(J_2/J_1) > 1$, and the range of stiffness ratio over which the system behaves like a single-degree-of-freedom system, shrinks appreciably.

(iii) Over the range where the system behaves approximately as a single-degree-of-freedom system, the added mass of fluid appears to be little affected by frequency. This is in agreement with the findings of previous workers, notably Todd [30].

(iv) The vibration experienced with the valve is not a resonance phenomenon. In preliminary vibration tests the observed frequency of vibration has always been much lower than the natural frequency of the system in water for the relevant spring stiffness.

(v) The damping in the system when vibrating in water appears to have increased by a factor of about 2 compared to the case of free vibrations in air.

CHAPTER 5

THE DYNAMIC BEHAVIOUR OF THE VALVE

5.1 Introduction

In this chapter, the dynamic behaviour of the check valve as designed originally by the manufacturer is studied, its limits of stability are determined and the influence of change of parameters in the region of instability is examined. Based on these experimental studies the key parameters apparently governing the instability are determined. Valve vibration is shown to be self-excited, and the region of self-excitation on a stability map is shown to have two zones with slightly different characteristics. A mechanism of instability is then postulated.

Before proceeding with the work in this chapter, the use of springs without an external damper on the model must be justified. The significant conclusion drawn from the preliminary experiments carried out on the externally damped prototype valve is that for high enough damping the damper became inoperative and the dynamic behaviour of the valve became dependent only on the elastic deflection of the pivot shaft and hydraulic oil damper connections. It was this elasticity plus the initial angle of valve opening which determined the frequency and amplitude of the observed valve vibration.

5.2 Static System Characteristics

As part of the programme to develop an understanding of the valve's behaviour, the theoretical hydrodynamic torque required to just overcome the spring arm restoring torque at the point of closure was calculated.

It was assumed that in this limiting condition, the equilibrium of the valve is determined solely by the restoring force in the spring and the effective pressure difference across the valve. The equilibrium equation is determined by taking moments about the centre of the pivot shaft as shown in Fig. 5.1. The moment due to the submerged weight of the disc and swing arm were found to be negligible compared to the moments due to the spring and hydrodynamic forces in the system. The resulting equation is:

$$K_{eq}\,\theta_o = (P_u\,A_u - P_d\,A_d)\,r_o \qquad (5.1)$$

where

$$K_{eq} = \left(\frac{K_s K_\theta L^2}{K_\theta + K_s L^2}\right) \qquad (5.2)$$

and $K_s = k_1 + k_2$

θ_o = initial angle of valve opening, in radians

P_u = average pressure (30.34 kPa) acting on upstream valve face A_u (0.04137 m^2),

P_d = average pressure (4.099 kPa) acting on downstream valve face A_d (0.0348 m^2),

r_o = effective radius arm from the centre of pressure to the centre of rotation (0.1222 metres).

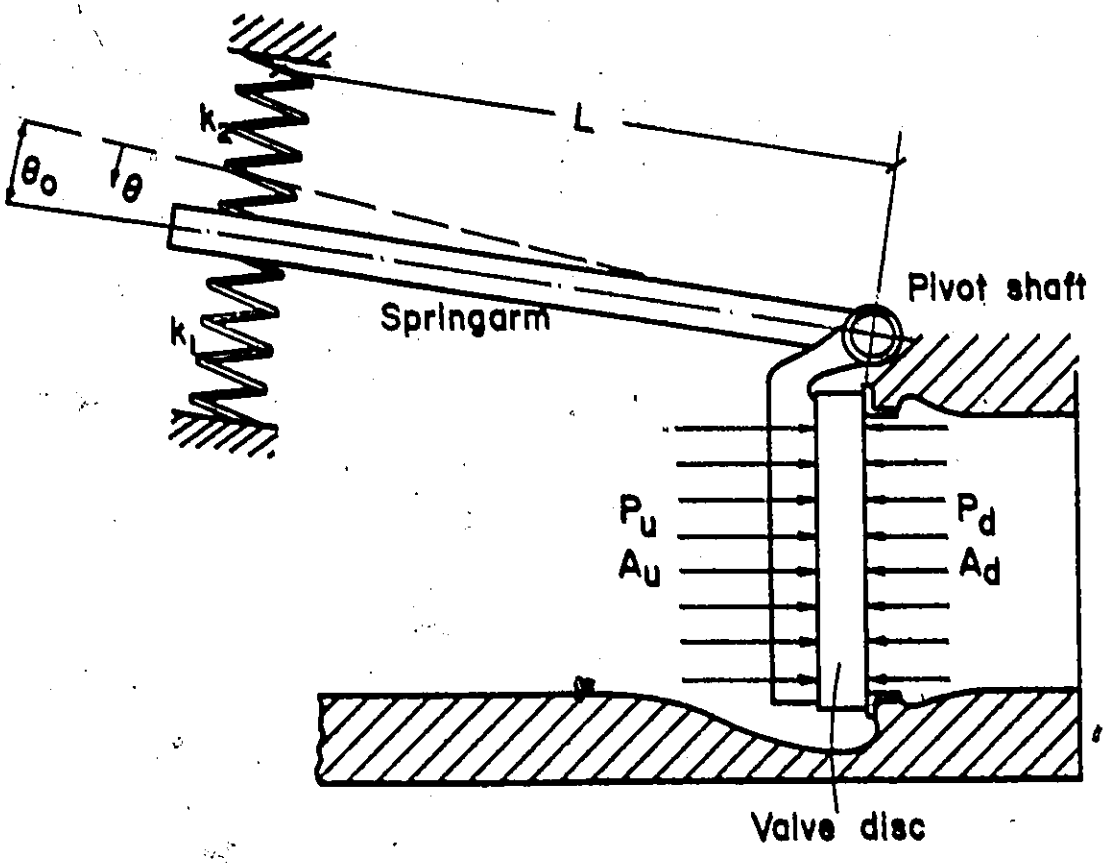

Figure 5.1. Limiting Condition of Equilibrium of the Valve.

L = distance from the spring support to the centre of rotation (0.3048 metres) and

K_θ is the stiffness of the pivot shaft, (10.876147 kN-m/radian).

As long as the hydrodynamic torque exceeds the spring restoring torque ($K_{eq}\ \theta_o$), the valve remains closed. The valve can open up only if the hydrodynamic torque reduces below this critical value.

A static characteristic for the valve has been derived using equation (5.1) and the appropriate areas, radius and hydrostatic pressures, i.e.,

$$\theta_o = \frac{1.3595 \times 10^3}{K_{eq}} \qquad (5.3)$$

The result is plotted in Fig. 5.2. The shape of this characteristic is dependent on the hydrostatic pressure and will move up or down depending on whether the pressure is higher or lower. This curve is based on the available hydrostatic head and is of significant importance in understanding the valve's dynamic behaviour.

All points to the left of the curve ideally should be stable in the sense of the valve closing and remaining closed because the available hydrostatic pressure in the system is sufficient to overcome the spring restoring force. To the right of this curve, the restoring torque from the spring at closure is greater than the torque exerted by the available hydrostatic pressure. Hence in this regime the valve will not close unless the hydrodynamic pressure exceeds

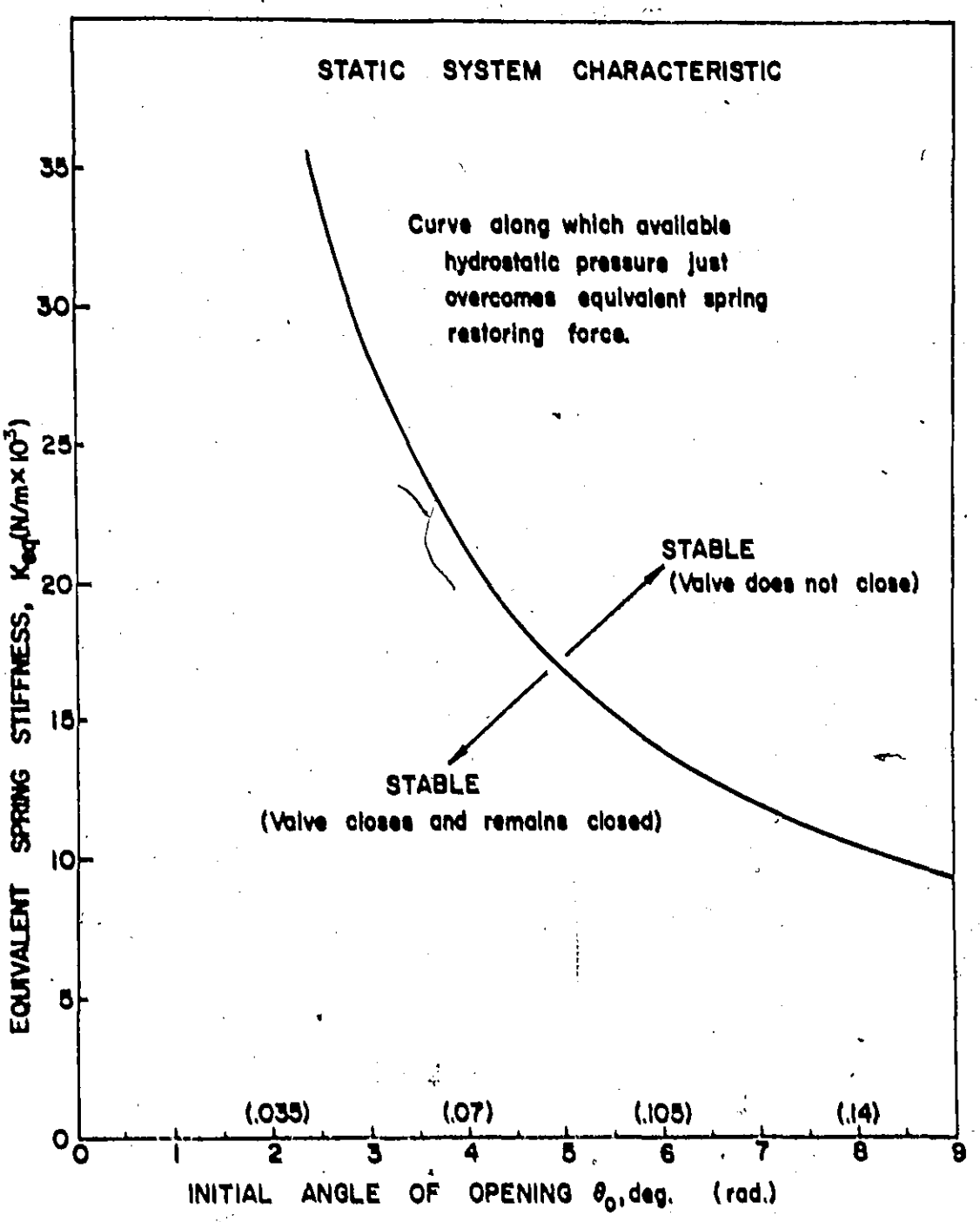

Figure 5.2. Static System Characteristic of the Valve.

the hydrostatic pressure.

5.3 Variable Parameters

For studying the dynamic behaviour of the valve, the parameters that can be varied are the spring stiffness and the initial angle of opening. Hence the natural frequency of free vibration and restoring torque at closure can be controlled. While the valve dynamics are also dependent on the total available hydrostatic pressure, this could not be varied with the existing experimental set-up.

5.4 Parametric Vibration Tests

In these tests, the pipeline was completely filled with water and the upstream gate valve was shut so that no flow occurred. A predetermined spring stiffness was arranged in the spring arm, and the valve opened to a desired initial angle. The upstream gate valve was then opened fully and the valve allowed to close from this initial angle.

5.4.1 Spring Stiffness kept Constant, Initial Angle of Opening Varied

These experiments have the same effect as holding the natural frequency of the valve constant and increasing the restoring torque at closure.

At small initial angles, depending on the spring stiffness, the valve slammed shut, bounced weakly once or twice and remained shut.

As the initial angle was increased, the valve suddenly began to oscillate with what appeared to be constant amplitude. Further increase in initial angle led to larger amplitude, lower frequency, limit cycle oscillations.

A large enough initial angle was eventually reached at which the valve slammed shut, bounced back once and remained open at a small angle. Any further increase in initial angle beyond this point merely increased the angle at which the valve finally stayed open. For these larger initial angles the hydrostatic pressure in the system was insufficient to keep the valve closed against the particular spring combination used.

5.4.2 Initial Angle of Opening kept Constant; Spring Stiffness Varied

In this series, not only is the restoring torque at closure increasing with increasing stiffness, but the natural frequency of the valve is also increasing.

For sufficiently small spring stiffnesses, the valve slammed shut and remained closed.

As spring stiffness was increased the valve suddenly began to execute limit cycle oscillations. Further increase in spring stiffness increased the violence of the oscillations.

A high enough spring stiffness was eventually inserted for which the valve slammed shut, bounced back once and remained open at a small angle. Any further increase in stiffness merely increased the angle at which the valve finally stayed open.

5.5 Dynamic Stability Diagram of the Valve

Stability data from the above parametric studies is plotted on a graph of stiffness against initial angle to form the stability map shown in Fig. 5.3. The curve represented by the broken line is the static characteristic of Fig. 5.2. Points on the diagram where vibration was observed experimentally are represented as dynamically unstable. It appears that the region of instability is almost evenly divided on either side of the static system characteristic.

The symbolic division of the unstable region into two sub-regions is not artificial. In the lower sub-region the valve is expected to close and remain closed since the available hydrostatic pressure is large enough to overcome the restoring force of the spring. This is shown further by experiments in which the valve was held shut for a few seconds and then released. It remained shut and no vibrations ensued. It follows that the cause of valve opening in this sub-region includes dynamic as well as static forces in the system.

In the upper sub-region the valve is expected to remain open since the available hydrostatic pressure is not sufficient to close it. The fact that it did close indicates that closure in this portion is effected by the addition of a hydrodynamic component to the available hydrostatic pressure bringing the total closing pressure to a value sufficient to overcome the spring restoring force. This additional hydrodynamic pressure component must be the result of the rate of change of discharge and local flow effects. Once the valve

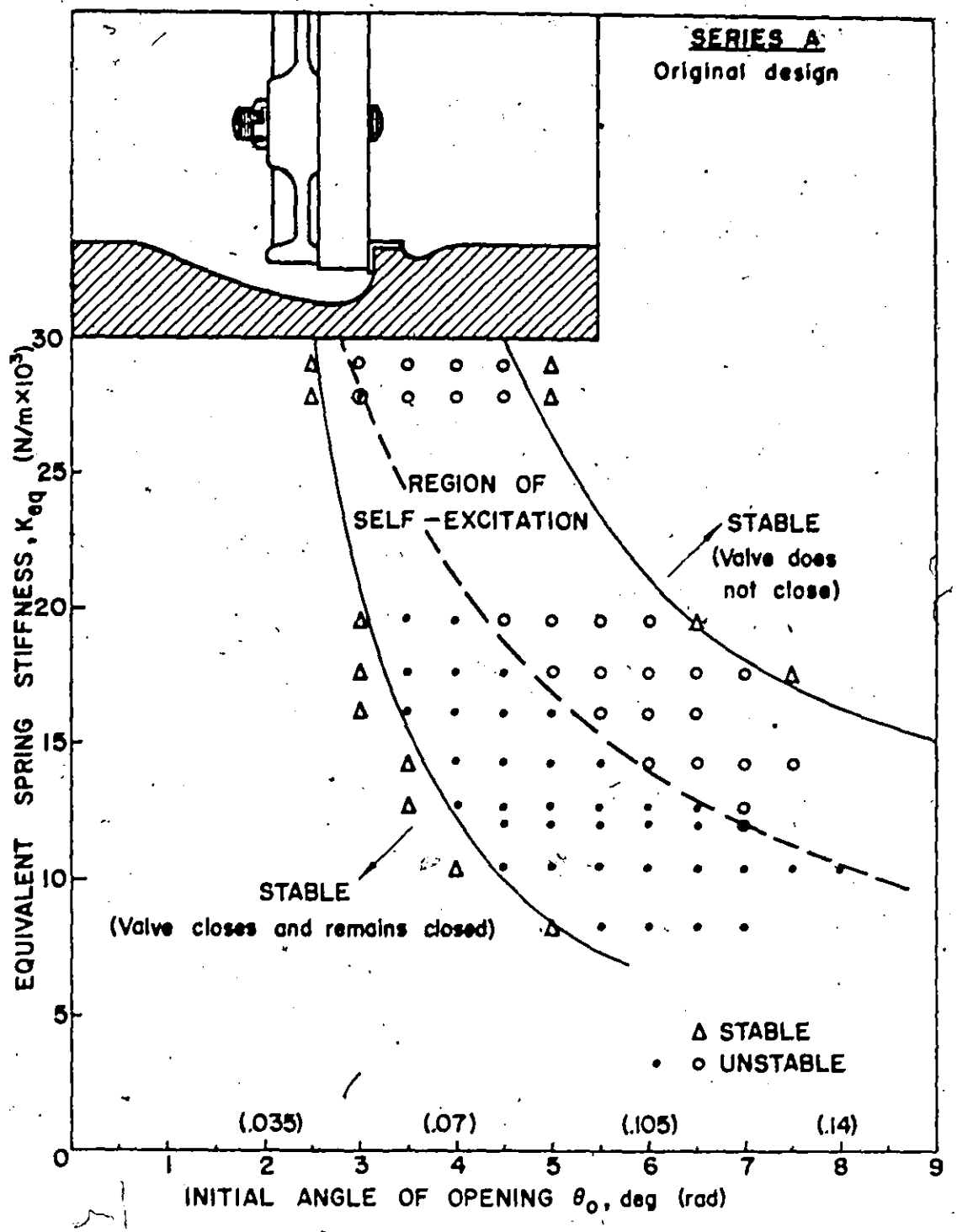

Figure 5.3. Stability Map of the Valve's Dynamic Behaviour.

closed, however, these dynamic pressure effects disappear and the valve is pulled open, at least initially, by the spring restoring force. Once open, the flow is re-established in the system, and the cycle repeats itself. Experiments in this sub-region show that the valve opens and vibration is instantly re-established on removal of an external static force holding the valve closed.

To the left of the lower sub-region of instability is a stable region where the valve always closed and remained closed. To the right of the upper sub-region of instability is another stable area where the valve does not close. In both these stable regions, all efforts to induce valve vibration failed.

5.6 Closer Examination of the Dynamic Instability

Having made the foregoing qualitative observations, it was decided to study in depth the dynamic measurements taken at five judiciously chosen points within the region of self-excitation shown in Fig. 5.3. These oscillographic records, shown in Figs. 5.4 to 5.8 display the instantaneous values of the upstream pressure, the downstream pressure, the resultant pressure difference across the valve, the valve displacement and the torque. From each of these figures the following general features of the vibration process are observed.

At the maximum angle of opening, the valve is just beginning to resume closure. There are waterhammer waves travelling back and forth within the pipeline and these waves

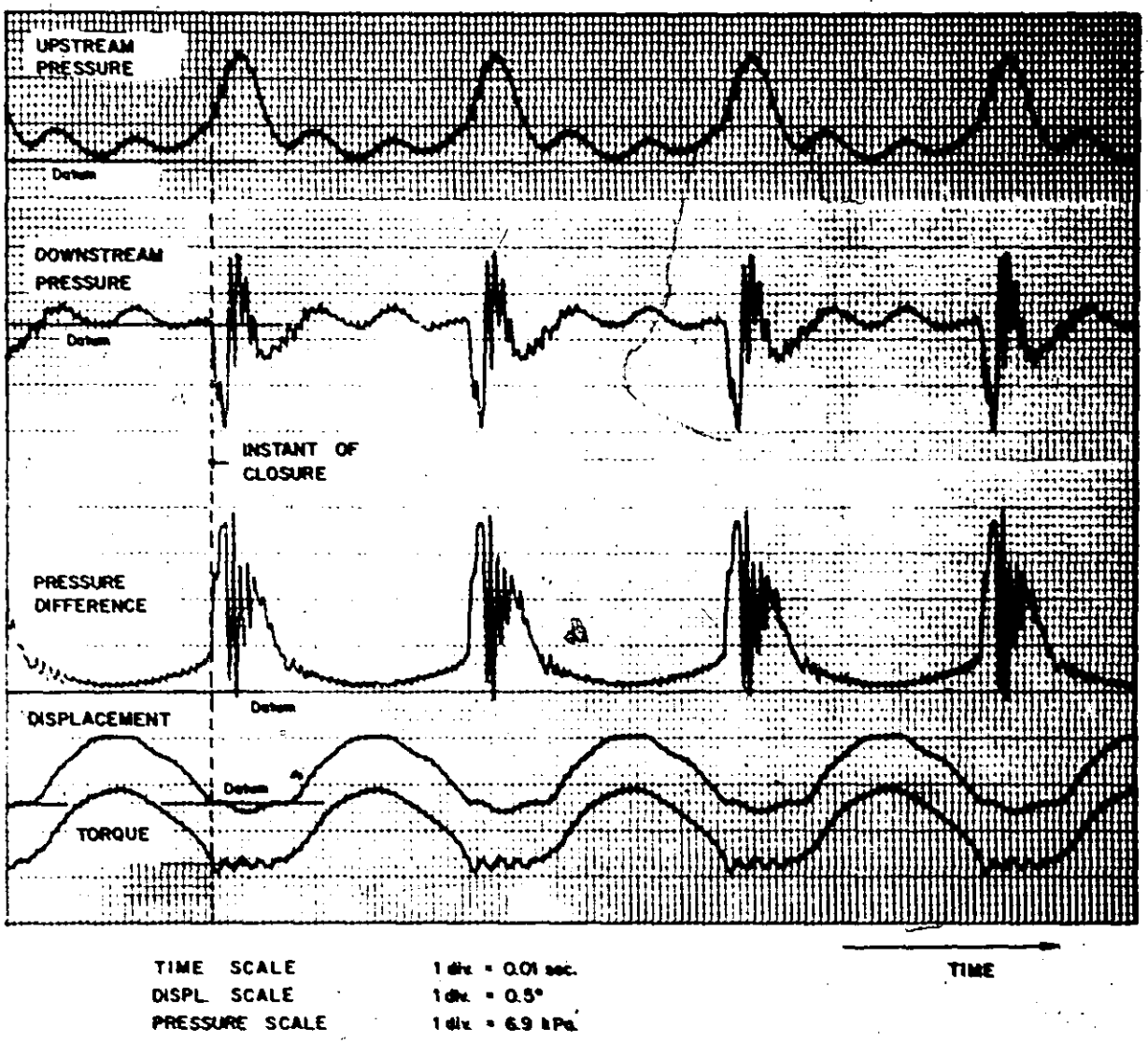

Figure 5.4. Dynamic Measurements: K_{eq} = 10.305 kN/m; θ_o = 4 1/2°.

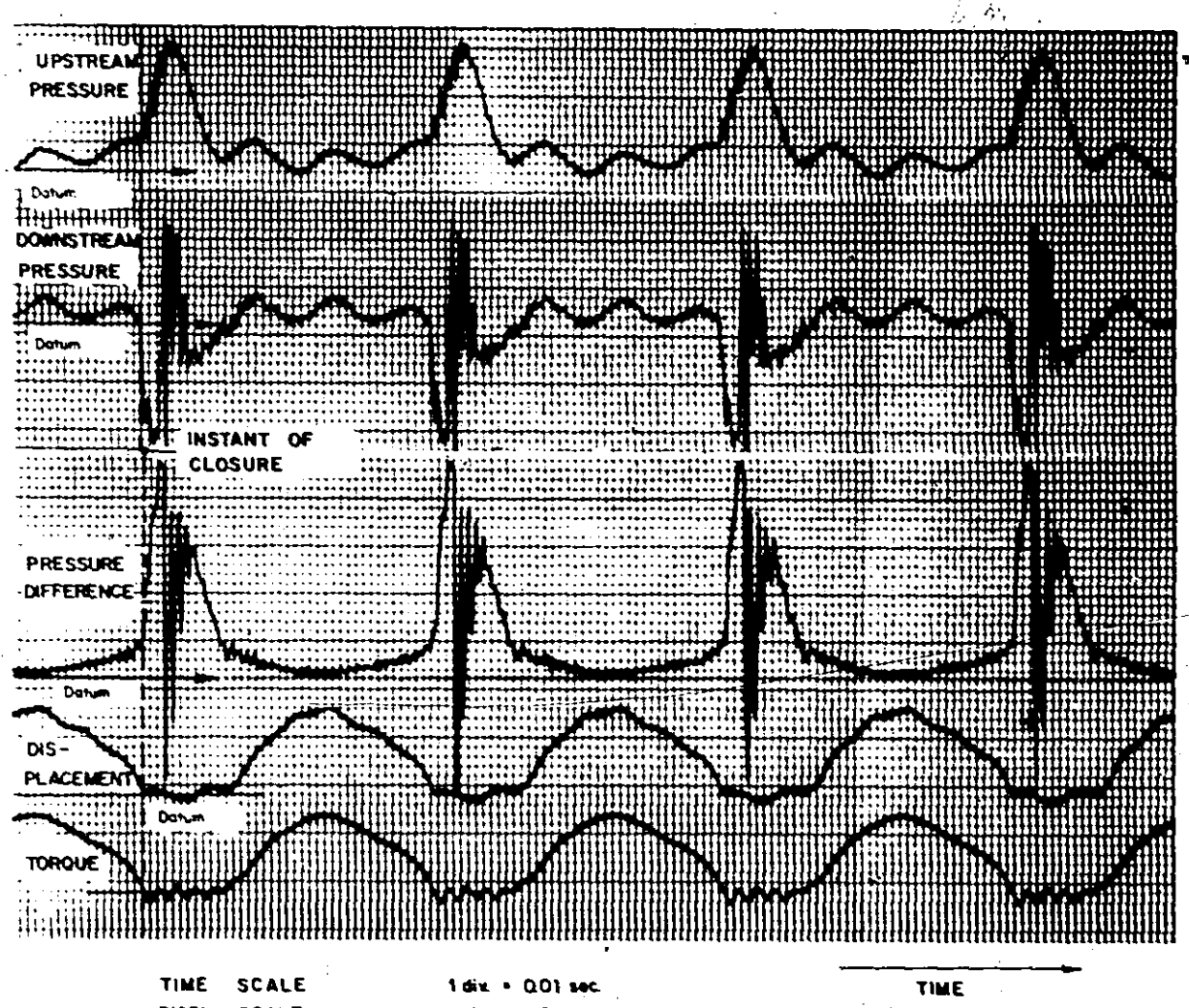

Figure 5.5. Dynamic Measurements: K_{eq} = 14.168 kN/m; $\theta_o = 4^o$.

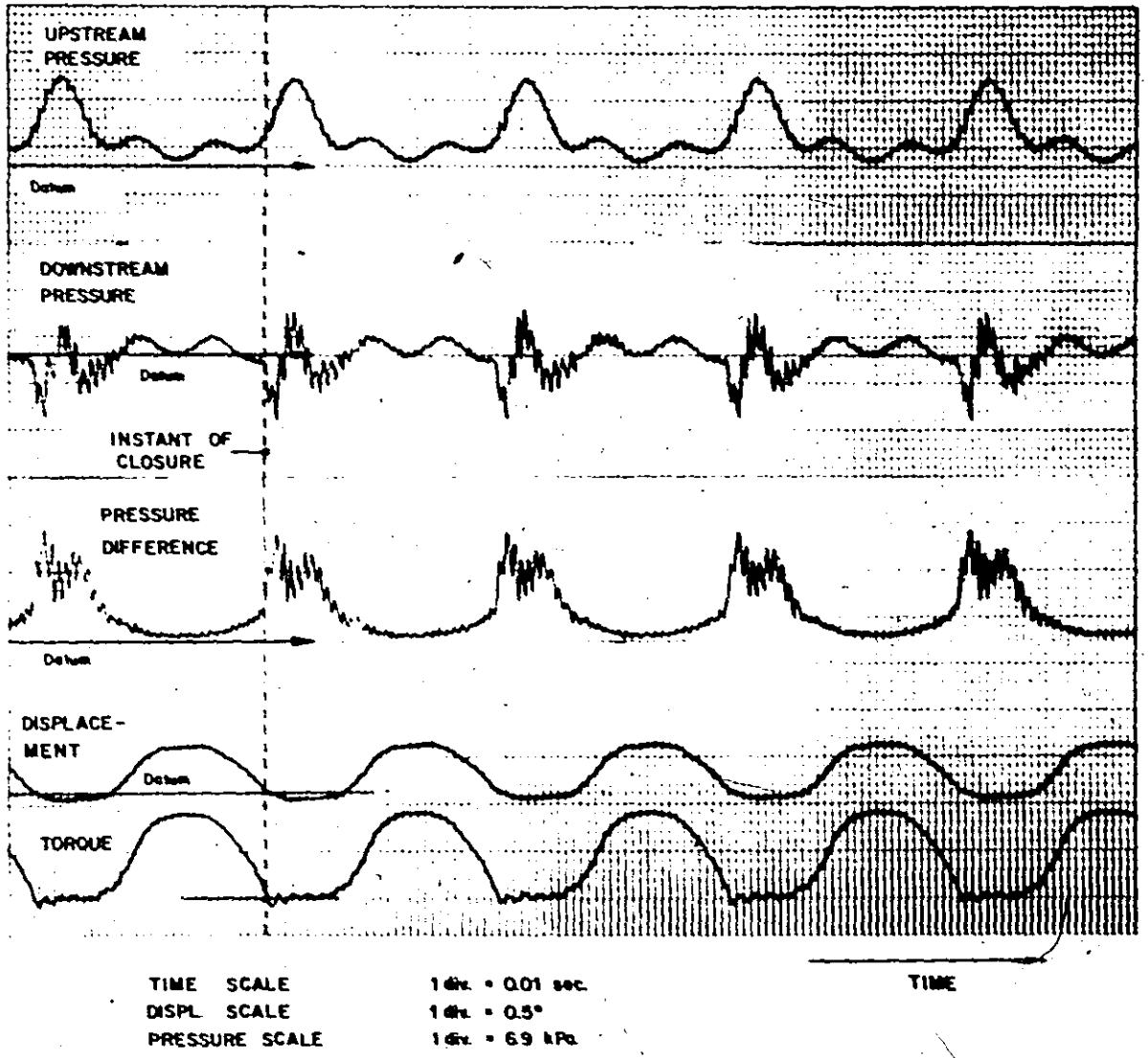

Figure 5.6. Dynamic Measurements: K_{eq} = 28.85 kN/m; $\theta_o = 3^o$.

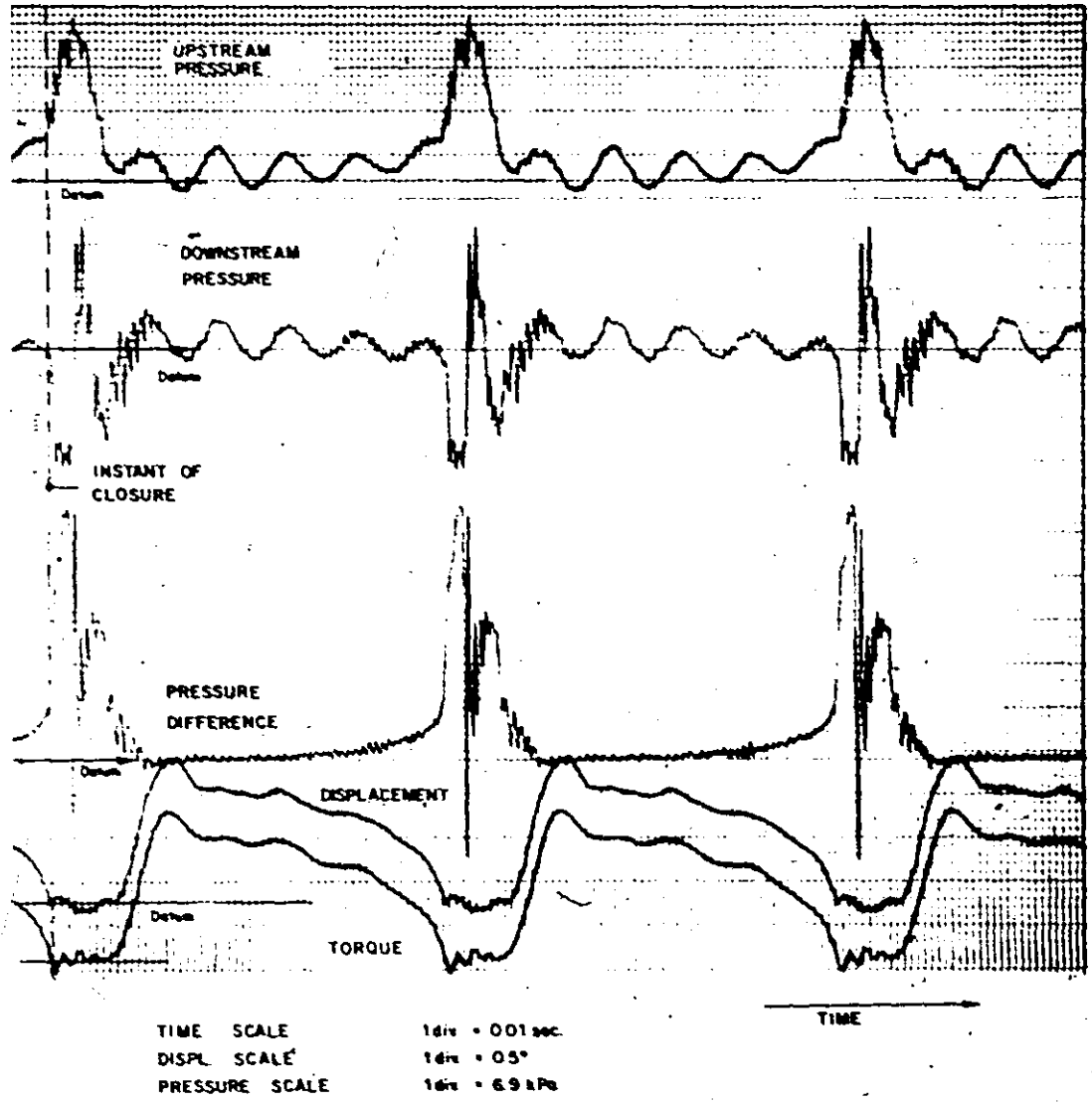

Figure 5.7. Dynamic Measurements: K_{eq} = 14.168 kN/m; θ_o = 7°.

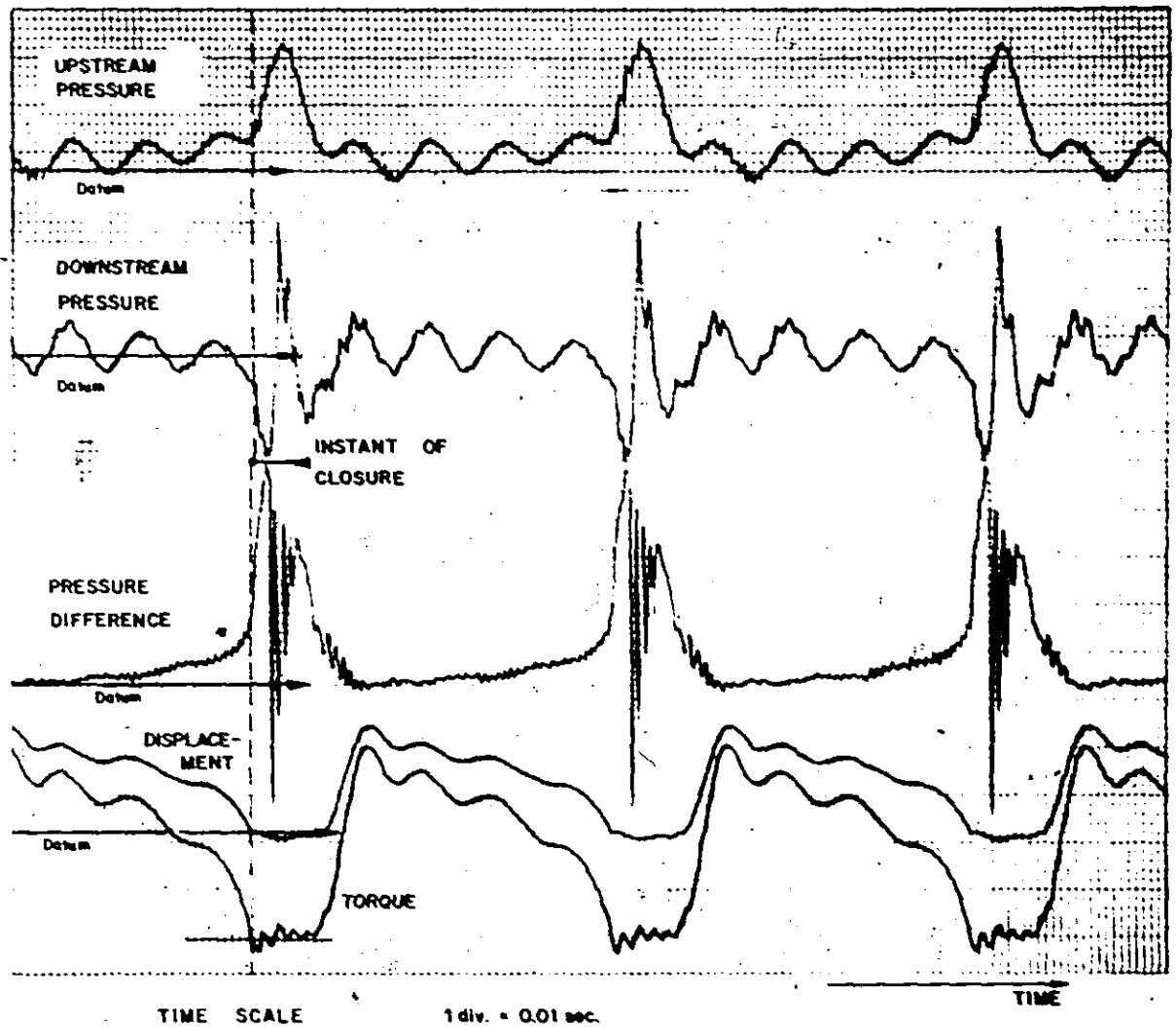

Figure 5.8. Dynamic Measurements: K_{eq} = 28.85 kN/m; θ_o = 4 1/2°.

can be seen in the upstream and downstream pressure traces. However, the valve responds only to the effective pressure difference which can be seen at this point to be relatively smooth. The valve begins to drift close under the influence of this pressure difference, which is sufficient to just overcome the spring force. As the disc nears the seat it begins to accelerate as the pressure difference begins to rise. This process is an interactive one. A small increase in the pressure difference advances the disc a small distance towards the seat. This reduces the flow area, leading to an increasing head loss and reduction in the discharge, and hence a further rise in pressure difference. This rise in pressure is evident in the upstream pressure trace where the decaying waterhammer waves are superimposed on an increasing mean upstream pressure. At the same time the mean downstream pressure is decreasing. At rather small angles the pressure difference is relatively large and the disc accelerates rapidly towards the seat.

At closure the valve impacts heavily on the seat. Instantly there is a sharp increase in upstream pressure and a sharp drop in downstream pressure as the velocity head of the fluid is converted into a pressure head. The resulting pressure waves travel independently in the pipeline while the valve remains closed - the upstream positive pressure wave travelling back to the high level reservoir to be reflected as a rarefaction wave, and the downstream pressure wave travelling to the open end of the pipeline to be reflected as

a positive pressure wave. The records of upstream and downstream pressure show that while the valve remains closed the downstream pressure wave performs approximately one complete cycle while the upstream pressure completes only one-half a cycle. This is because the length of the pipeline downstream of the valve is approximately half the upstream pipe length. Interestingly the flexibility of the transition section reduces the average waterhammer wave speed to about 500 feet per second and leaves the wave shape nearly sinusoidal.

The torque record indicates that the impact of the disc on the seat excites free vibrations of the sub-system of the torque arm, shaft, and springs about the seat as shown schematically in Fig. 5.9. Analysis shows that the natural frequency of this system is given by

$$f_n = 1/2\pi \sqrt{\frac{3(K_\theta + K_s l^2)}{m l^2}} \qquad (5.4)$$

where m is the mass of the torque arm. By substituting the relevant values into this equation the calculated values of the natural frequency may be compared with those shown on the torque records. The calculated and experimental values were found to be in close agreement at between 51 and 56.7 Hz.

The small disturbances seen on the pressure traces could be attributed to two independent factors - the influence of pipeline motion which Wood [48] (1969) showed would result in jagged pressure response, and the possibility of cavitation which Duc [49] (1965) claimed would lead to the

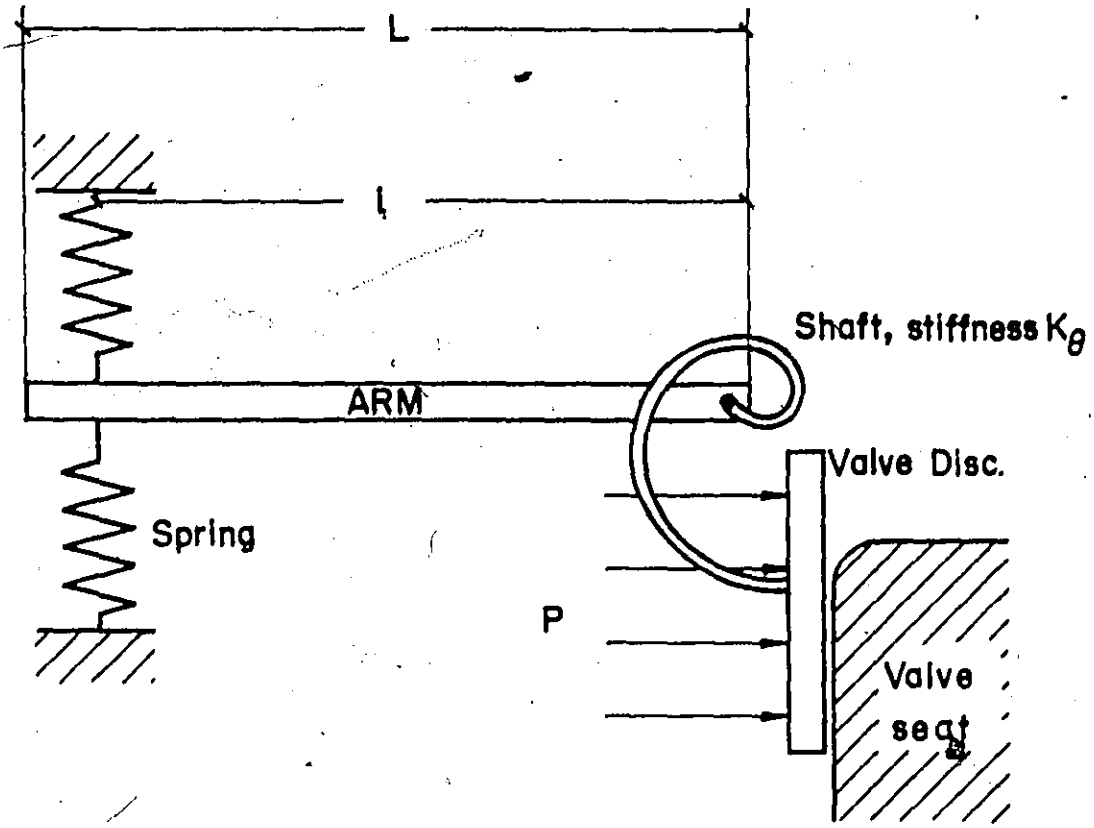

Figure 5.9. Subsystem Excited into Free Vibration while Valve Remains Closed.

same effect. Since both the downstream pressure trace and the pressure difference across the valve indicate these pressure values close to the vapour pressure of water at the prevailing temperature over a very small time interval, it is impossible to discount the possibility of cavitation. Moreover, the pipeline was freely supported and was observed to move quite substantially during the experiments which involved valve vibration. It is therefore suggested that the high frequency peaks of the pressure response may be a consequence of both of these factors.

The pressure difference records show conclusively that for those points chosen in the sub-region where the hydrostatic pressure is sufficient to overcome the spring force, (Figs. 5.4 and 5.5), the valve opens only after the pressure difference falls below the value required to close it. Hence in this sub-region the dynamic pressure wave action is solely responsible for opening the valve. Once the valve is partially open, flow is re-established, the pressure difference continues to decrease and opening continues.

For points to the right of the static system characteristic, (Figs. 5.6, 5.7 and 5.8) closure of the valve depends on the hydrodynamic pressure exceeding the maximum available hydrostatic pressure by an amount sufficient to overcome the spring force. The valve remains closed until the pressure difference drops below that necessary to overcome the spring forces. Thus in this sub-region of instability it is the combined effect of the spring force and the pressure

wave action that causes the valve to re-open. Again the valve is seen to open very quickly. Once the maximum displacement is reached, the cycle of events is repeated.

Figs. 5.10 to 5.14 give pressure difference across the valve disc plotted against angle of opening. These results, obtained from Figs. 5.4 to 5.8, indicate that the pressure difference is greater during closing than during opening for the same angle. Thus, more energy was added to the system during the closing part of the cycle than was taken out of the system during the opening part of the cycle. This hysteretic effect is an indication of the nonlinear nature of the phenomenon and the limit cycle oscillation suggests that this net energy addition per cycle is exactly balanced by the energy dissipated by the damping forces in the system. Any excess energy addition beyond that dissipated by damping would have resulted in oscillations of continuously increasing amplitude. On the other hand, if the work done by the damping forces were to exceed the net energy input per cycle, these oscillations would have been damped out.

The values of the available hydrostatic pressure, and the approximate theoretical pressure difference

$$\left(\Delta p = \frac{K_{eq}\,\theta_o}{r_o A}\right)$$

required to just overcome the spring arm restoring torque are indicated on each diagram by the broken lines. The relative position of the two lines is an indication of the part of the stability diagram which the curve represents. As

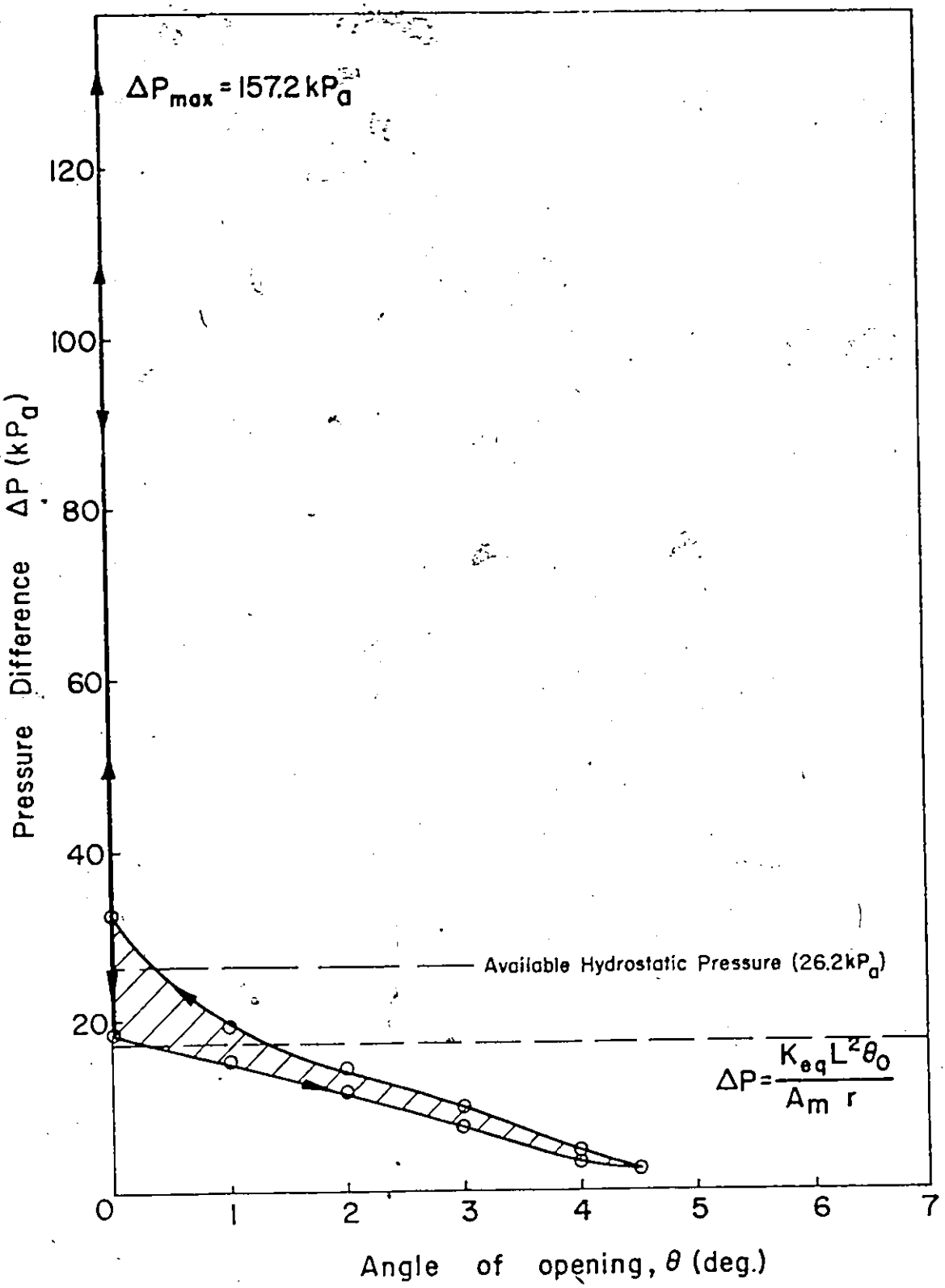

Figure 5.10. Pressure Difference vs Angle of Opening, K_{eq} = 10.305 kN/m; θ_o = 4 1/2°.

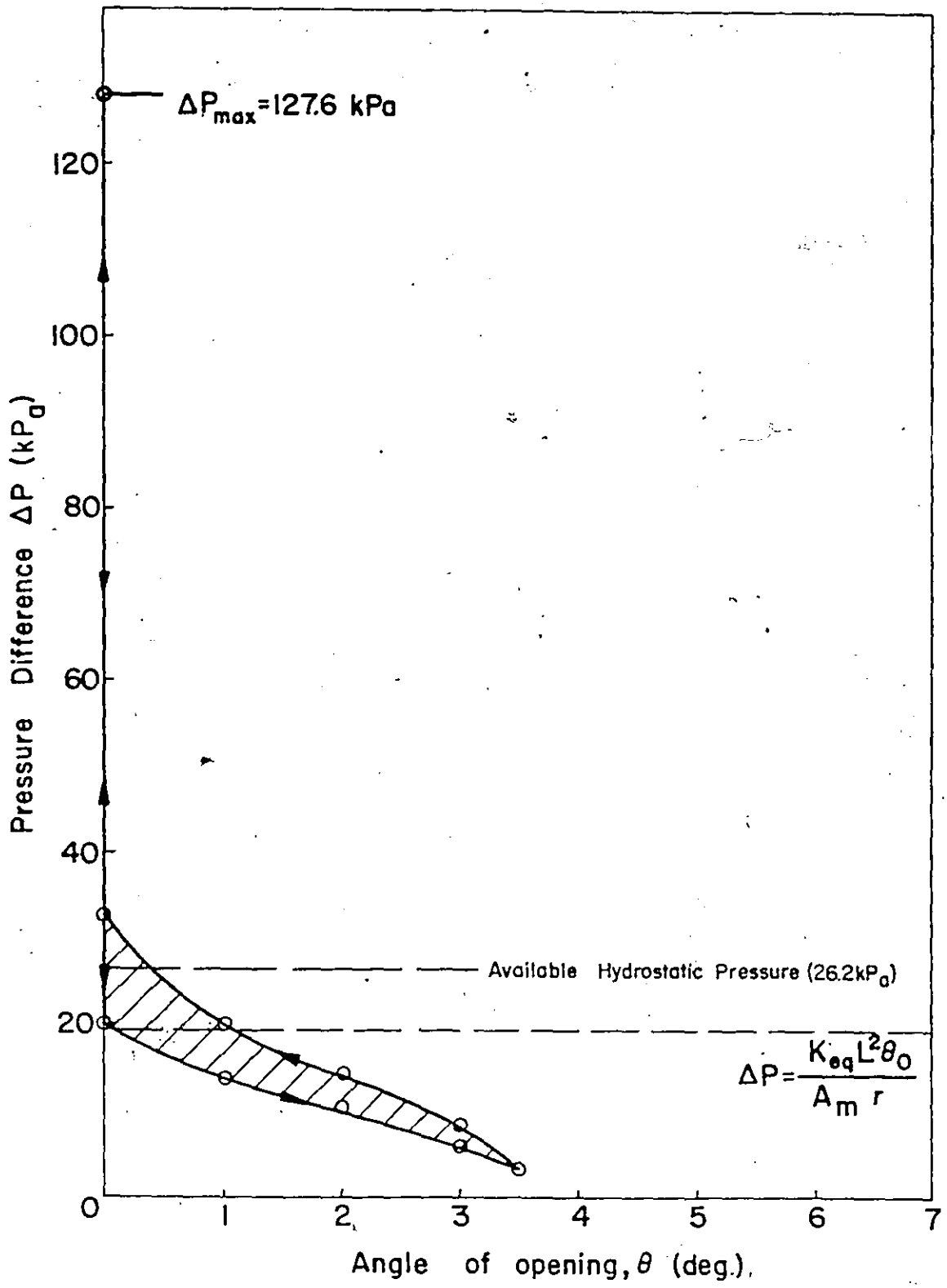

Figure 5.11. Pressure Difference vs Angle of Opening, K_{eq} = 14.168 kN/m; $\theta_o = 4^0$.

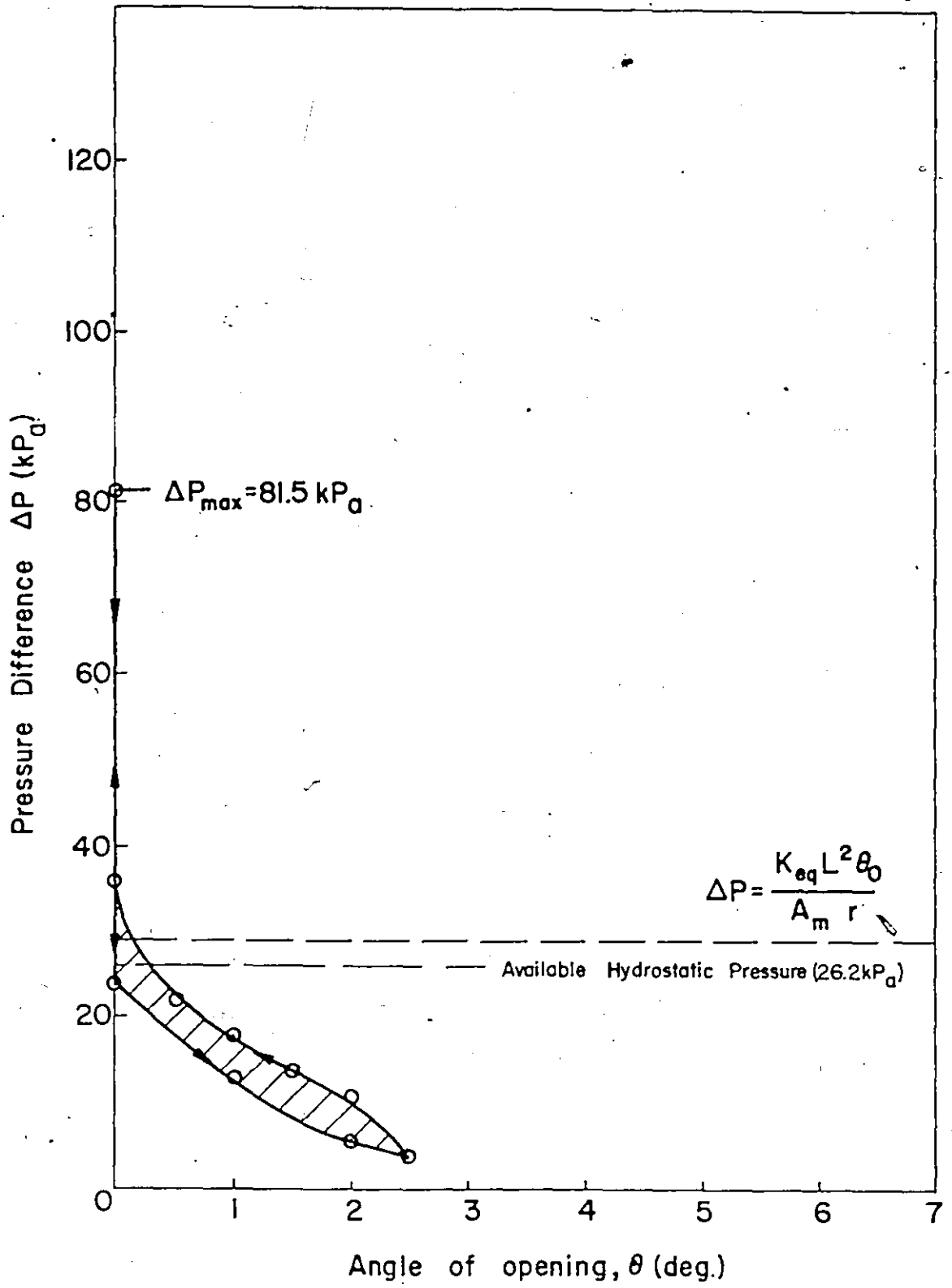

Figure 5.12. Pressure Difference vs Angle of Opening, K_{eq} = 28.85 kN/m, θ_o = 3°.

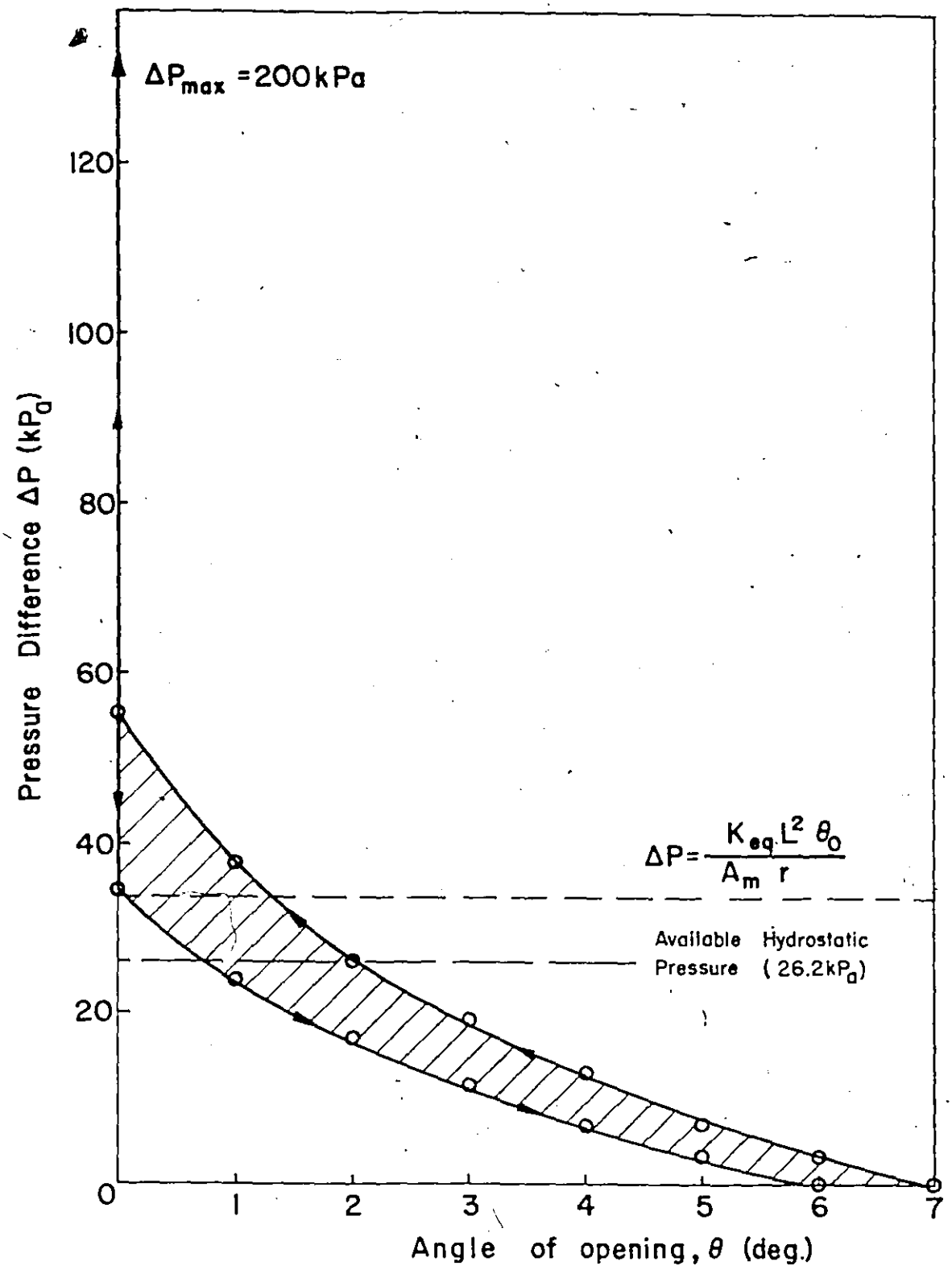

Figure 5.13. Pressure Difference vs Angle of Opening, K_{eq} = 14.168 kN/m; $\theta_o = 7^0$.

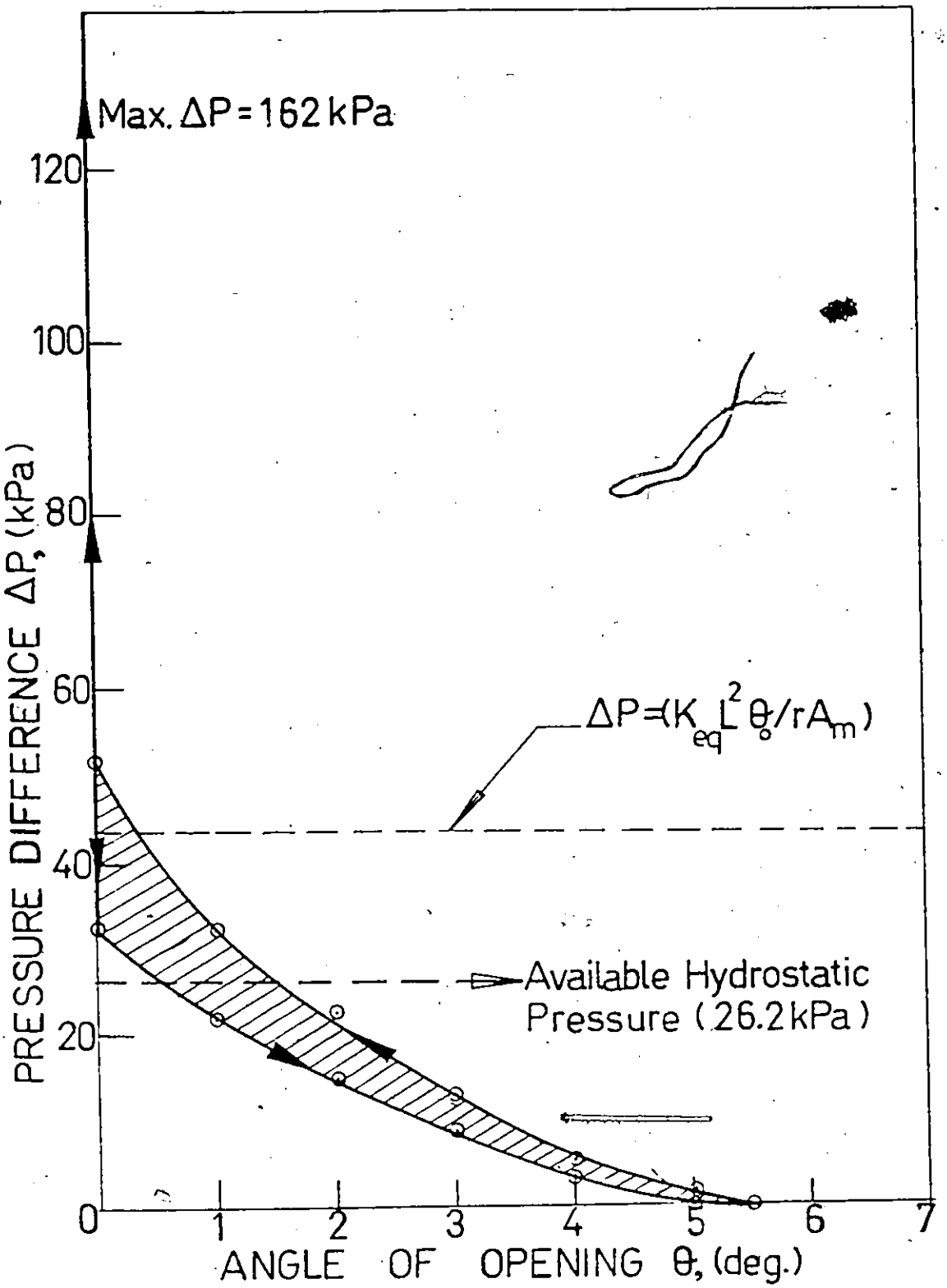

Figure 5.14. Pressure Difference vs Angle of Opening, K_{eq} = 28.85 kN/m; θ_o = 4 1/2°.

indicated in Figs. 5.10 and 5.11, the available hydrostatic pressure is higher than the theoretical static pressure difference, required to overcome the springs at closure so that the valve should close and stay closed. The two points on the stability diagram represented by these curves therefore are from the region of instability to the left of the static system characteristic. In Figs. 5.12, 5.13 and 5.14 the available hydrostatic pressure is lower than the theoretical static pressure difference required to overcome the spring at closure indicating that the valve should not close. The points on the stability diagram represented by these diagrams are from the region of instability to the right of the static system characteristic. Both of these observations are to be expected in light of the results. The pressure difference during the closing part of the cycle increases sharply as the valve approaches its seat especially for closing angles less than about 2^{o}.

The enclosed area in each diagram is proportional to the net energy input to the system per cycle of vibration. The size of each area, as well as the maximum pressure difference attained subsequent to closure, appear to be related to the maximum angle of opening, and therefore the violence of the vibration. Experimental observations show that the larger the enclosed area the more violent was the vibration.

5.7 Parametric Studies

Experiments were conducted to determine the influence of change of parameters (stiffness and initial angle of valve

setting) on the frequency and amplitude of vibration at constant upstream pressure.

These experiments were carried out as described in sections 5.4.1 and 5.4.2.

Both the frequency of oscillation and the maximum displacement of the valve were determined from the Visicorder strip chart records of these experiments. These results are summarized in Figs. 5.15, 5.16 and 5.17. In Fig. 5.15 the ratio of frequency of vibration to the fundamental frequency of the valve in quiescent water for each spring combination is plotted against the stiffness ratio, $(K_s L^2/K_\theta)$. All the curves are for full upstream hydrostatic pressure and each curve represents a different initial setting of the valve. In Fig. 5.16 the maximum displacement of the valve is plotted against the equivalent spring stiffness K_{eq} given by equation (5.2). In Fig. 5.17 the initial angle of valve opening θ_o is plotted against the maximum dynamic displacement of the valve for different stiffness ratios.

Figs. 5.15 and 5.16 show that for a constant available hydrostatic head and initial angle of opening, the amplitude of vibration of the valve increases while the frequency decreases as spring stiffness increases. This is, of course, contrary to the effect of increased stiffness on free vibrations. The apparent explanation for this phenomenon is that the increased spring force meant increased resistance to valve closure. This slows down the closing part of the cycle considerably, thus changing the form of the hydrodynamic

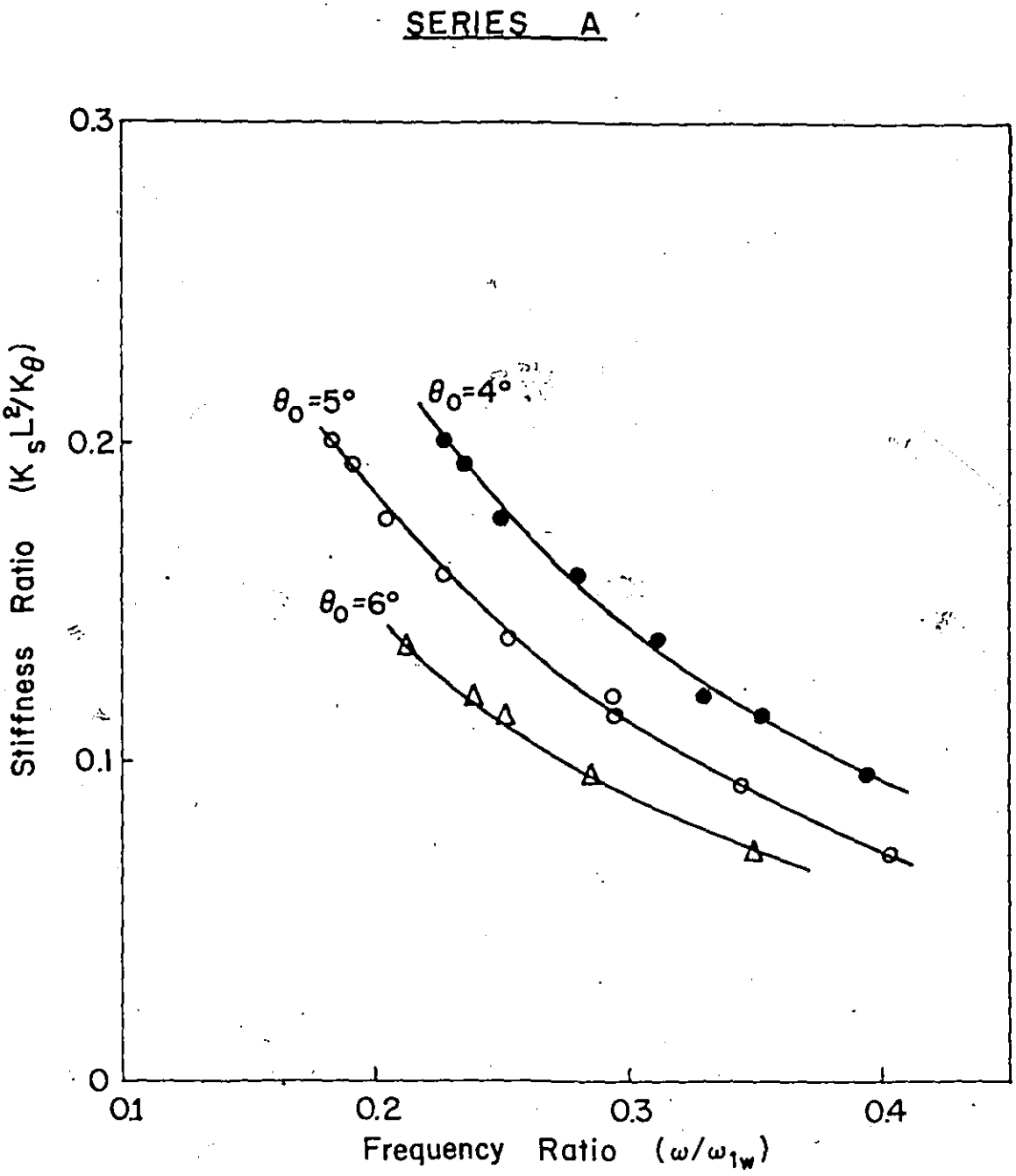

Figure 5.15. Results of Parametric Tests: Frequency Ratio vs Stiffness Ratio for Constant Applied Pressure.

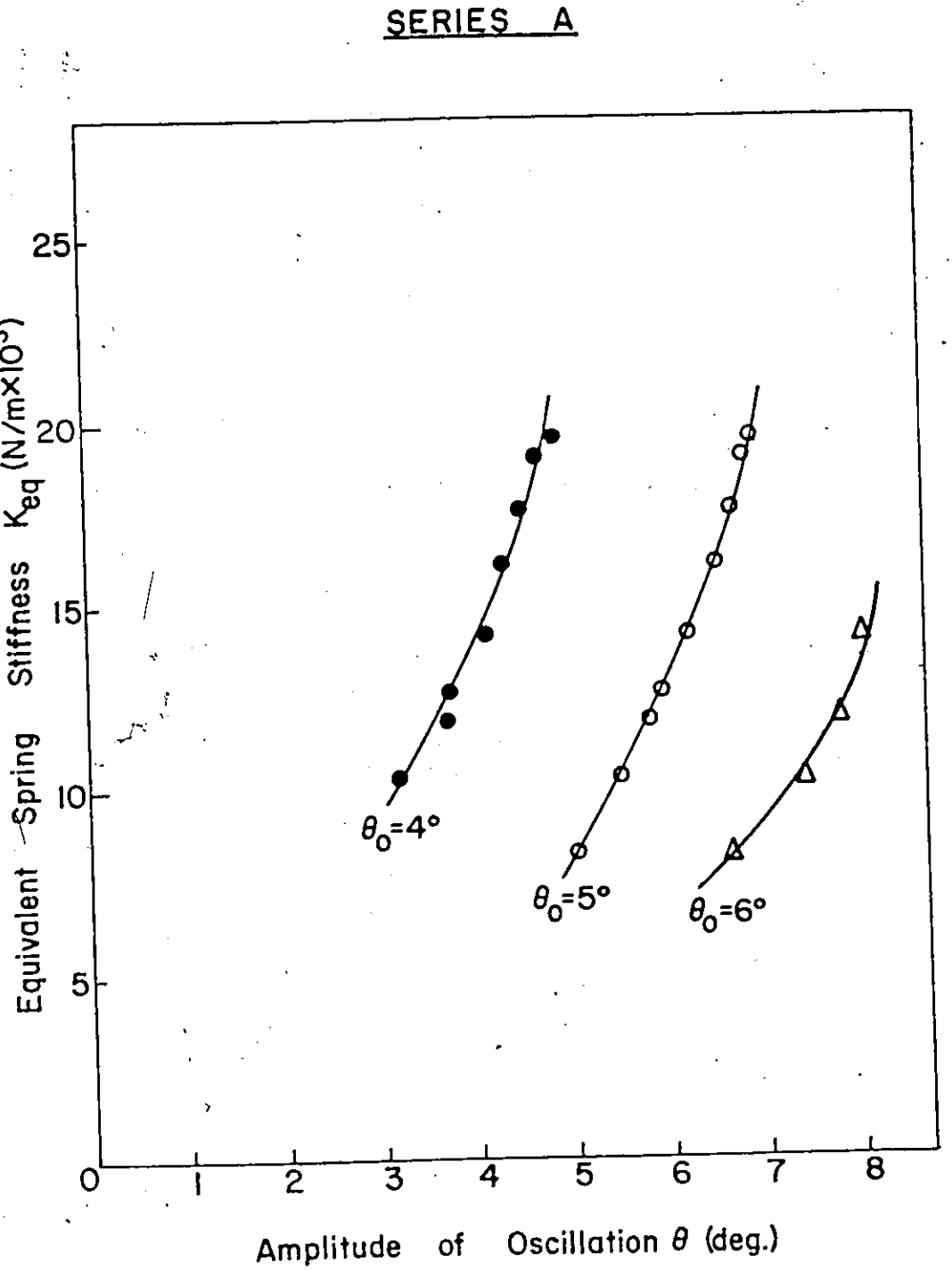

Figure 5.16. Results of Parametric Tests: Maximum Angle of Opening vs Equivalent Spring Stiffness.

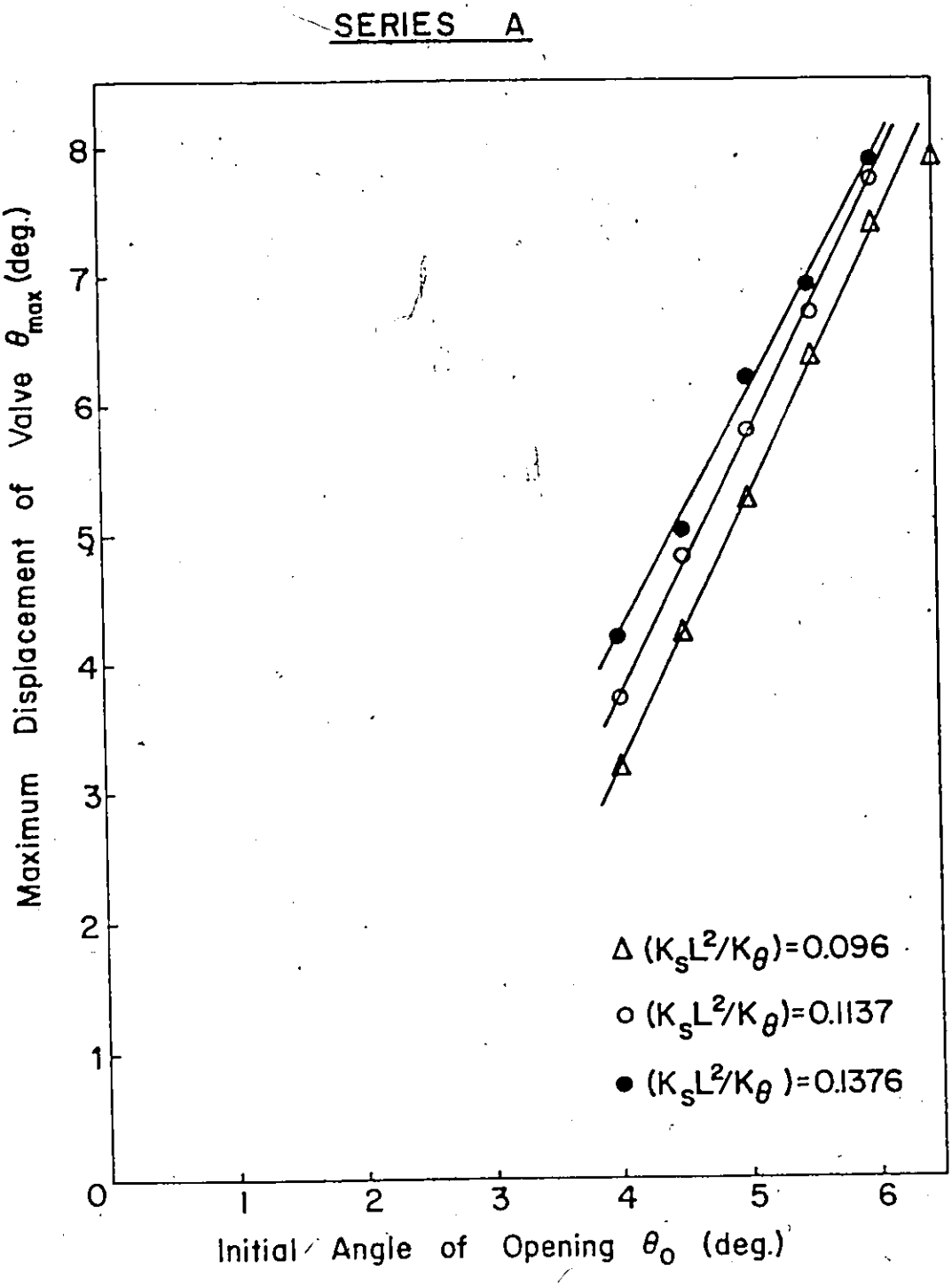

Figure 5.17. Results of Parametric Tests: Initial Angle of Setting vs Maximum Valve Displacement.

closing load which is a path-dependent, non-conservative force. The net result is a lowering of the frequency of vibration with increasing spring force. Fig. 5.17 shows that for constant hydrostatic head and valve stiffness the maximum valve displacement is linearly dependent on the initial angle, at least in the range, of all the measurements.

Thus, the effect of increasing stiffness and initial angle on frequency and amplitude of vibration are qualitatively the same. Both increase the violence of the vibration, thereby threatening the structural integrity of the model at the larger values of both parameters.

5.8 Flow Visualization Studies

5.8.1 Expectations from the Flow Visualization Programme

The main reason for the considerable emphasis in this research programme on flow visualization was the expectation that the vibration phenomenon would be accompanied by observable variations in flow pattern and fluid behaviour in the valve apron during valve vibration. Quantitative results were obtained from the flow visualization films for the vibrating valve, while only qualitative results were obtained from fluid flow through the valve open and held stationary at particular angles.

The oscillation frequency for the unsteady tests was made low, and the amplitude of oscillation large. The best photographic results were obtained for large amplitude, low frequency oscillations.

5.8.2 Photographic Method

As discussed in Chapter 3, section 3.5.4, the Bolex H16 Reflex 16mm cine-camera was used for all the cine-photography described in this thesis.

A series of multiple picture sequences on 16mm, plus-X Negative film was taken using this cine-camera, which could be operated up to a maximum of 64 frames per second.

Using either of the light sources described in section 3.5.2 at full power, enough aluminium tracer was injected into the closed-circuit experimental system to obtain a light meter reading of between 9.5 and 10 on the Bolex camera light meter. This value was arrived at on the basis of numerous experiments which gave the best photographic results for this amount of light entering the camera. Injection of aluminium tracer was stopped once this light meter reading was obtained, thus eliminating particle concentration from photographic considerations.

In order to make detailed comparisons possible between opening and closing portions of the vibration cycle, the same vibration sequence was filmed at 12, 24, 32, 48 and 64 frames per second. Closeups were also filmed to focus on some important details of the flow. These films were synchronised with the records obtained on the Visicorder oscillograph through a common trigger mechanism.

For the steady flow tests, still photography was done with an Asahi-Pentax Spotmatic 35 mm single lens reflex camera. Kodak Tri-X Ektachrome 35mm black and while film

having a speed rating in sunlight of 125 ASA was used. By injecting more aluminium tracer than was used for cine-photography, it was possible to obtain reasonably good photographs of the flow at the different angles of valve opening at shutter speeds up to 1/250 second.

5.8.3 Results and Discussion

Fig. 5.18 shows a full view of the valve during a vibration cycle taken with the still camera using a wide angle lens. This picture shows the flow both upstream and downstream of the valve and also shows the valve in the last stages of its acceleration towards the seat. It shows that the flow entering the valve from the transition section is reasonably two-dimensional. This is true whenever the streamlines of flow do not cross one another and it is evident from the picture that the streamlines are reasonably parallel as the flow enters the valve. The flow downstream of the valve is seen to be quite turbulent.

Steady flow through the valve at different angles is featured in the next sequence of photographs up to around 8^{o}, Figs. 5.18(b). An attempt was made in these photographs to eliminate the three-dimensional view seen in Fig. 5.18(a). This resulted in loss of part of the field of view. The increase in fluid velocity in the valve apron as the angle increased is evident from these photographs taken at the same shutter speed. Again the turbulent nature of the flow in the valve wake is obvious.

Figure 5.18(a) Flow Visualization of Full View of Valve During Vibration.

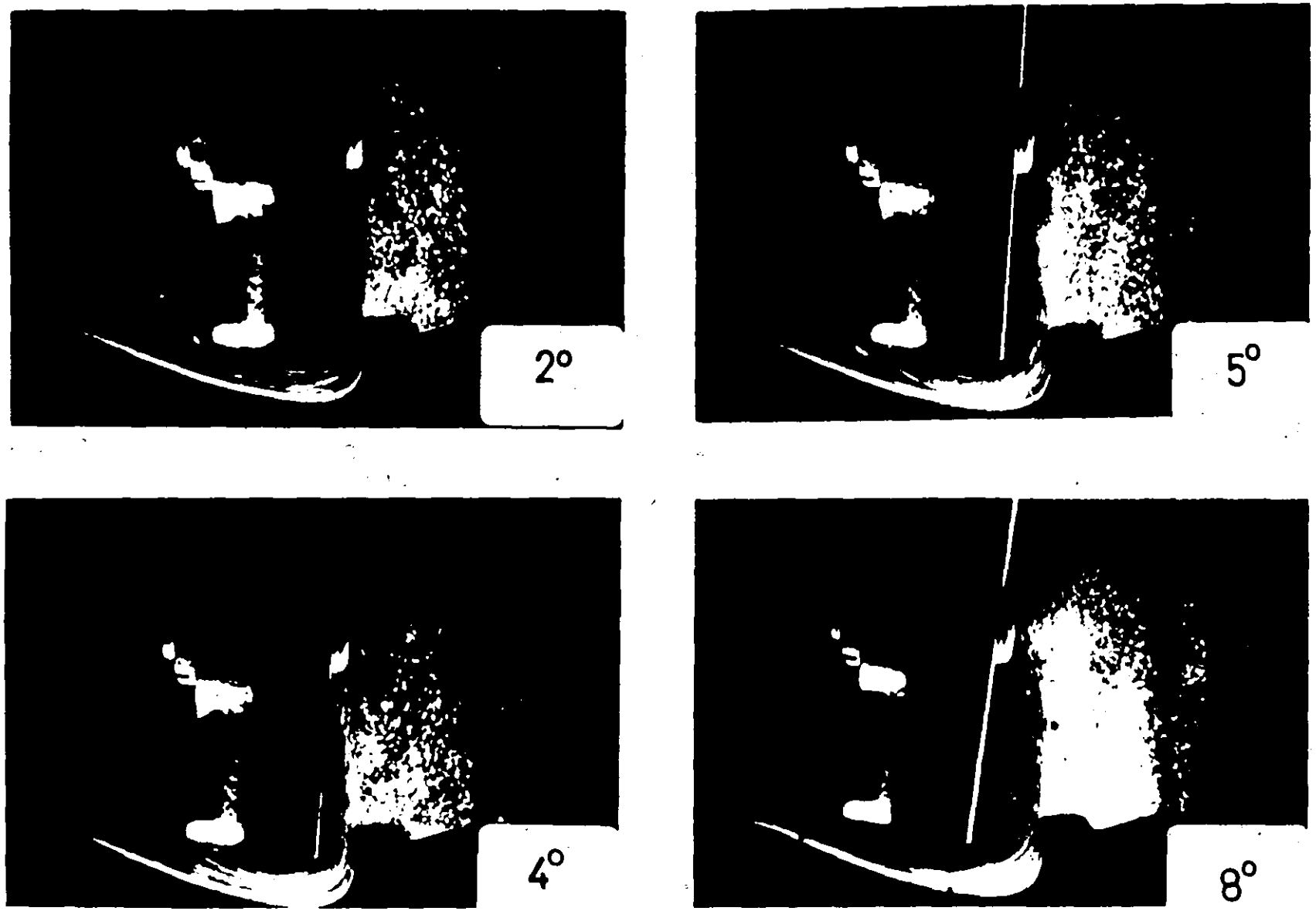

Figure 5.18(b). Flow through Static Valves at Various Angles.

A study of these and other similar photographs led to the conclusion that all the significant fluid-dynamic events are taking place in the area close to the valve seat - in the apron just upstream of the seat and in the slot. Any possibility of the presence of a significant vortex trail in the wake capable of dominating the valve's behaviour was discarded on the basis of the photographic evidence. Hence all the photography of the unsteady flow during valve vibration was concentrated around this area.

Fig. 5.19 shows a sequence of photographs depicting one full cycle of valve vibration. The approximate exposure time interval of each of these frames is marked on the synchronized record shown in Fig. 5.20. These prints are from a segment of film shot at 12fps (1/33 sec. shutter speed).

As the pressure difference across the valve begins to increase the valve starts to accelerate. Simultaneously, the flow velocity through the valve increases, as is shown by the longer streaks in pictures 2, 3, and 4 of Fig. 5.19. Between pictures 2 and 3 the valve, which has been closing steadily up to this point is actually stopped and driven back slightly open (generally less than one degree). This is shown clearly in the displacement record of Fig. 5.20. This event always coincides with a vortex rolling up and separating from the valve seat at around this closing angle.

When flow separates from a boundary, the separation streamline coincides with a free shear layer across which a steep velocity gradient exists and along which there is a flow of vorticity. Such a shear layer is seen in, for example,

picture 1 of Fig. 5.19 and in all the pictures of Figs. 5.21 and 5.22, as a result of flow separation from the downstream edge of the valve disc. As the valve closes, the motion of the disc generates a disturbance of this free shear layer. The vorticity of the free shear layer becomes concentrated in the growing disturbance as shown in picture 3 of Fig. 5.21 and pictures 11 to 16 of Fig. 5.22 and leads to the formation of the vortex shown in these pictures. This vortex grows in size as it entrains fluid from the valve wake.

As the relatively large vortex leaves the seat (pictures 14 and 15, Fig. 5.22), the downstream pressure momentarily increases, thereby arresting the closing motion. The closing motion resumes as the vortex is swept into the wake flow.

As flow area decreases, the fluid velocity increases and this can be seen from pictures 3, 4 and 5 of Fig. 5.19. Between pictures 4 and 5 there is a radical increase in pressure difference across the valve, Fig. 5.20. This causes the valve to begin its sudden acceleration towards the seat. This acceleration is clearly evident in picture 5 of Fig. 5.19 which shows the disc blurred and the fluid moving at a relatively high velocity. As the disc slams on the seat, this fluid velocity is reduced suddenly to zero. The main effect observed on the films is the appearance of "tad-pole" like streaks, which are shown in the pictures of Fig. 5.23. The occurrence of very high waterhammer pressure waves and their reflections results in the high pressure difference seen in Fig. 5.20, keeping the valve closed against the seat. The

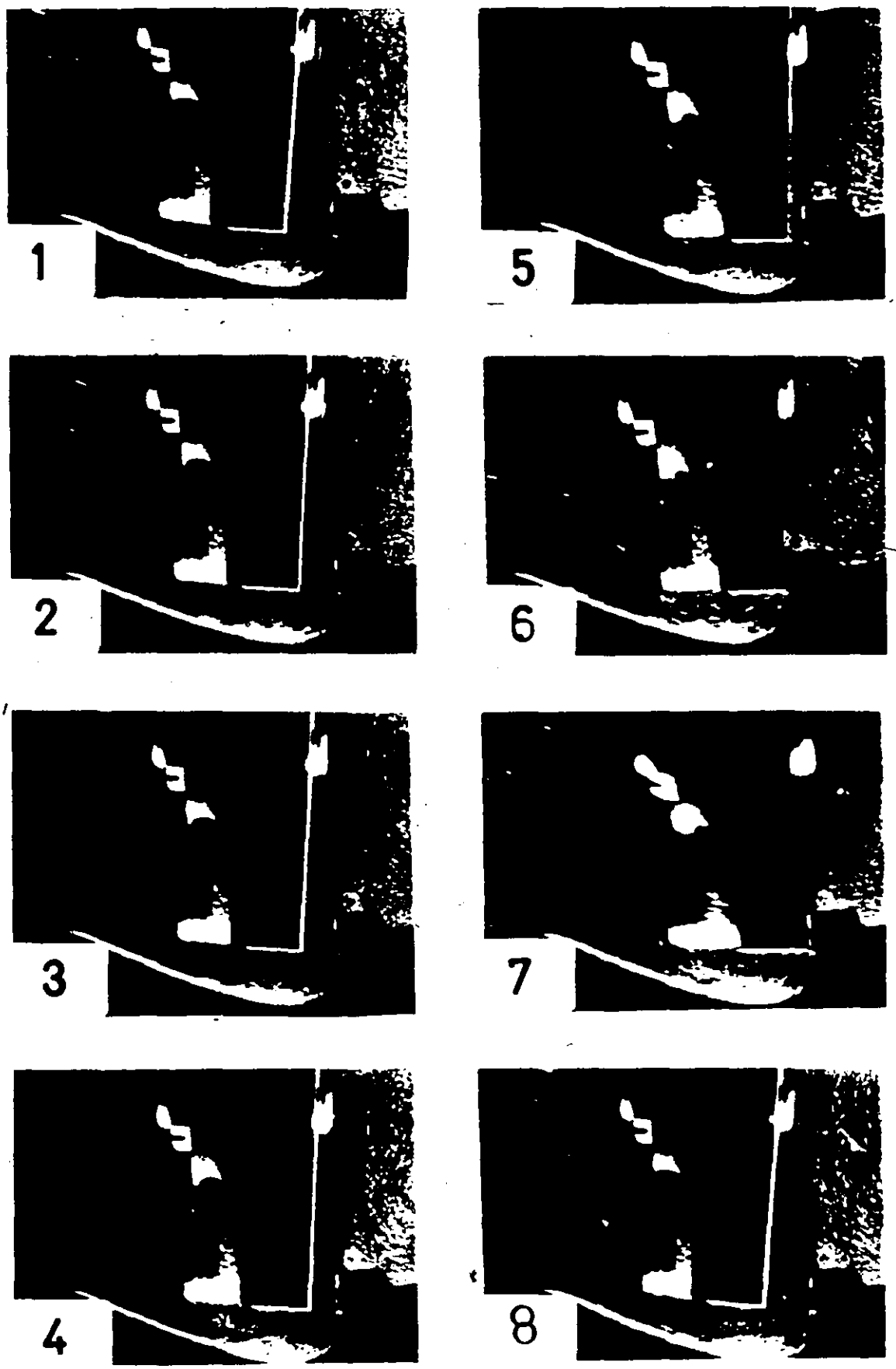

Figure 5.19. Flow Pattern Variation over One Cycle of Valve Vibration: Framing Rate = 12 fps; K_{eq} = 14.168 kN/m; θ_0 = 6°.

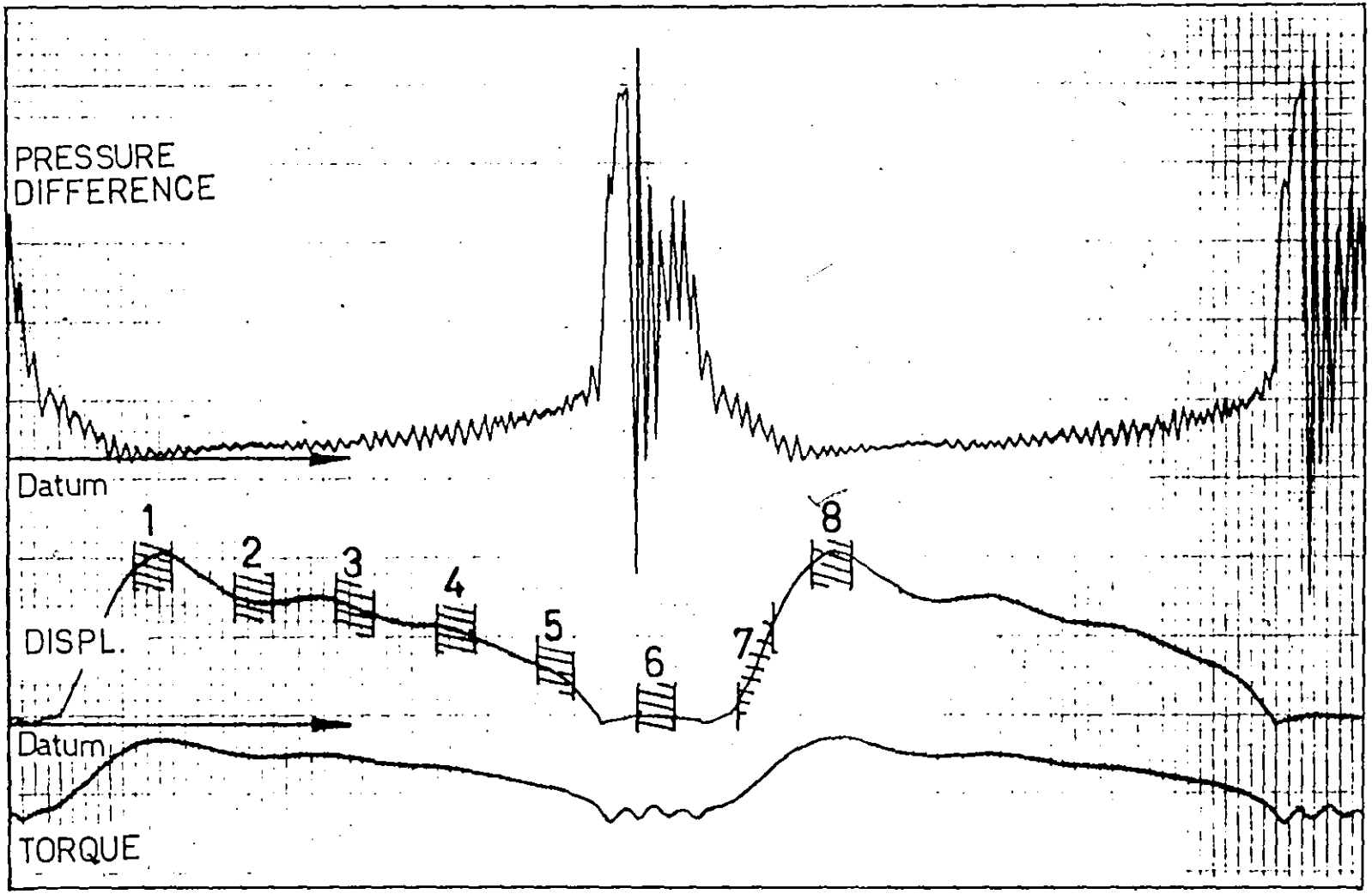

Figure 5.20. Synchronised Dynamic Measurement of Vibration Recorded in Figure 5.19.

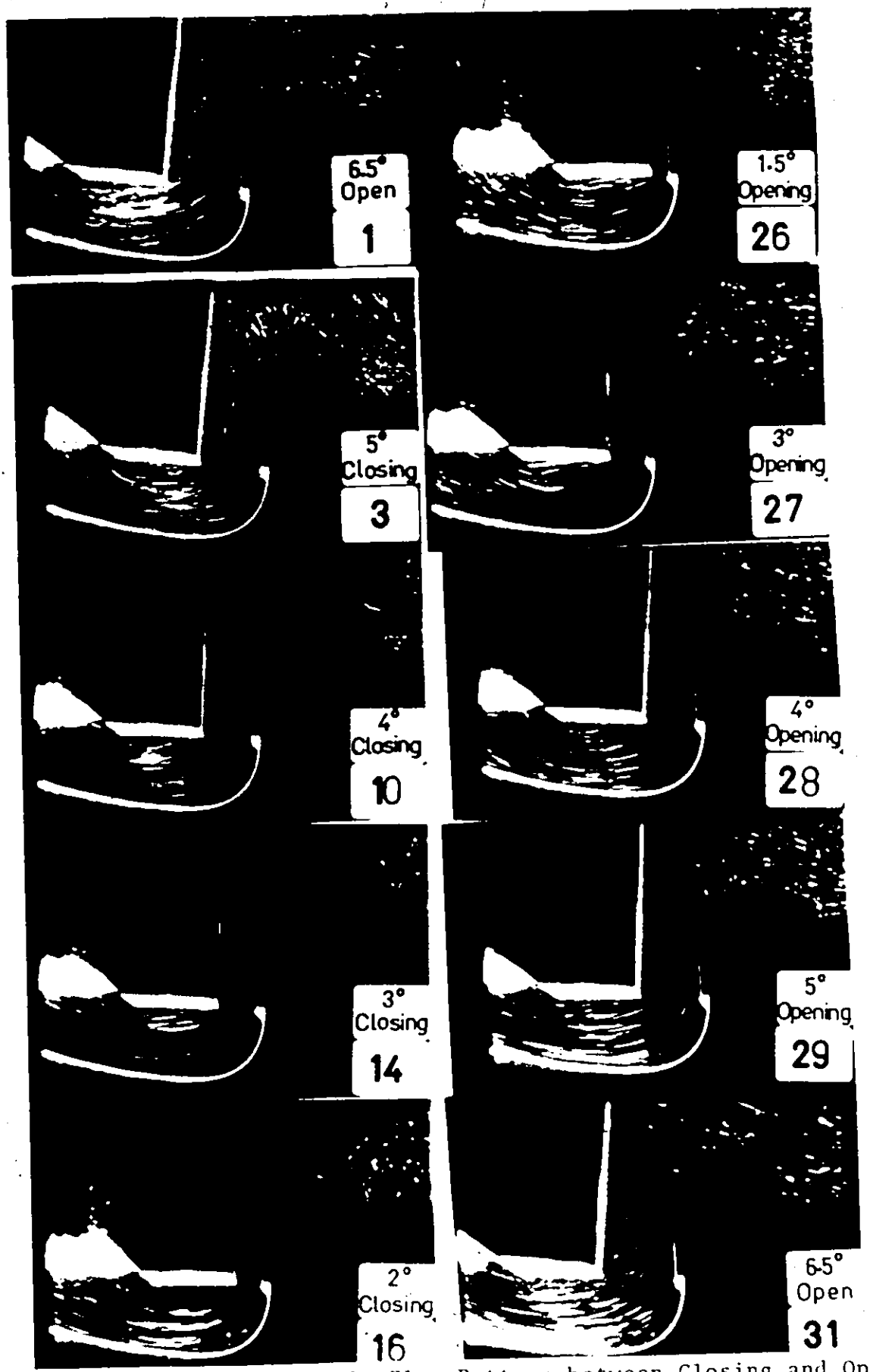

Figure 5.21. Differences in Flow Pattern between Closing and Opening Parts of the Vibration Cycle: Framing Rate = 64 fps; K_{eq} = 11.956 kN/m; θ_o = 5.5°.

total time during which the valve remains closed depends on the length of the pipeline and the waterhammer wave celerity. As the pressure difference falls very sharply below the value necessary to overcome spring resistance, the valve opens rapidly. This is clearly shown in picture 7 of Fig. 5.19 where the disc is moving so quickly it is once again blurred. Flow velocity at this angle of opening is definitely much less than at the corresponding closing angle as can be seen from the photographs. The rapid opening of the valve continues until maximum valve displacement is attained under the influence of the decreasing pressure difference and the restoring action of the spring. Picture 8 of Fig. 5.19 shows the valve at its maximum angle of opening. This picture also shows the flow impinging on the downstream face of the disc, an occurrence which is not evident in any of the photographs in the closing part of the vibration cycle. The synchronised record shows that the pressure difference is now once again a minimum, signalling the beginning of a new cycle and explaining the similarity between picture 1 and picture 8.

5.8.4 Special Effects

(i) Vortex Action

The action of the vortex discussed in the last section is shown more clearly with the photographs of Figs. 5.22. These pictures show a closeup view of the disc and the seat and were shot at 64 frames per second (exposure time 1/180 sec.). Pictures 11 to 17 of Fig. 5.22 show quite clearly

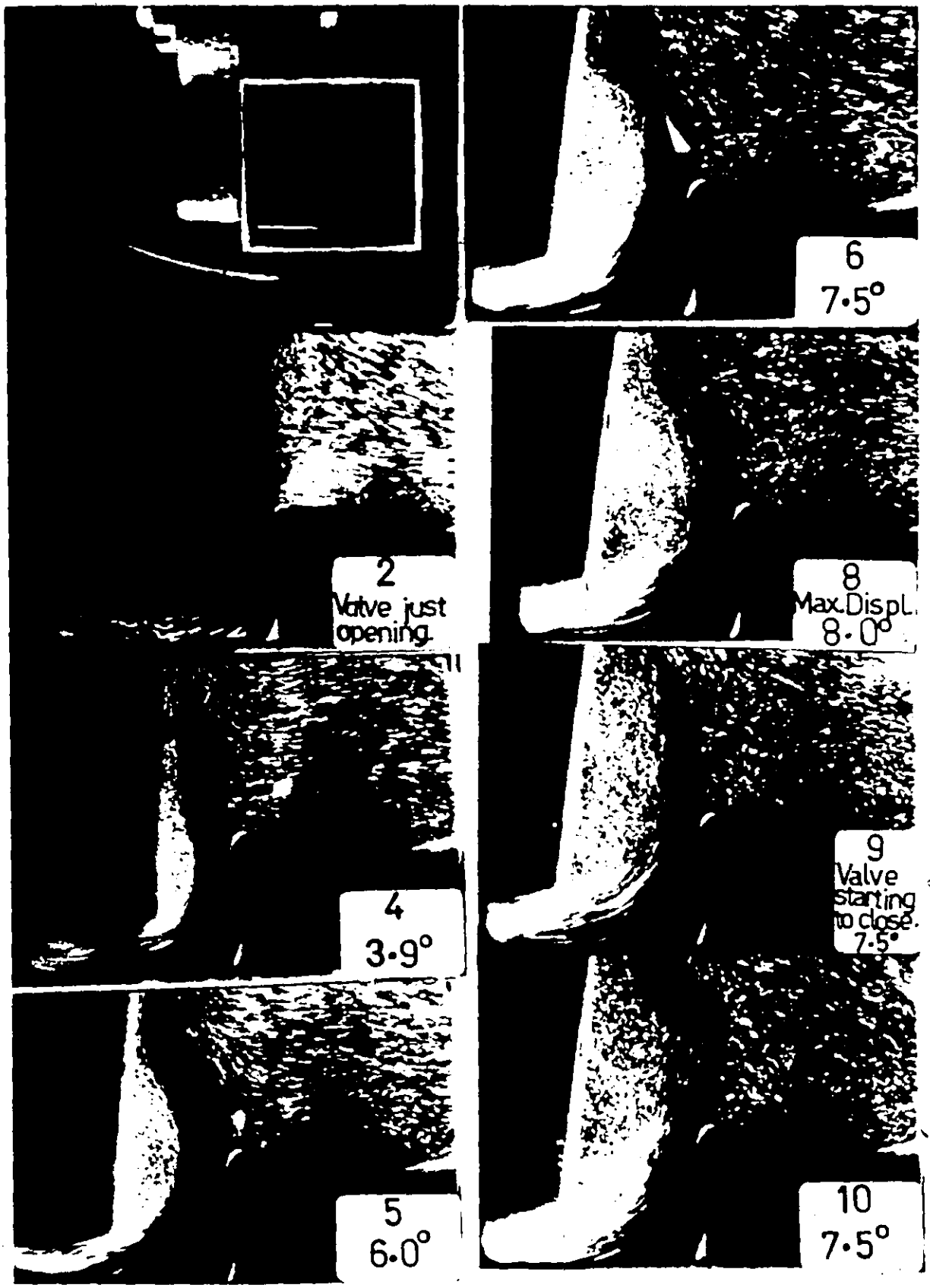

Figure 5.22. Special Effects: Vortex Action: Framing Rate = 64 fps, K_{eq} = 14.168 kN/m; $\theta_o = 6^o$.

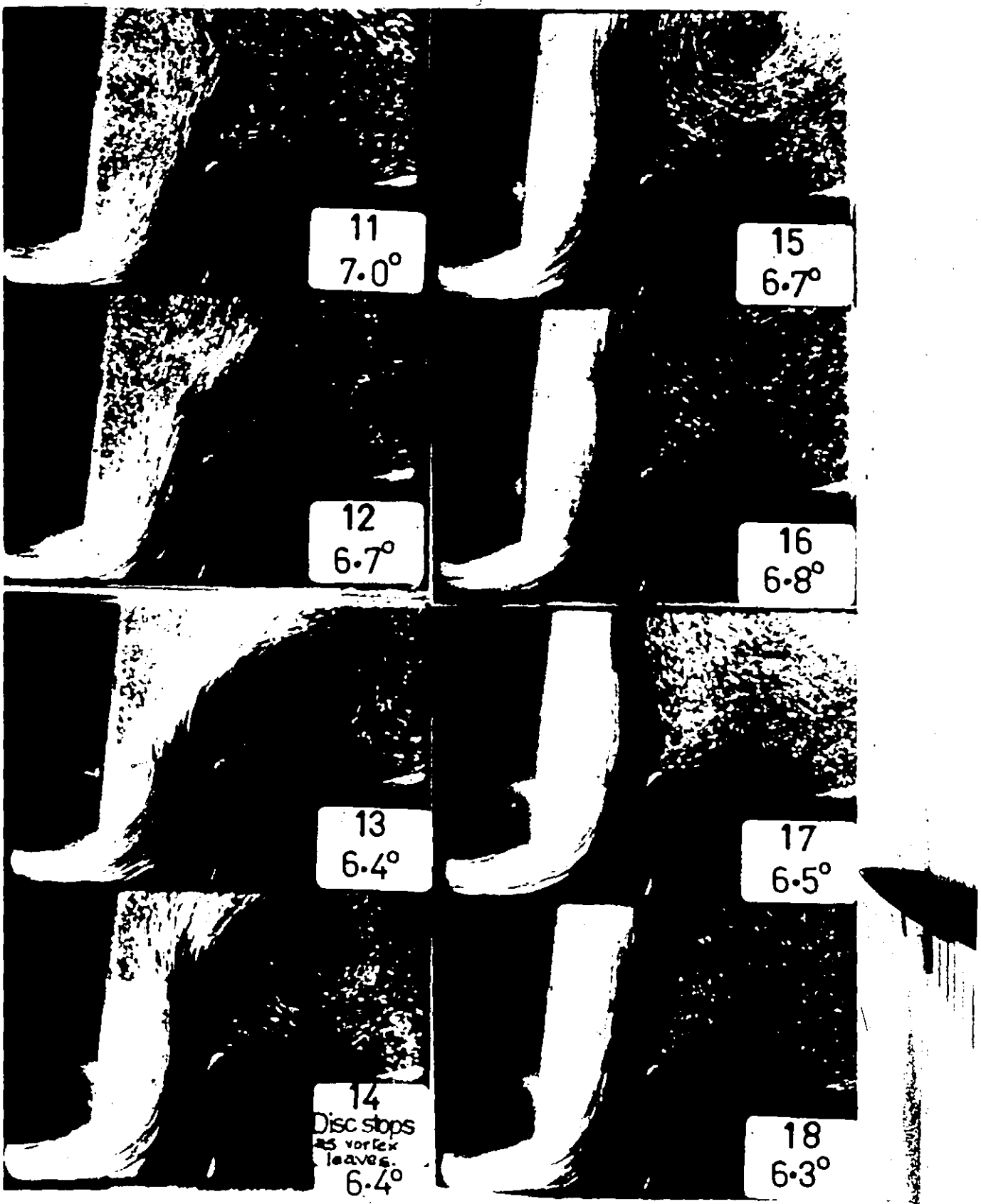

Figure 5.22. Continued.

that the motion of the disc is arrested as the vortex rolls up and leaves, (Fig. 5.22, picture 16).

(ii) Appearance of "Tadpoles"

Pictures 1 and 2 of Fig. 5.23 show the effect produced when the fluid motion is suddenly stopped by the valve closure. The effect on fluid motion of the rapid opening of the valve is shown in picture 3. Both rapid deceleration and acceleration produce "tadpole"-like streaks, the body end resulting from the longer photographic exposure of the stationary aluminium particle. Of course, the tail of these "tadpoles" are produced when the fluid is moving. Hence, the tails point upstream when the valve shuts, and point downstream when the valve suddenly opens.

In summary the following general comments are offered on the difficulties of the flow-visualization for this problem.

(a) At lower framing rates (between 12 and 24 frames/sec) the flow in the valve apron appears as well-defined long streaks making reasonably precise flow-velocity measurements possible. However, the flow in the slot is not so well-defined because the high flow velocity does not allow sufficient time for film exposure of the particles. Also, the high velocity of the valve disc near closure and opening results in its blurred appearance.

(b) At higher framing rates (between 32 and 64 frames/sec), the flow in the apron appears as shorter streaks because of the smaller exposure time. Velocity measurements at these framing rates are therefore more susceptible to error. However, a much

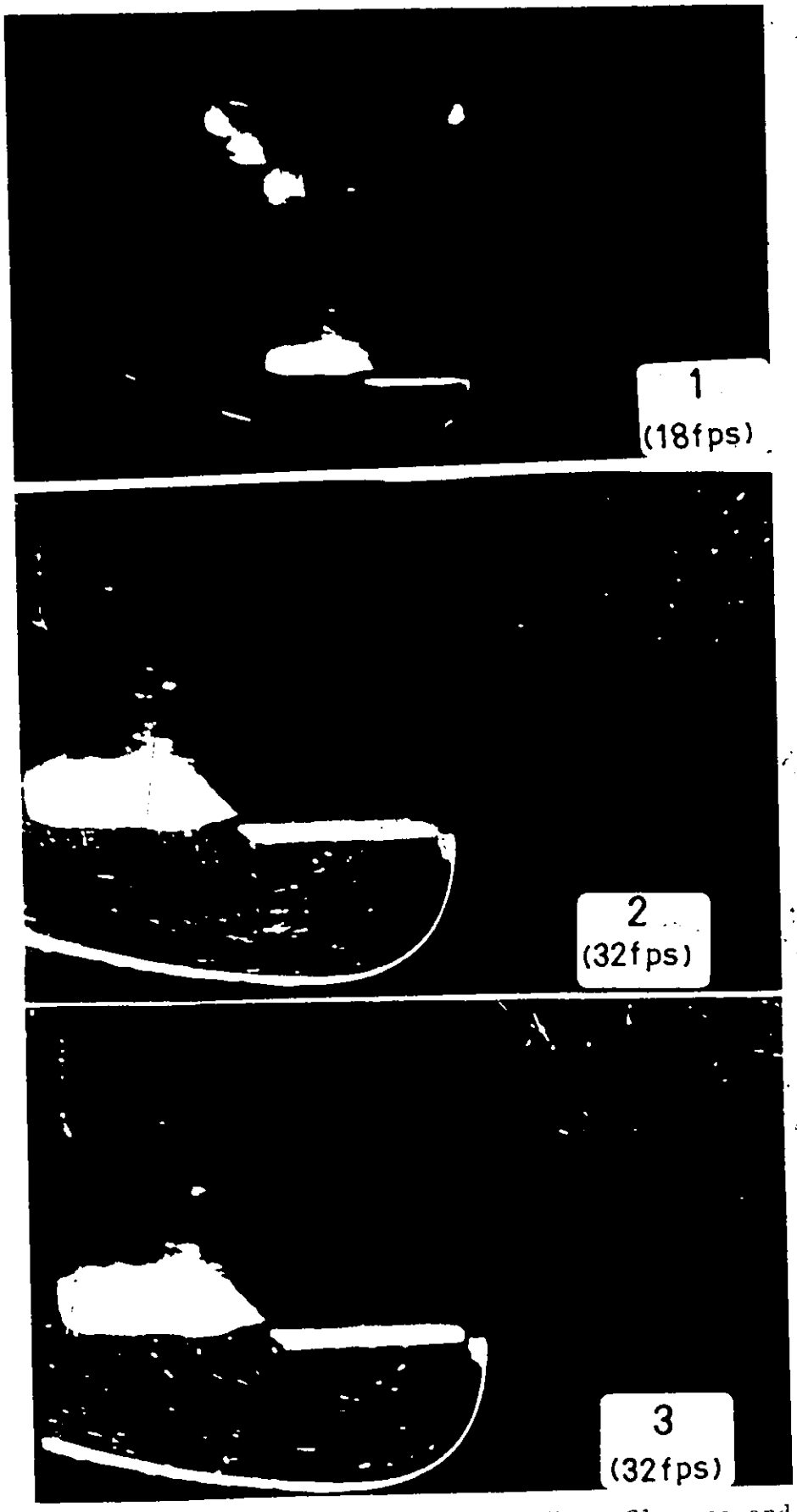

Figure 5.23. Special Effects: "Tadpoles" at Closure and at Opening of Valve.

clearer definition of the flow in the slot is obtained, expecially of the separation region on the downstream face of the disc. The disc still appears blurred at small angles of opening and closure, but much less so.

(c) Flow details like the vortex rolling off the seat during the initial stages of closure are not clearly seen at lower framing rates because the time interval between pictures is relatively large.

(d) The relatively large size of the valve restricts the field of view, especially if a strictly two-dimensional picture is desired.

(e) The motion picture sequence shows pipeline movement after each valve closure but this effect cannot be illustrated with still photographs.

(f) Finally, the events described by the flow-visualization illustrate the great difficulties involved in any attempt at modelling the hydrodynamic forces mathematically.

5.9 Fluid Behaviour During Vibration

An attempt was made to obtain quantitative fluid velocity measurements from the films. The average velocities were measured across the same section of the flow in the valve apron for the different angles of valve opening during one cycle of vibration. The results plotted in Fig. 5.24 are for one such section at approximately $\theta_o = 20^o$. These measurements were made by dividing the actual length of the streaks by the shutter speed applicable at the framing rate.

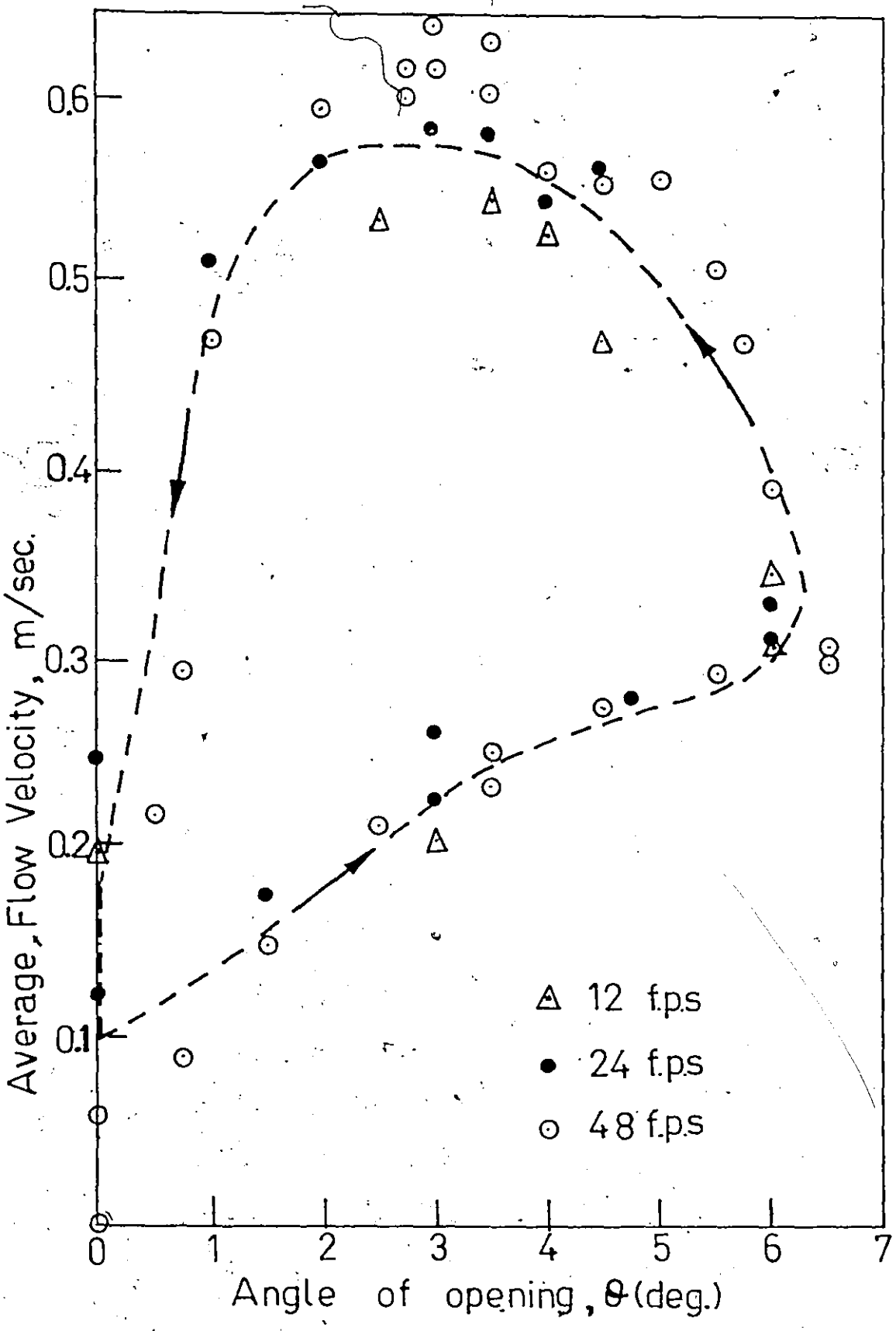

Figure 5.24: Velocity Measurements Across a Section of the Valve Apron During a Typical Cycle of Vibration.

An average for a number of such measurements was taken across the section on each frame and the valve angular displacement represented on the frame was also determined.

In Fig. 5.24, the same vibration sequence was filmed at 12, 24 and 48 frames per second, and the measurements were made across the same section in the valve apron. The results indicate quite clearly that at the same valve angular displacement, fluid velocities are much greater during closing than during the opening part of the cycle. A visual examination of the pictures shown in Fig. 5.19 confirms this. In the closing part of the cycle the flow velocity increases to some maximum value around 3^{o} valve angular displacement and thereafter drops rapidly towards zero as the disc accelerates towards its seat.

Because the flow is unsteady, a change in the total pressure drop across the valve is needed to accelerate and decelerate the fluid within the system. The conjugate pair of variables, P, Q, used to describe such unsteady flow must satisfy the equation

$$I \frac{dQ}{dt} = \Delta P \qquad (5.5)$$

where I is the pipeline inertance,

Q is the discharge, and

ΔP is the pressure difference.

The development of the inertia pressure becomes conceptually obvious from this equation as the flow passage diminishes very

rapidly in the last few degrees of closure.

5.10 Reverse Discharge Characteristics of the Valve

In order to examine the change in discharge as the valve closed, steady state experiments were conducted in which the valve was held fixed at different angles and reverse flow through it was measured. These tests involved determining the time required to collect a known volume of fluid discharging under the influence of a constant hydrostatic pressure. The results are shown in Fig. 5.25.

This diagram shows that the discharge remains relatively constant between 20^{o} and 8^{o}. Thereafter the discharge drops very rapidly especially from about 3^{o} to 0^{o}. The non-zero discharge at 0^{o} is due to leakage between the disc edges and the front and back perspex cover plates of the model. The clearances were quite small and were necessary to guarantee unrestricted motion of the disc as well as to prevent scratching of the perspex.

Considering the rate of change of momentum over these last few degrees before closure, it will be appreciated that the resulting hydrodynamic closing forces would be substantial. Thus, even when the pressure drop across the valve due to the hydrostatic pressure is not enough to close the valve against the spring forces, there is an indication here that the rate of change of fluid momentum provides enough of an additional pressure difference to overcome the spring forces and close the valve.

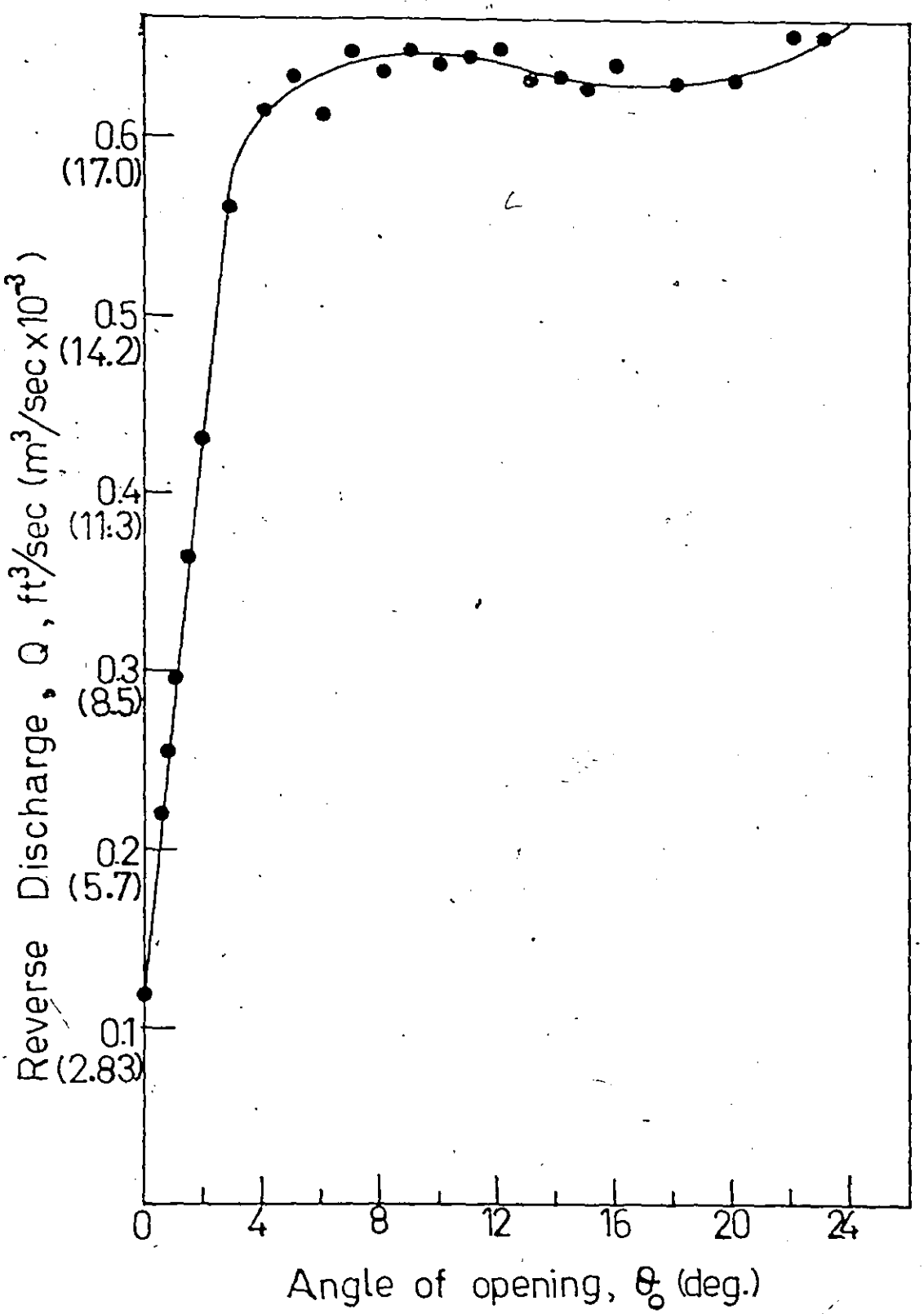

Figure 5.25. Static Reverse Discharge Characteristics of the Valve.

It is emphasized here that the static discharge characteristic of Fig. 5.25 does not apply quantitatively under the unsteady flow conditions of valve vibration. However, it provides a qualitative indication of the reverse discharge during valve closure.

It appears that the sudden drop in discharge occurs at slightly smaller angles while the increase in discharge occurs at larger angles under dynamic conditions.

For these experiments the pressure difference across the valve was also measured at each fixed angle. Based on the equation

$$Q = C_d A \sqrt{\frac{2\Delta P}{\rho}} \qquad (5.6)$$

a curve of the reverse discharge coefficient against angle of closure was plotted as shown in Fig. 5.26. This curve is based on the actual minimum area available to the flow. This behaviour agrees very well with that of the prototype valve reported by Weaver, Kouwen and Mansour [50].

5.11 Summary of Results: Mechanism of Instability

By summarizing the main results of the work reported in this chapter, it is possible to deduce the mechanism by which the dynamic instability observed with this valve is generated.

Analysis of the records of the valve vibration indicate that there is a sudden increase in hydrodynamic

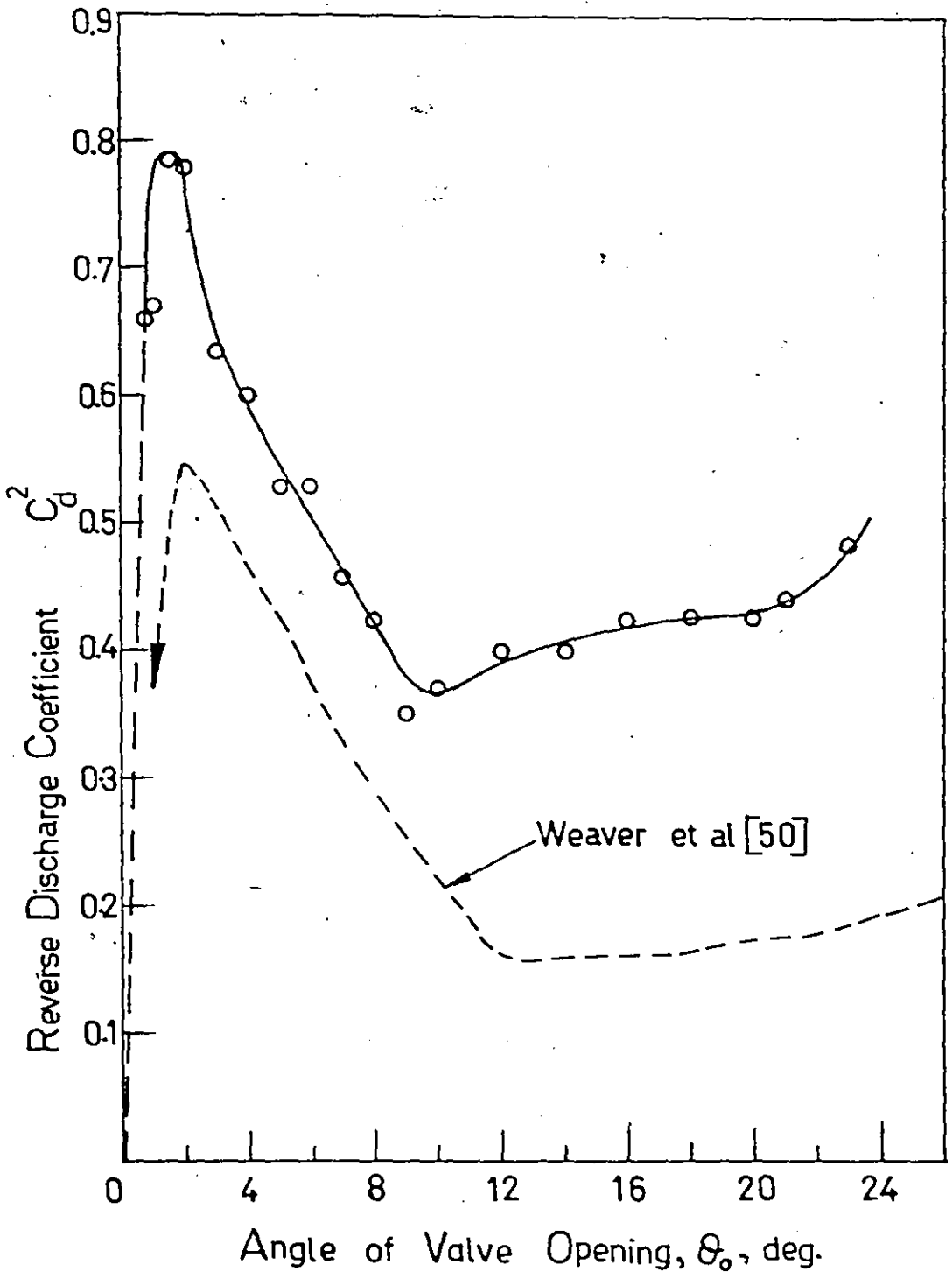

Figure 5.26. Actual Reverse Discharge Coefficient vs Fixed Angle of Closure.

closing load as the valve approaches its seat, Figs. 5.4 to 5.8 and Figs. 5.10 to 5.14. The cause of this sudden increase in closing load is the changing discharge characteristic of the valve especially in the last few degrees of closure.

As the valve slams onto its seat waterhammer pressure waves are generated upstream and downstream of it. The valve, responding only to the pressure difference across it, remains on its seat until this pressure difference reduces to a point where it either forces the valve open, or allows the spring restoring forces to initiate opening. As Figs. 5.10 to 5.14 show, the hydrodynamic closing load is substantially less during the opening part of the cycle than it is at the same angle during the closing part. This hysteretic effect indicates that there is a net energy transfer from the fluid during each cycle and the vibration is perpetuated.

Thus the mechanism of excitation of the valve vibration is governed mainly by the nature of the hydrodynamic closing load which is closely controlled by the reverse discharge characteristics of the valve.

CHAPTER 6

INVESTIGATION OF DESIGN CHANGES TO ELIMINATE VALVE VIBRATION

6.1 Introduction

The vibration experienced with the valve was self-excited. Its mechanism of excitation was found to depend mainly on the dynamic discharge characteristics during the last stages of closure. It was therefore realised that the vibration could not be eliminated by adjustments of damping or other structural parameters and that only a change in valve geometry, which changed the discharge characteristics, could provide relief from the dynamic instability. In particular, it is necessary to reduce the discharge over a much greater angle of closure so that there is no sudden rise in closing pressure difference across the valve.

Various changes to the design of the valve were evolved; each design change was capable of generating a more gradual reduction in reverse discharge at small angles of valve opening than the original design. However, it could not be known beforehand precisely how each modification to the valve geometry would modify the flow rate to achieve the desired result. In order to determine the most effective and economical measure to eliminate the valve vibration, a number of changes

(i) to the valve apron geometry,

(ii) to the valve plate, and

(iii) to the valve seat

were tested on the model to determine their effectiveness singly and in various combinations. The results of this experimental investigation leading to a practical solution of the vibration problem are reported in this chapter.

A major design criterion specified by the manufacturer was that it must be possible to pass, through the valve, a steel sphere of the same diameter as the pipe for which the valve is used. This criterion was fulfilled in all the design modifications tested.

6.2 Criterion for an Effective Solution

A completely successful solution of the vibration problem requires that the dynamic behaviour of the modified valve must match the static system characteristic of Fig. 5.1. This means that the valve must be stable at all points on its stability map. Below the static system characteristic the valve must close without vibration and remain closed; above the static system characteristic the valve should remain open at a small angle determined by the difference between spring force and available hydrostatic pressure. The degree of effectiveness of a given design modification is indicated by how closely the dynamic behaviour of the modified valve conforms to the above.

In evaluating a design modification, the stability diagram has been chosen as the sole indication of its effectiveness. In a number of cases the static reverse discharge

characteristic was determined for comparison with that of the original design and to foster an understanding of the reason for their effectiveness or lack of same.

The modified designs tested were arbitrarily labelled series B, C, D, E or some combination of these for identification purposes. On this basis the series of experiments on the original design was called series A. Series B generally involved valve body geometry modification; series C involved the use of appendages to the valve plate, and series D involved a change in the valve seat geometry.

6.3 Series B Experiments and Results

Series B experiments involved tests carried out on the valve with only the valve apron modified. The principle of the design modification was to reduce the discharge at small angles before the valve reached its seat. This was carried out by filling the apron as shown in Fig. 6.1 with a perspex plate attached to it with silicone sealant adhesive. Shown on the valve drawing in dotted line is the actual shape desired. It was observed that the limiting streamline very closely conformed to the desired geometry. The approximation had the advantage of being much less expensive to make as well as being easily removable.

Also shown on Fig. 6.1 is the stability map for the valve modified in this way. The static system characteristic of Fig. 5.2 is shown in dashed lines on the graph.

Comparison with Fig. 5.3 shows that the region of self-excitation both above and below the static system

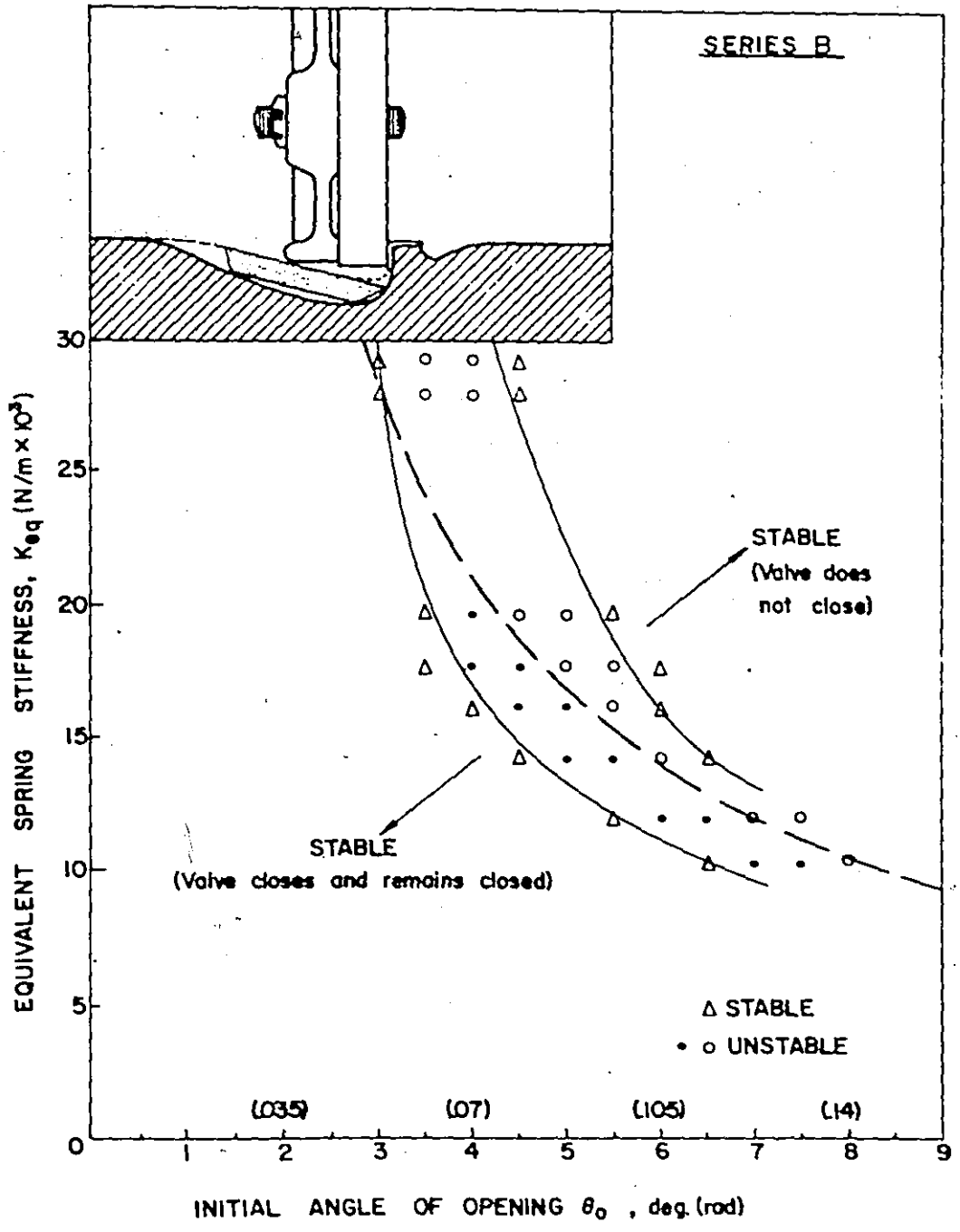

Figure 6.1. Series B Experiments: Design Modification and Stability Map.

characteristic is considerably reduced. Within the region of self-excitation, experiments showed that the vibration was much less violent than in the tests with the original design, series A. The amplitude of oscillation was also considerably lower in this case than it was at the same initial setting for series A.

In order to better understand the reason for the partial success of this modification, the static reverse discharge characteristic of the valve was determined. This curve, shown in Fig. 6.2, indicates that the reverse discharge decreased more gradually than series A until an angle of closure of 2^{o}; from this point it drops very sharply until complete valve closure is attained. This relatively high rate of change of discharge once again sets up the inertial component of hydrodynamic pressure which leads to the instability. However, since the discharge at 2^{o} is considerably less than series A, the region of instability is reduced and the vibration is less violent. Comparison of the reverse discharge characteristics of series B and series A shows that the slopes are very nearly equal between 0^{o} and 1^{o}.

6.4 Series C Experiments and Results

In this series of experiments the only modification in the design involved attaching appendages to the downstream face of the valve plate as shown in Fig. 6.3. These appendages were made of 0.5 inch thick perspex plate and attached to the valve plate at an angle of 45^{o} with silicone sealant adhesive. In the closed valve position the clearance

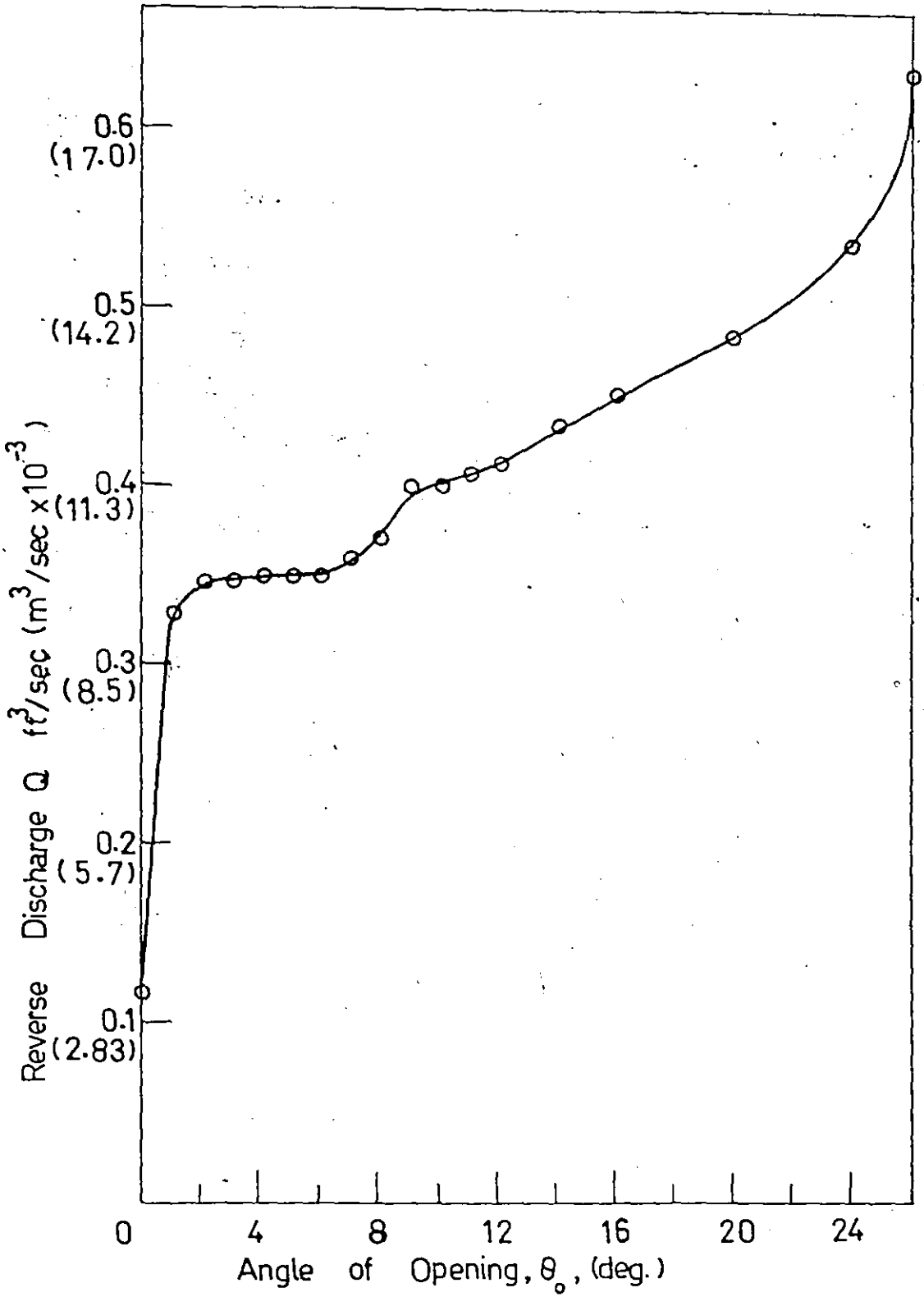

Figure 6.2. Series B Experiments: Static Reverse Discharge Characteristics of the Modified Valve.

between the seat and the nearest point on the appendage was 3/16 inch.

Also shown in Fig. 6.3 is the resulting stability map of the valve. The static system characteristic is shown in dashed lines on the map.

Comparison of this diagram with Fig. 5.3 shows that the region of self-excitation is reduced slightly in its upper half and hardly at all in its lower half. This indicates that this modification does not result in any dramatic improvement in the discharge characteristics; however experimental results showed that the amplitudes of vibration were reduced about 50% and the frequency increased slightly over that of series A.

6.5 Series C1 Experiments and Results

In this series the gap between the seat and the nearest point on the appendage when the valve was closing, was reduced to 1/16 inch. This modification, and its stability map are shown in Fig. 6.4. Comparison with series A and series C shows the drastic reduction in the region of self-excitation; the entire upper sub-region of instability now is stable while the lower sub-region is clearly reduced.

This means that dynamic pressure due to reduction in discharge is never very much greater than the hydrostatic pressure difference when the valve is closed. However, there is sufficient pressure reduction due to waterhammer wave reflection to open the valve once it is closed.

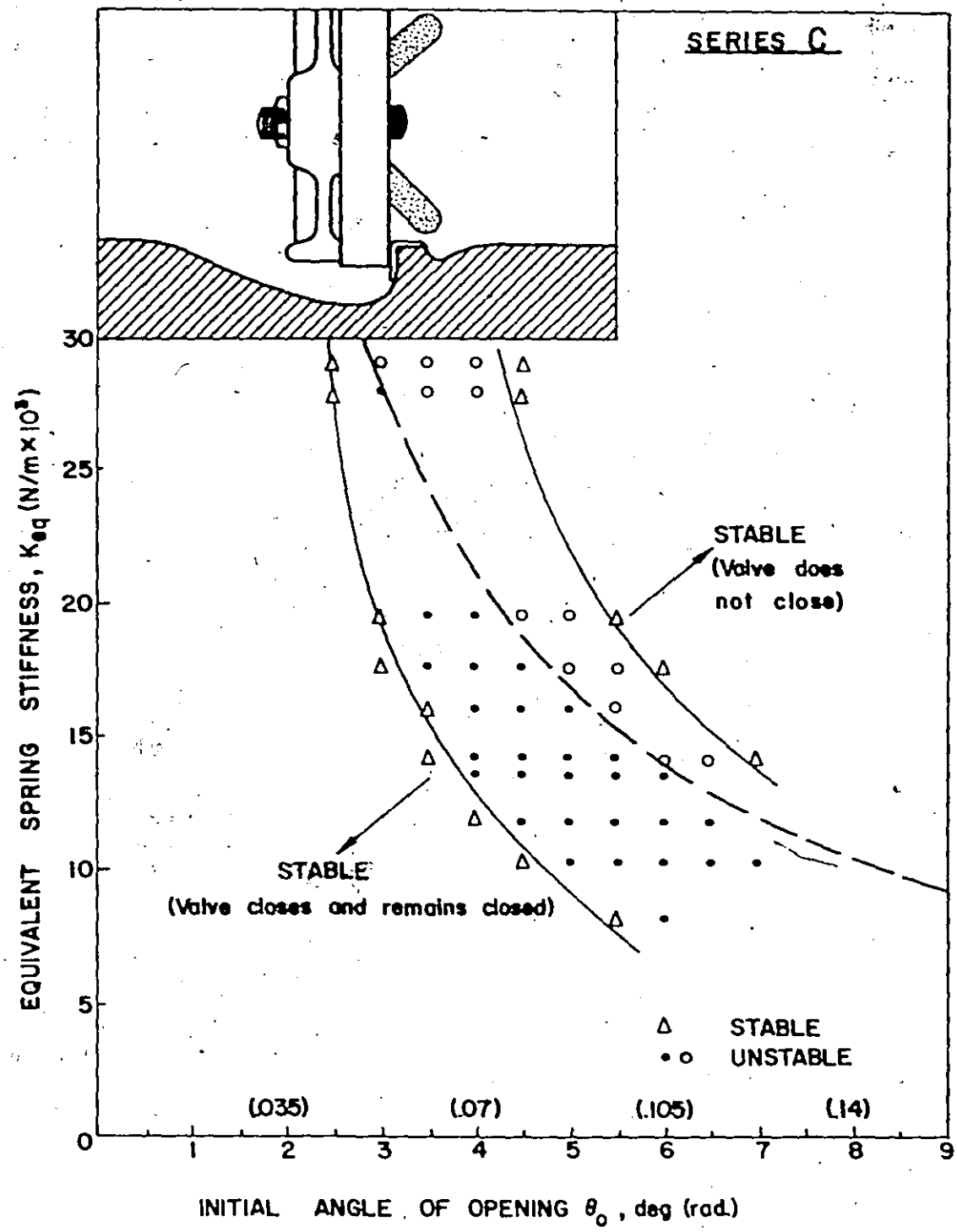

Figure 6.3. Series C Experiments: Design Modification and Stability Map.

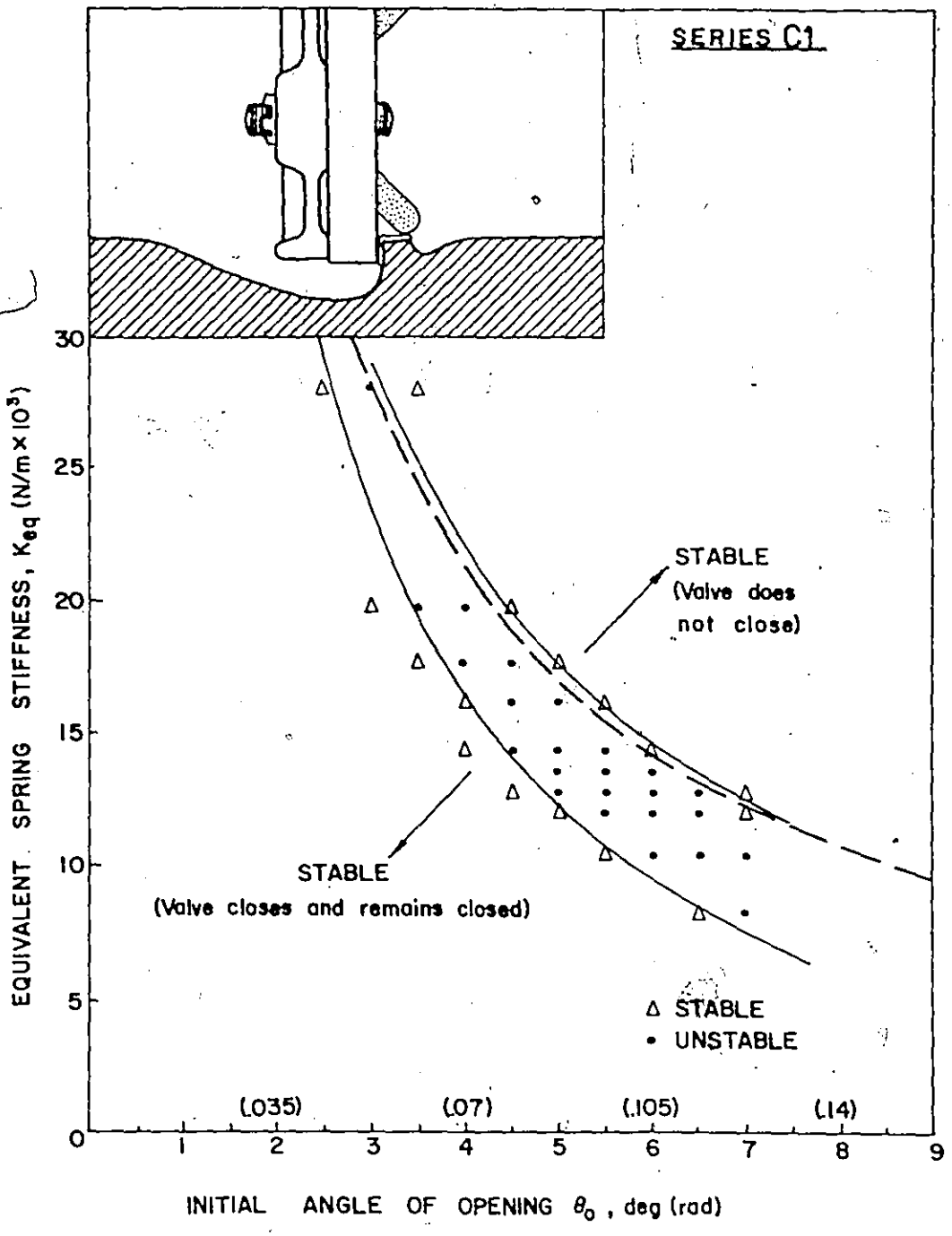

Figure 6.4. Series C1 Experiments: Design Modification and Stability Map.

This modification by itself does not appear capable of effecting a large enough reduction in the rate of change of discharge to provide complete relief from the vibration. Once again the amplitude of vibration in this case was reduced by more than 50% compared to series A and the frequency increased slightly, (see Appendix A) and Fig. 6.5. Fig. 6.5 shows the comparison between vibration records for series A and series C1 for the same initial angle of valve setting, spring stiffness and upstream head. The record shows that the vibration is much less violent in the case of series C1 than in series A.

6.6 Series B-C1 Experiments and Results

Series B-C1 experiments involved the combination of the modifications carried out for series B and C1. It is shown in Fig. 6.6, together with its stability map.

Apparently the addition of the apron filler does not improve the behaviour over the disc appendage of modification C1. In fact, it seems to be a little worse. This is not surprising since in the case of series B-C1 the path of flow through the valve is less tortuous than in the case of series C1, and hence the pressure drop is less at larger angles. This apparently results in more reverse discharge and less pressure drop at a given angle of opening. Examination of Appendix A shows that both the valve maximum displacement and frequency of vibration are very similar for series B-C1 and series C1.

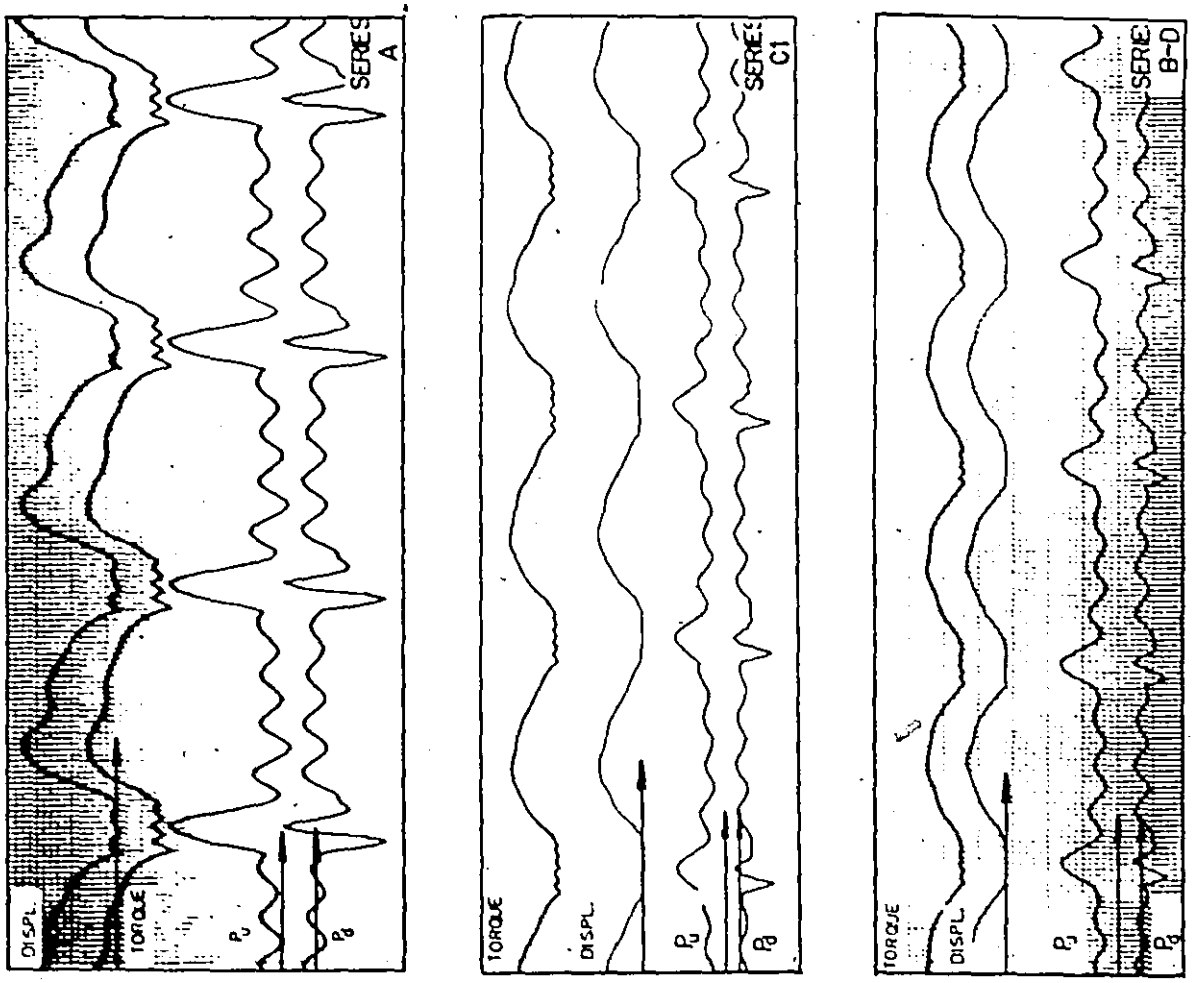

Figure 6.5. Comparison of Vibration Records of Series A, Series C1 and Series B-D for K_{eq} = 11.956 kN/m; $\theta_o = 6^o$.

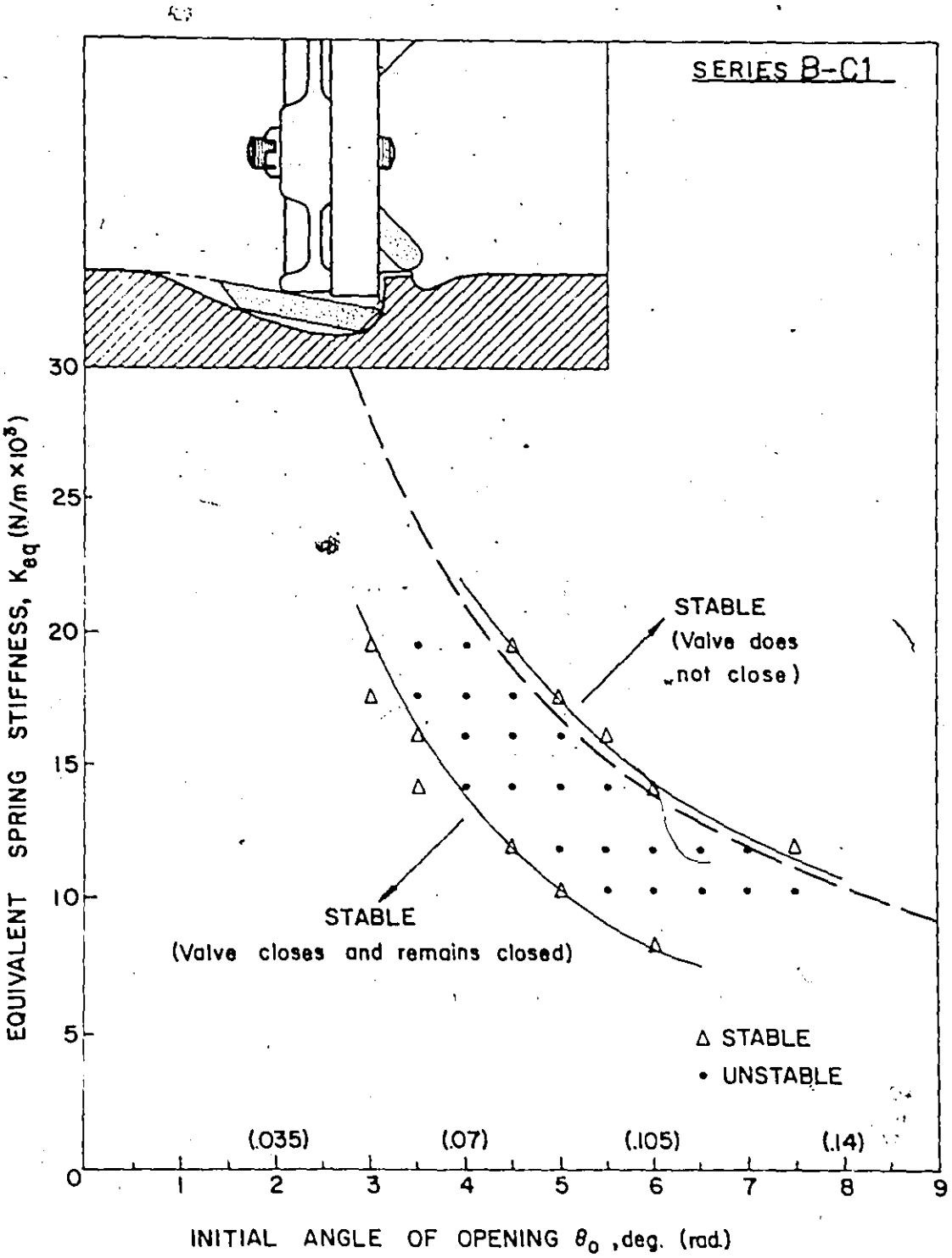

Figure 6.6. Series B-C1 Experiments: Design Modification and Stability Map.

6.7 Series B-C2 Experiments and Results

Fig. 6.7 shows the form of series B-C2 and its stability diagram. In this case the appendage was attached at 90^{o} to the valve plate. The minimum permissible clearance between appendage and seat was once again arranged. This experiment was carried out solely to observe what effect, if any, the angle of attachment of the appendage has on the dynamic behaviour of the valve. This information is of importance for the practical implementation of the successful solution as we shall see later, since an appendage to be attached at 90^{o} is less expensive and easier to manufacture than one to be attached at 45^{o}.

The resulting stability map, Fig. 6.7 shows that the dynamic behaviour of the valve is insensitive to the angle of attachment of the appendage, at least for acute angles, since the area of self-excitation in Figs. 6.6 and 6.7 are practically the same. The important parameter is definitely the clearance between appendage and seat since this parameter controls the discharge at a given angle.

Comparison of the vibration records of series B-C2 and series B-C1 shows the very close similarity of valve behaviour between the two.

Also shown in Fig. 6.8 is the static reverse discharge characteristic of the valve for this case. This curve exhibits the rapid drop at small angles indicative of a substantial rate of change of reverse discharge which is responsible for the dynamic instability. The more gradual

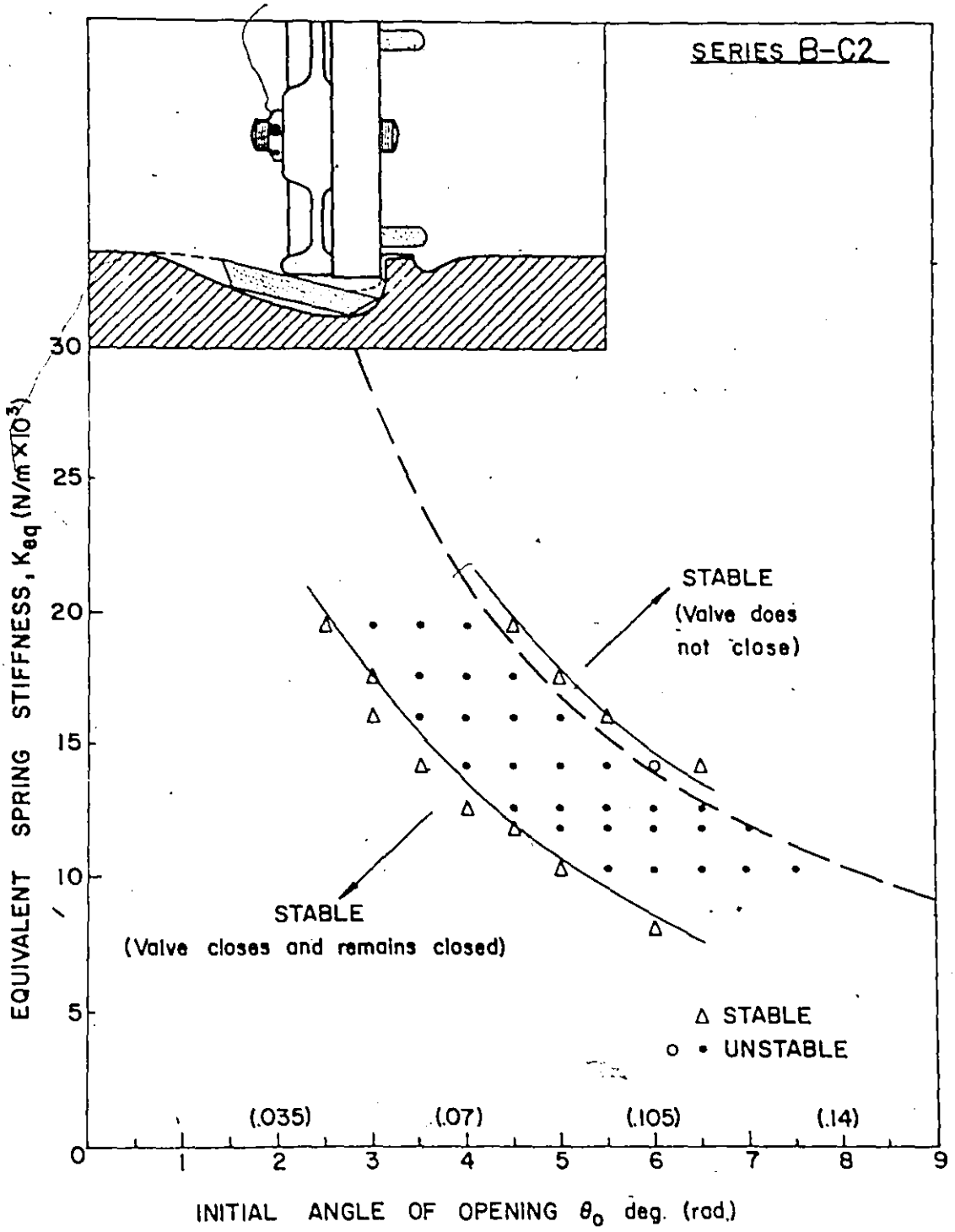

Figure 6.7. Series B-C2 Experiments: Design Modification and Stability Map.

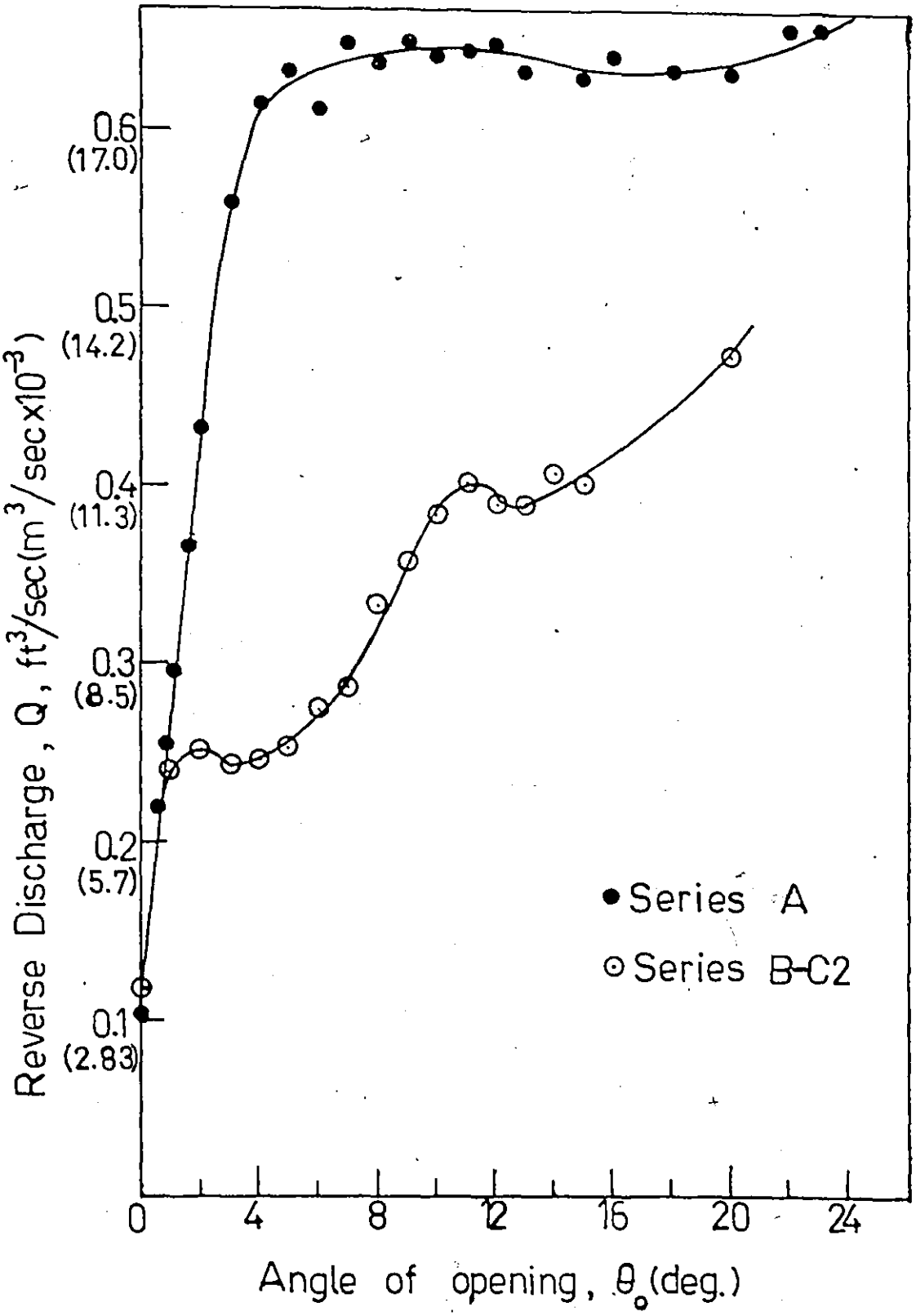

Figure 6.8. Comparison of Static Reverse Discharge Characteristics of Series A and Series B-C2.

change in reverse discharge between 2^{o} and about 7^{o} explains why the upper half of the region of self-excitation is now stable. It appears that some means of controlling the discharge characteristic in the region from 0^{o}-2^{o} is essential to removing the instability entirely.

6.8 Series B-D Experiments and Results

The results of the previous series of experiments showed that modifications involving changes to the valve apron or attachment of appendages to the valve plate, whether used alone or in combination will not sufficiently reduce the rate of change of discharge to eliminate valve vibration. Clearance between an appendage and the valve seat cannot be held below a certain value for all angles below about 6^{o}, otherwise contact between appendage and seat would result.

It was therefore decided that a more gradual reduction in the rate of change of reverse discharge in the region from 0^{o} to 2^{o} would be achieved only by modifications to the seat and valve plate. This is because of the possibility of holding the flow area to very small values with this arrangement without premature contact occurring.

In order to emphasize the critical importance of minimizing the available flow passage at small angles of opening, series B-D, shown in Fig. 6.9, was examined. In this series, a lip was attached to the valve seat and a corresponding portion cut away from the valve plate to allow proper valve seating. The valve apron was also modified

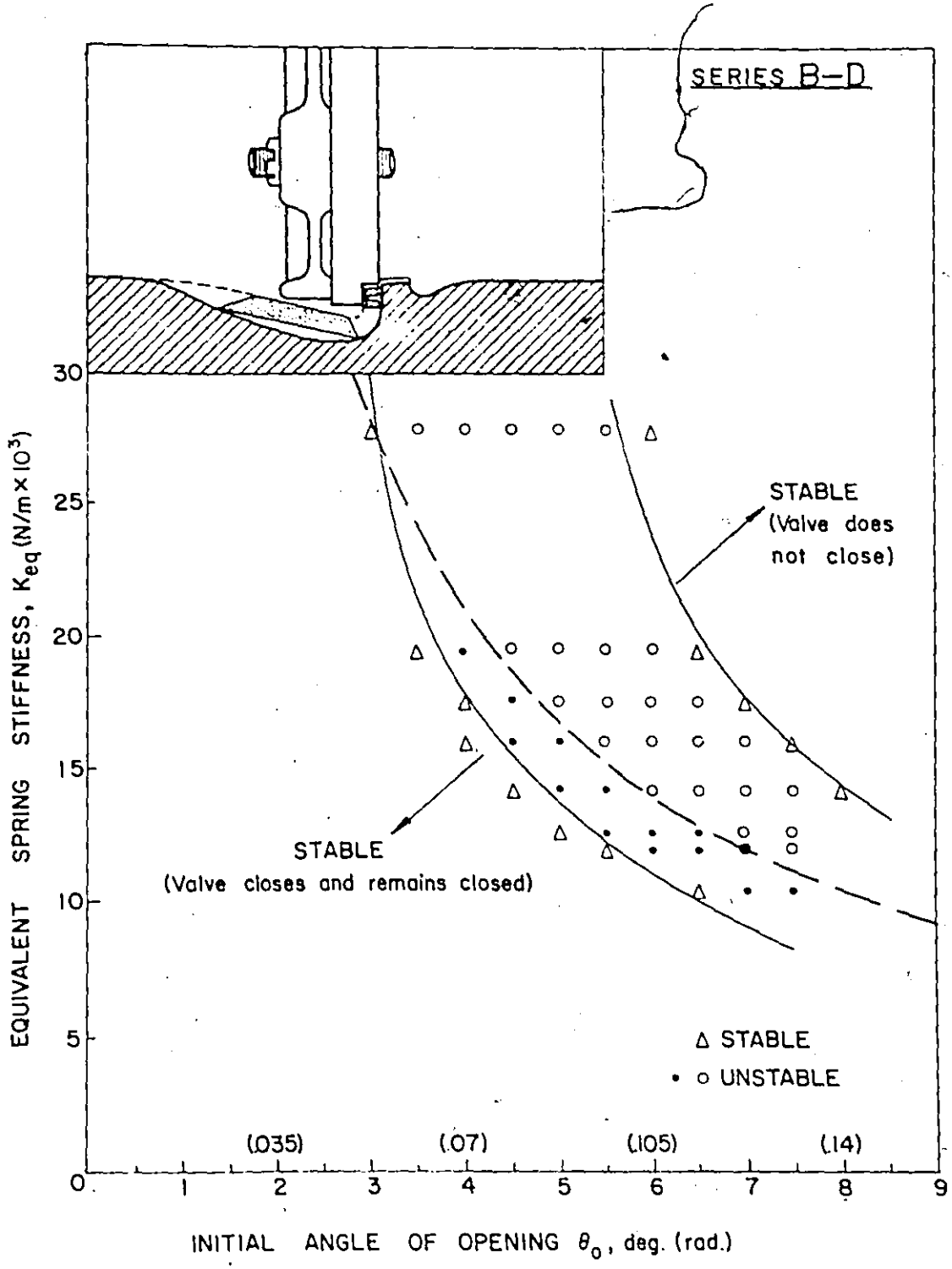

Figure 6.9. Series B-D Experiments: Design Modification and Stability Map.

as shown in Fig. 6.9. A clearance of 1/16 inch at complete valve closure between the cut-away portion of the valve plate and the lip was used in this series of experiments. The resulting dynamic behaviour of the valve is shown on the stability map of Fig. 6.9.

Comparison of results of series B-D with those of series A shows that the only improvement has occurred in the lower half of the region of self-excitation. However at those points where vibration occurred, the oscillations were less violent, the amplitude of vibration being reduced by an average of more than 50%. This is shown for one point of the stability map in Fig. 6.5.

6.9 Series B-D1 Experiments and Results

Series B-D was improved by reducing the clearance between the lip and the cut-away portion of the valve plate to a little less than 1/32 inch. This modification is shown in Fig. 6.10. Except for small leakage the valve is essentially closed at around 2^{o}.

The size of the lip used was not arbitrary. The reverse discharge characteristics of series A shows a high slope between about 6^{o} and 0^{o}. Examination of the vibration records of series A showed that the sudden acceleration of the valve towards its seat occurred between 1.5^{o} and about 3^{o} depending on the initial setting. The choice of lip size was based on preventing the sudden reduction in discharge in the last 2^{o} as seen in series B, (Fig.6.2) and B-C2, (Fig. 6.8).

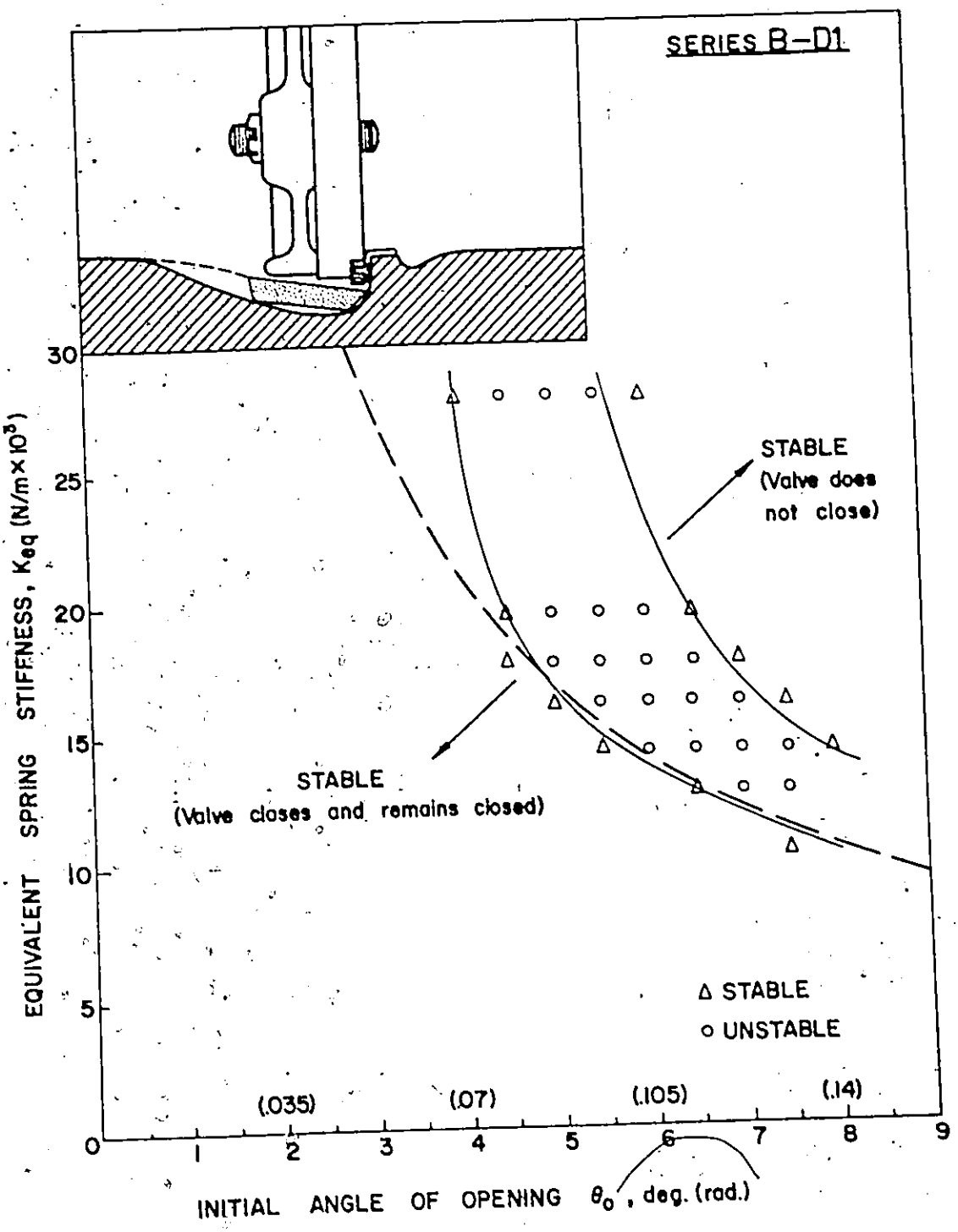

Figure 6.10. Series B-D1 Experiments: Design Modification and Stability Map.

A figure of 2^{o} was also chosen to safeguard the structural integrity of the valve plate as it slams onto the seat. This meant a cut-away of 1/4 inch by 1/4 inch by 9 inches in the present experiments. To further ensure the structural integrity of the model, the lip was lowered by 1/16 inch to allow contact of the valve plate with both the seat and the lip.

The dynamic behaviour of the valve modified in this way is shown in Fig. 6.10. The lower half of the region of self-excitation is now completely stable but a considerable area of instability remains in the upper half. This nevertheless represents a remarkable improvement in the dynamic behaviour of the valve. For the first time a modification in design was demonstrated to guarantee that if the spring stiffness used in the valve design is not stiffer than what the hydrostatic pressure in its system can overcome, no matter the initial angle of opening, the valve would be stable. This suggests that even if the dynamic pressure due to waterhammer wave reflection is sufficient to dislodge the valve from the seat by some small angle, the flow is not reestablished and the valve settles down on the seat again.

Normally if a valve is to be prevented from slamming by inclusion of springs in the valve system, rational design practice would ensure that the included springs would not be so stiff that the available hydrostatic pressure cannot close the valve against the spring force. However, as shown by the remaining area of instability this modification does not

represent a fool-proof practical solution of the vibration problem. If, due to changes in operating conditions the available hydrostatic head dropped, the valve could become unstable due to opening caused by the spring.

To understand why the valve was dynamically unstable at the larger angles, the static reverse discharge characteristic was determined. This curve is shown in Fig. 6.11. It shows a much gentler slope between 2^{o} and 0^{o}. However the slope is relatively steep between 2^{o} - 4^{o}. This enables the generation of an additional hydrodynamic pressure component due to fluid inertia which forces the valve shut against the spring. Once the valve is closed however, the dynamic pressure due to fluid inertia disappears whereupon the spring restoring force initiates valve opening. It follows that a combination of B-D1 and B-C1 should eliminate the unstable region entirely.

6.10 Series B-C1-D1 Experiments and Results

The results of series B-D1 showed that the only region of instability left was the top half. It was relatively easy at this point to synthesize a complete practical solution of the valve problem by combining series B-D1 with either series C1 or series C2. One such combination is shown as series B-C1-D1 in Fig. 6.12. Also shown in Fig. 6.12 is its dynamic stability characteristics.

Clearly this represents a complete practical solution of the vibration problem. Its dynamic stability characteristic

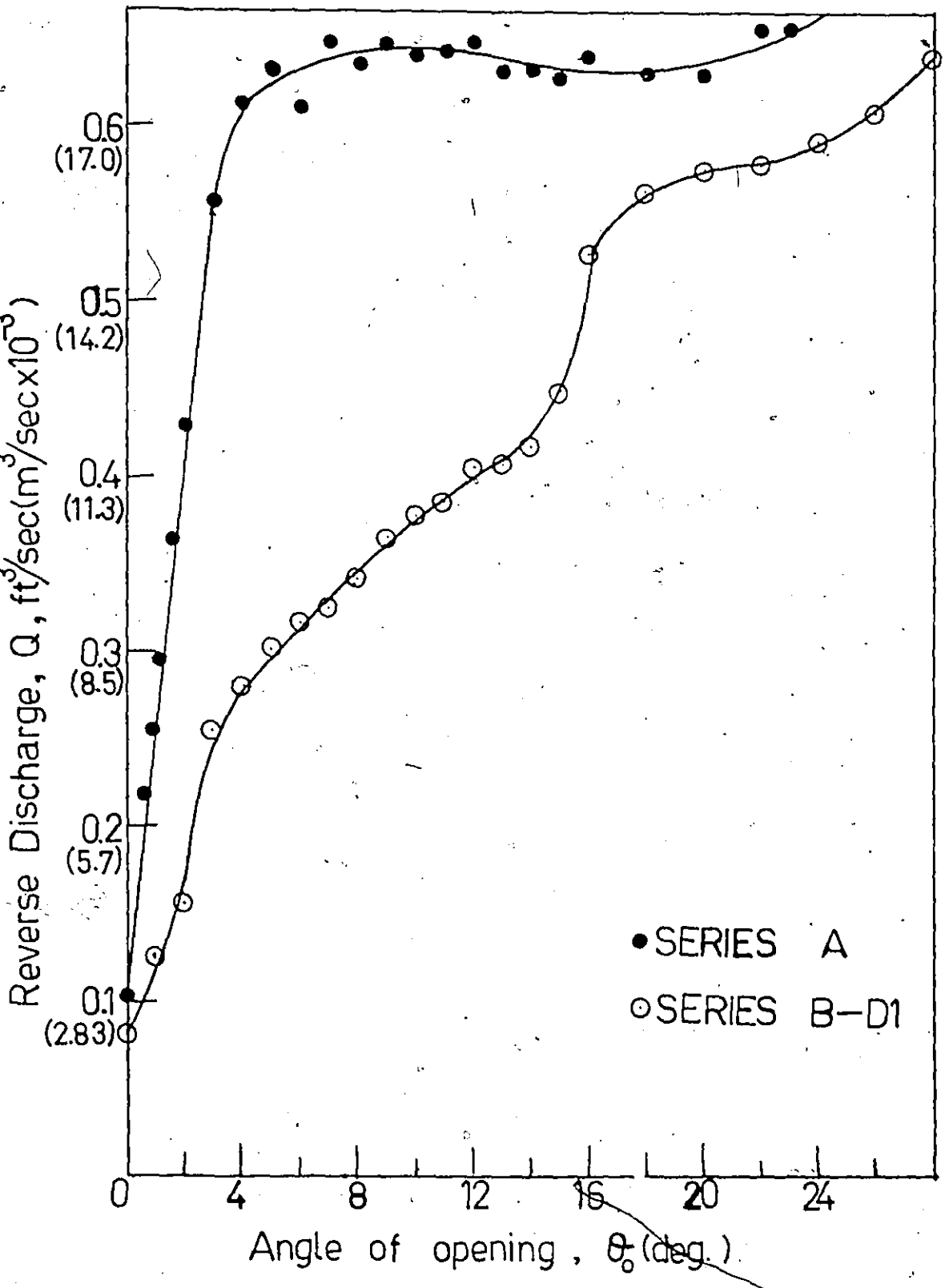

Figure 6.11. Comparison of Static Reverse Discharge Characteristics of Series A and Series B-D1.

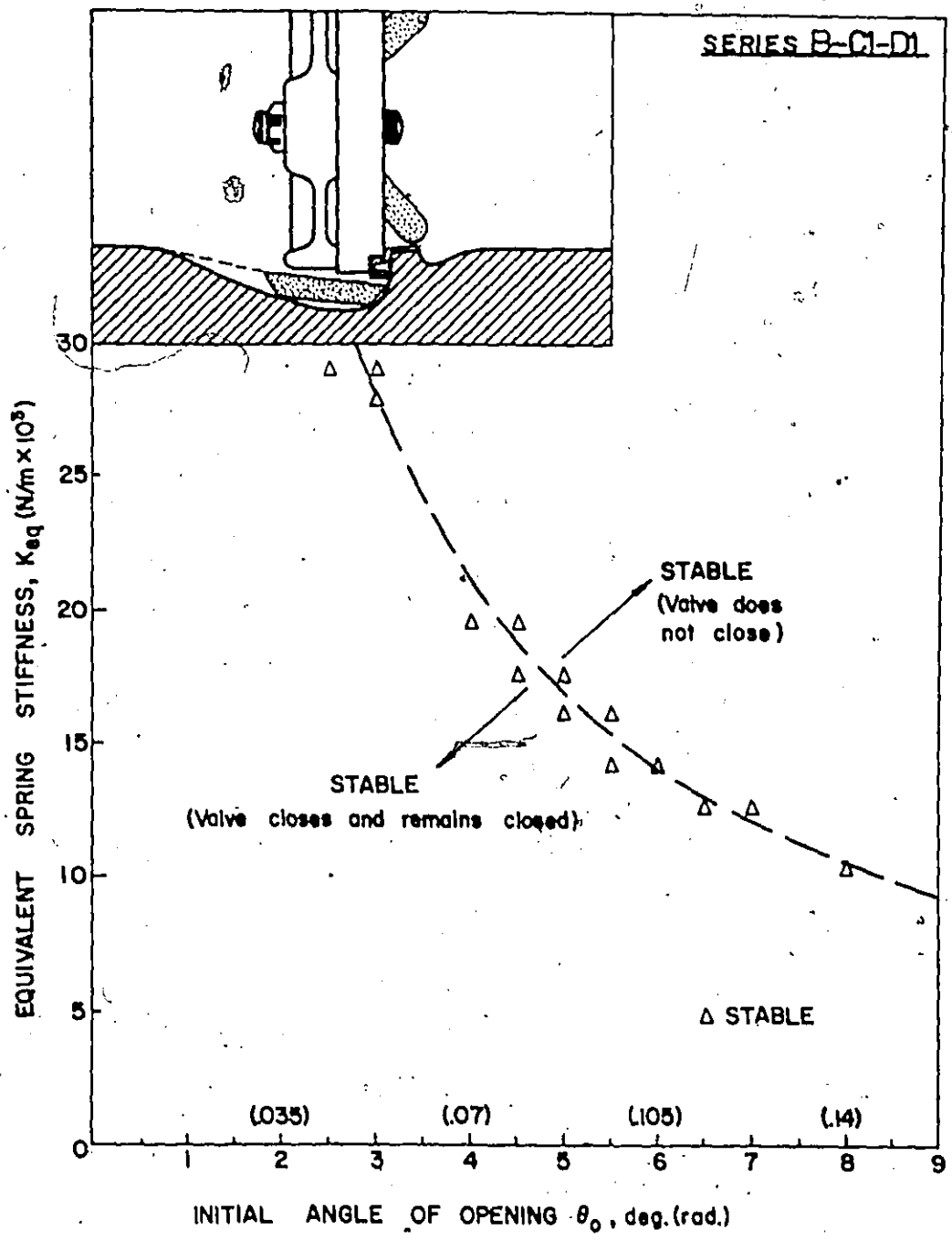

Figure 6.12. Series B-C1-D1 Experiments: Design Modification and Stability Map.

exactly matches the static system characteristic of Fig. 5.1 which has been indicated by dashed lines in Fig. 6.12. Figs. 6.13 to 6.16 show the dynamic behaviour of the improved design at four randomly chosen points on the stability map. In the region below the static system characteristic, represented by Figs. 6.13 and 6.14, the valve closed, bounced weakly once and remained closed. In the region above the static system characteristic, the valve closed once depending on the initial setting, bounced back and executed damped oscillations about some angle determined by the difference between spring force, initial setting and available hydrostatic pressure. All attempts to produce oscillations by letting the valve drop from large angles failed.

The reverse discharge characteristic for this case is shown in Fig. 6.17. Also shown for comparison is the reverse discharge characteristic for the valve of original design. The slopes of the two curves, especially at the smaller angles of opening (between 0° and about 6°) are dramatically different, the curve for the improved design showing a more gradual reduction in the discharge as the valve closed.

6.11 Series C1-D1 Experiments and Results

The results of earlier experiments with the modifications involving attachment of appendages to the valve plate (series C, C1 and C2) showed clearly that little improvement in valve stability resulted from modifying the valve apron

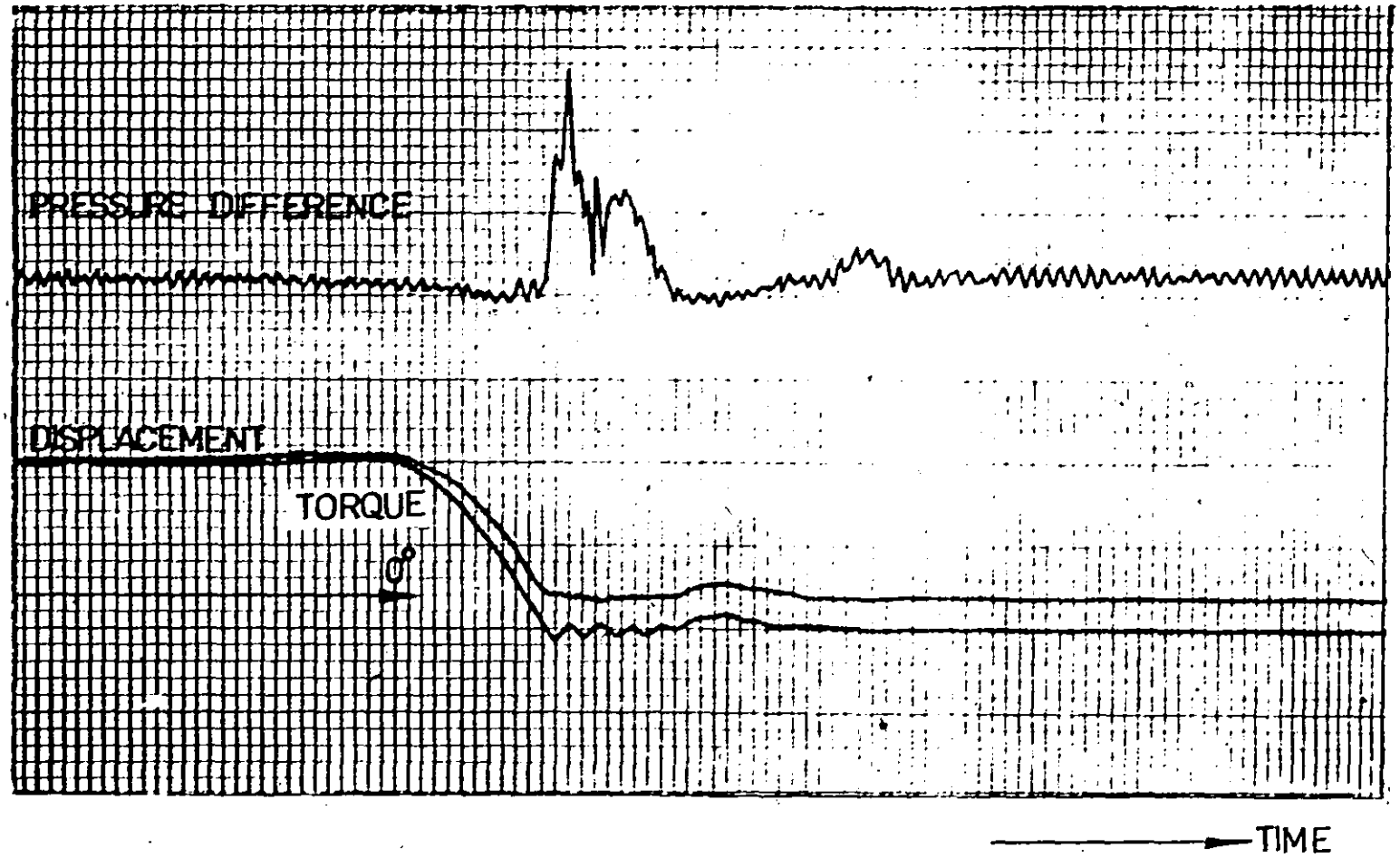

Figure 6.13. Series B-C1-D1: Dynamic Behaviour of Valve at K_{eq} = 10.305 kN/m; θ_o = 4 1/2°.

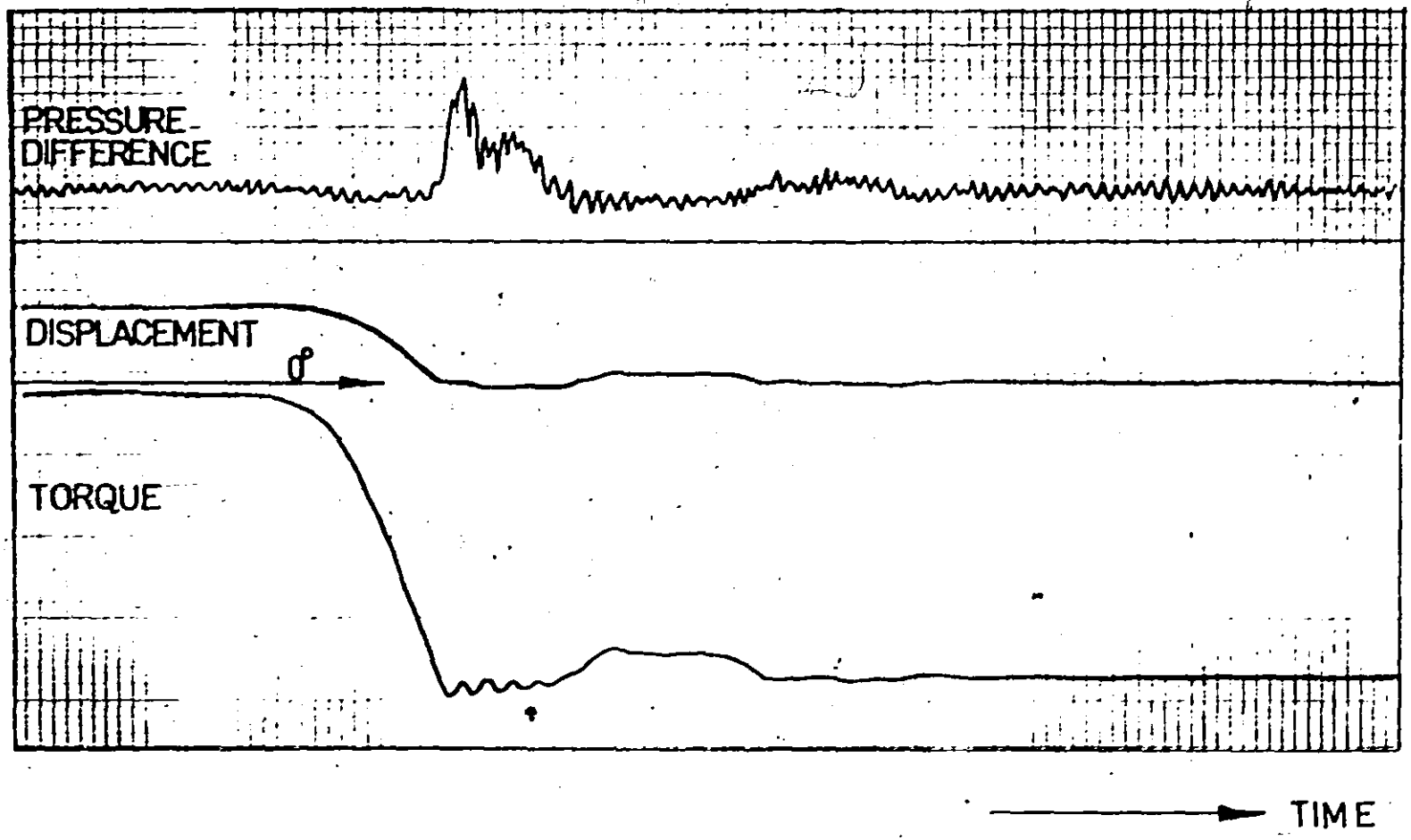

Figure 6.14. Series B-C1-D1: Dynamic Behaviour of Valve at K_{eq} = 28.85 kN/m; $\theta_o = 3^o$.

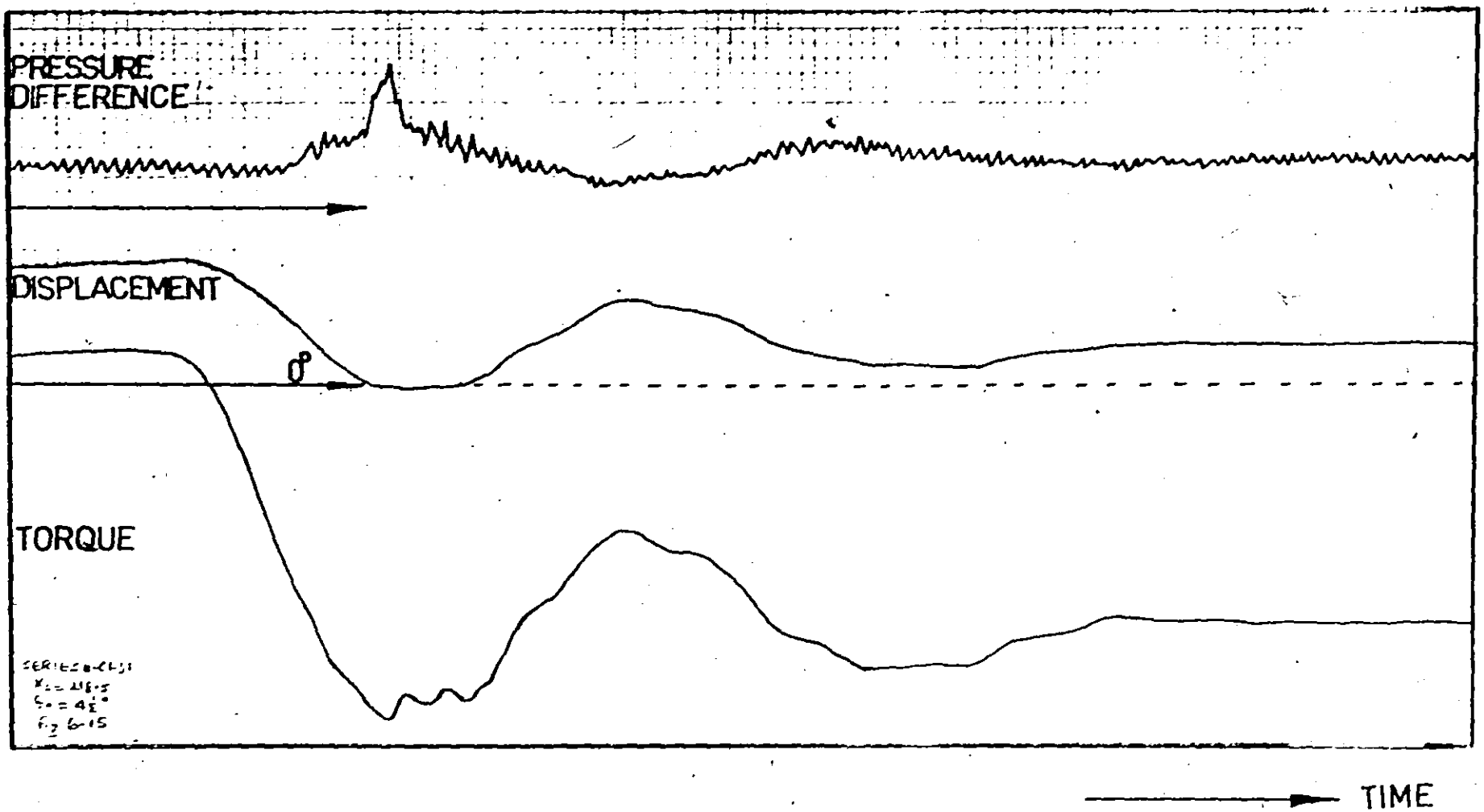

Figure 6.15. Series B-C1-D1: Dynamic Behaviour of Valve at K_{eq} = 28.85 kN/m; θ_o = 4 1/2°.

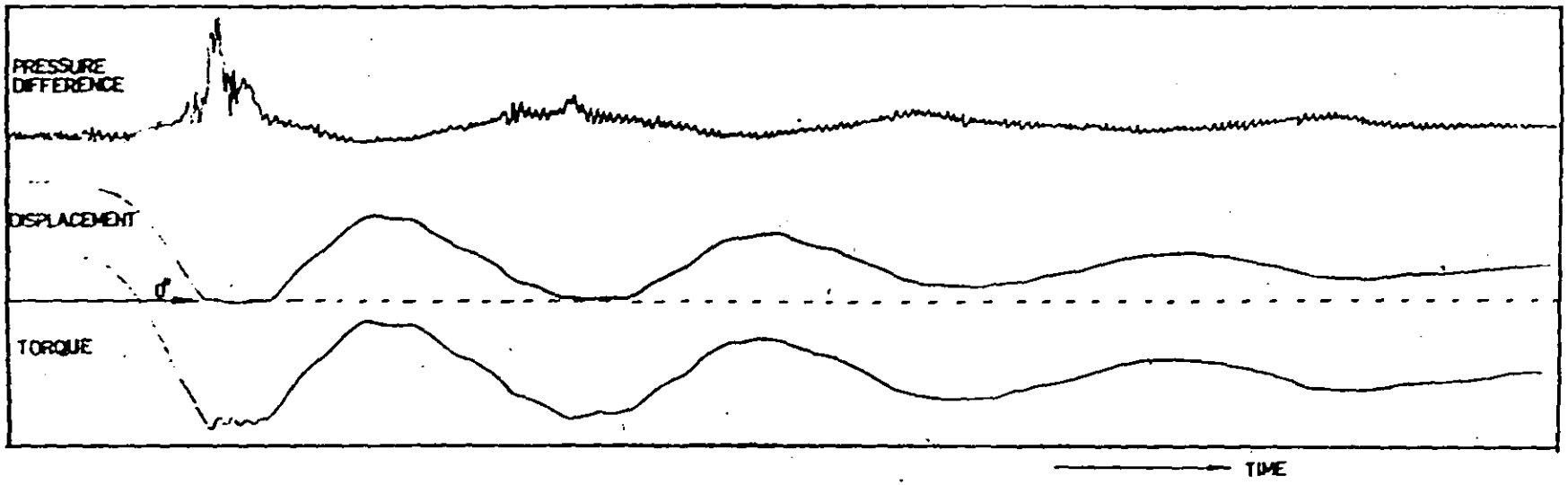

Figure 6.16. Series B-C1-D1: Dynamic Behaviour of Valve at K_{eq} = 14.168 kN/m; $\theta_o = 7^o$.

geometry. In fact whenever the apron was modified, a relatively less tortuous path of flow resulted; the fluid was discharged more or less as a horizontal jet so that no substantial improvement in the rate of change of discharge at very small angles was achieved. It followed that the solution achieved in series B-C1-D1 owed little to the modification of the valve apron. Besides, a modification to the apron constitutes the most difficult and expensive of all the improvements in design suggested. It was felt that removal of the valve apron modification should not affect the dynamic stability behaviour adversely; moreover, it represented a simplification of the final solution and a real cost-saver with respect to possible practical implementation in the prototype valve.

Thus, series C1-D1, shown in Fig. 6.18 was examined. The results, shown on the stability map of Fig. 6.18 confirmed the expected valve behaviour. It shows the valve stable at all points on its stability map and therefore represents a complete practical solution of the vibration problem.

Its reverse discharge characteristic, shown in Fig. 6.19 is practically identical to that of series B-C1-D1 between 0^{o} and 6^{o}. This is the critical zone where a very gradual reduction in the rate of change of reverse discharge is imperative if dynamic instability is to be avoided. Also shown on Fig. 6.19 for purposes of comparison is the reverse discharge characteristics of the original design.

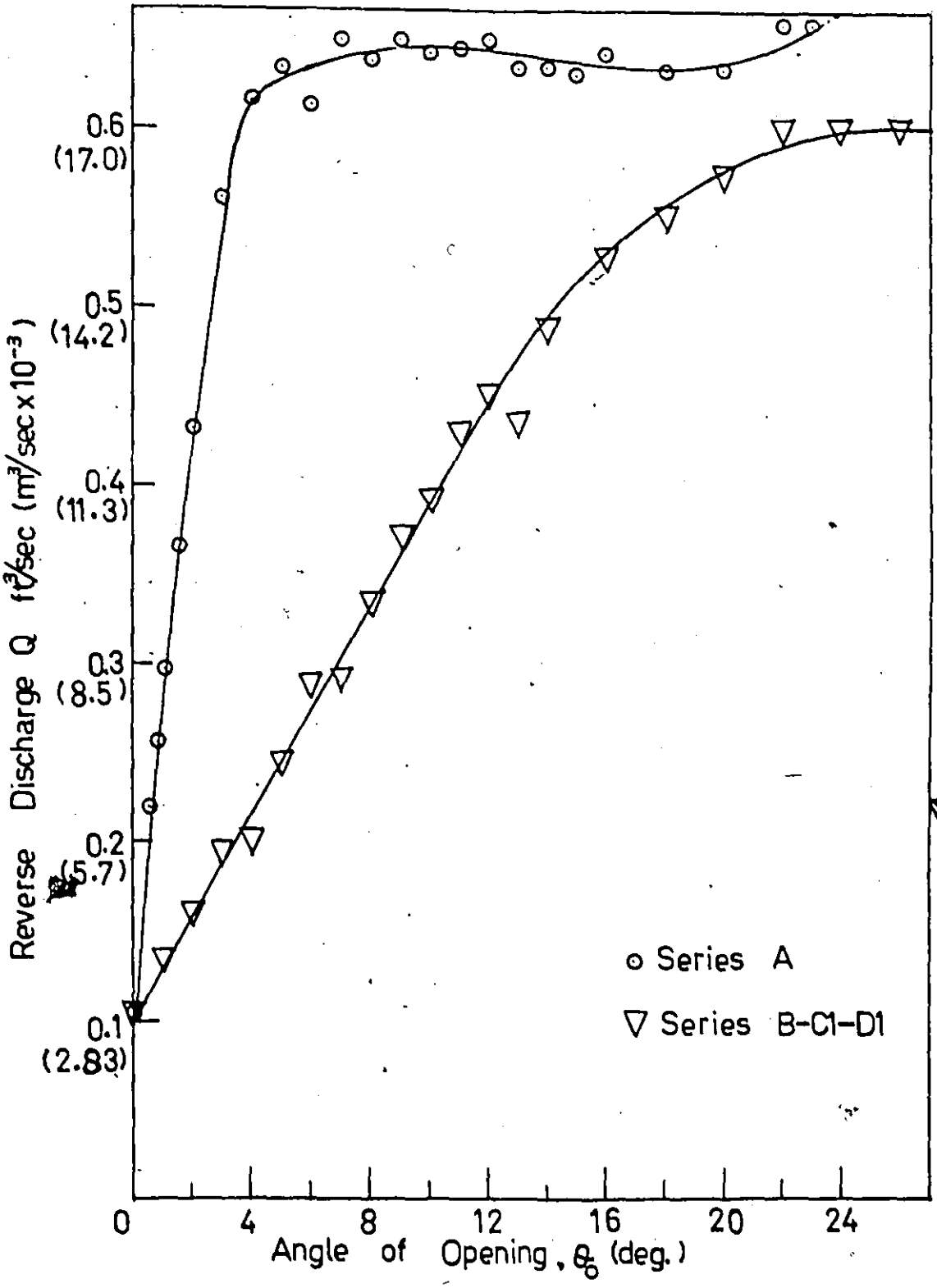

Figure 6.17. Series B-C1-D1: Static Reverse Discharge Characteristics Compared to Series A.

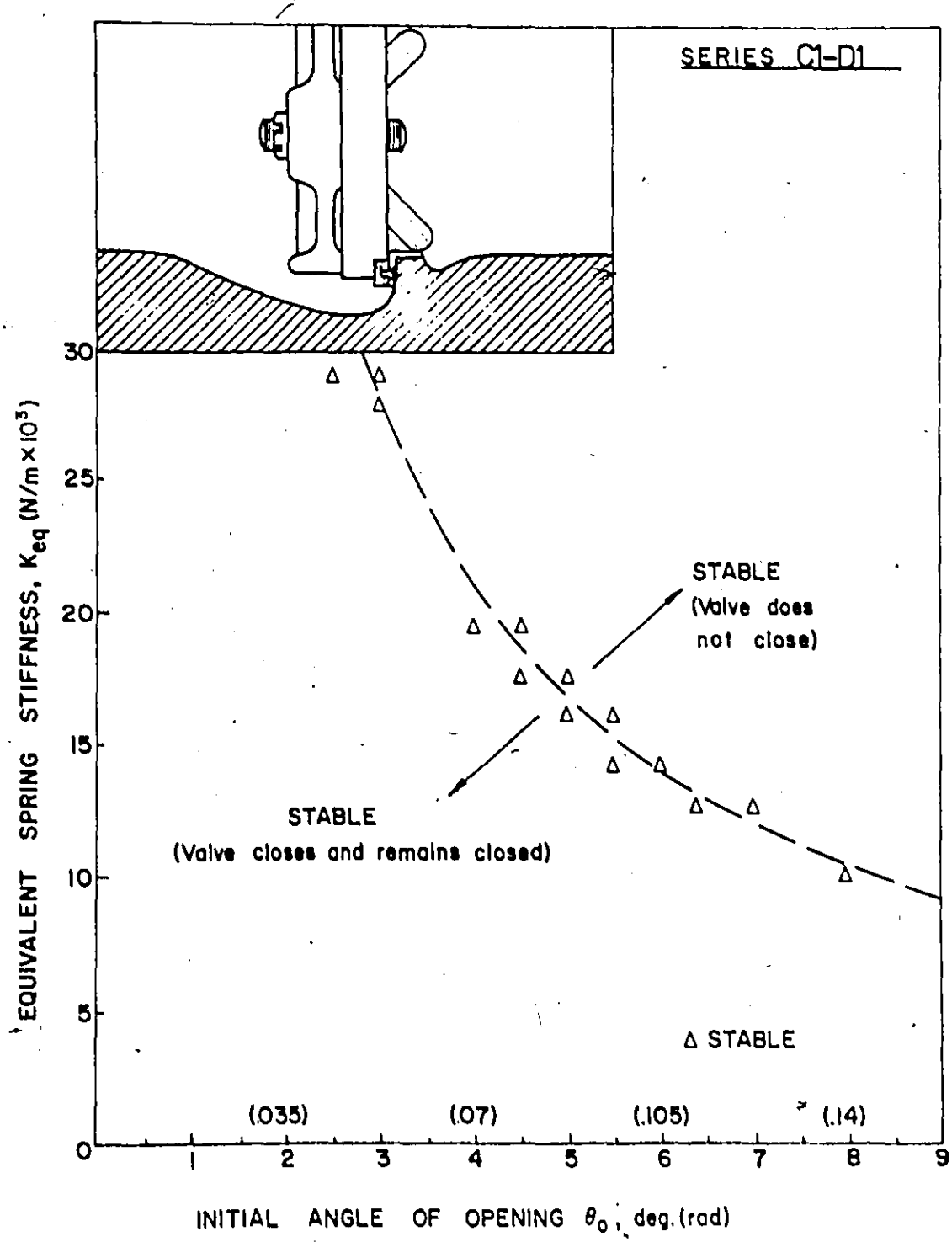

Figure 6.18. Series C1-D1 Experiments: Design Modification and Stability Map.

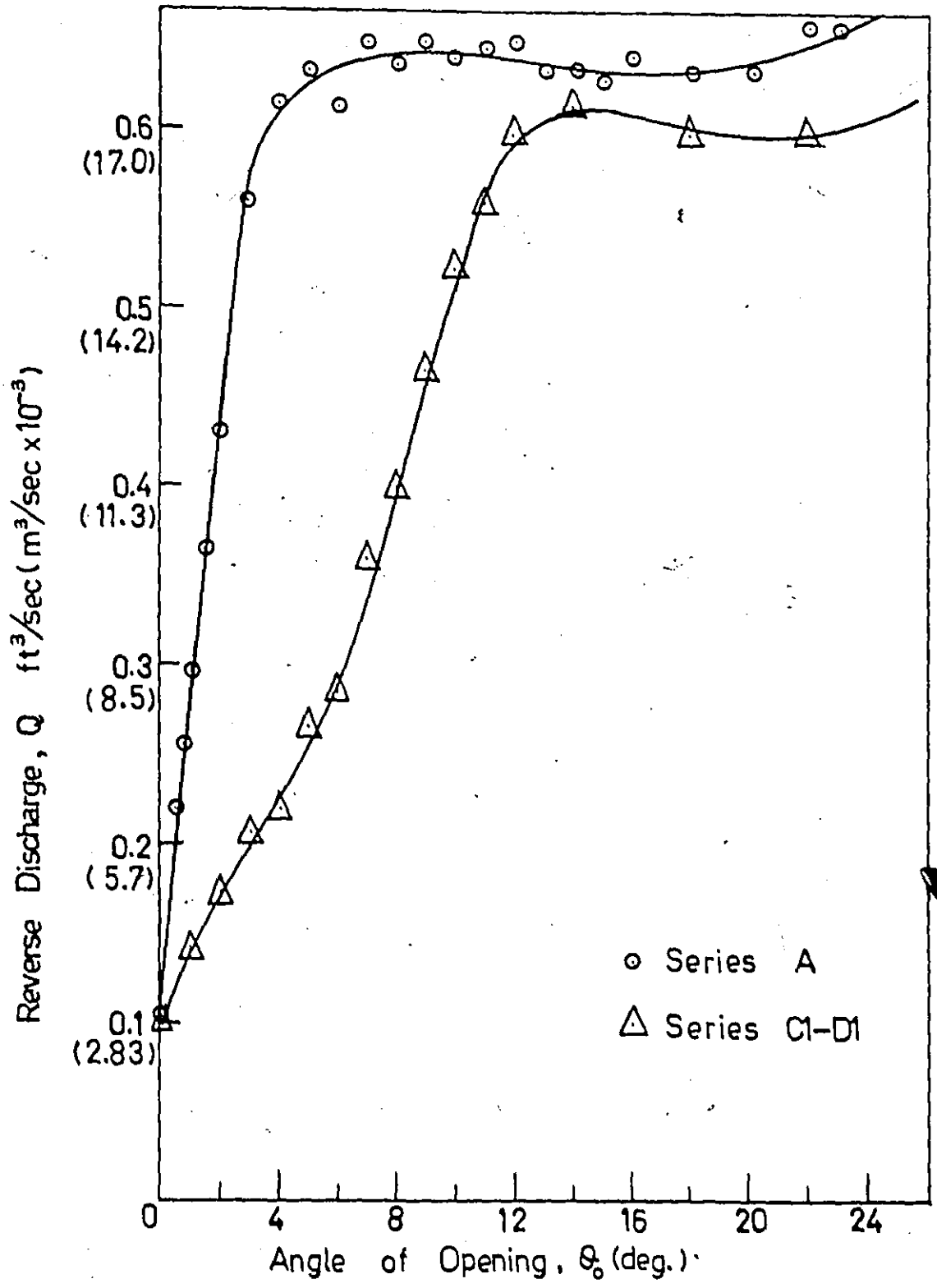

Figure 6.19. Comparison of Static Reverse Discharge Characteristics of Series C1-D1 and Series A.

6.12 Series E Experiments and Results

An attempt to reduce the reverse discharge at small angles of valve opening involving the use of counter-jets to the flow in the slot area was made. Eleven, 3/16 inch diameter holes were drilled at 60° to the downstream face of the disc and positioned in such a way that the holes were covered by the valve seat at complete valve closure. At small angles, flow through these holes was expected to reduce the flow velocity in the slot as it formed a counter-jet to the normal reverse discharge. This modification, together with its stability map, is shown as series E in Fig. 6.20.

Comparison with series A shows that the area of self-excitation was slightly extended. Results shown in Appendix A also indicate that the amplitudes of vibration were comparable to those of series A. The vibrations were observed to be very violent at the larger angles of initial setting and no attempt was made to determine the outer limits of the region of self-excitation as the structural integrity of the model was threatened.

Evidently the pressure difference across the valve disc is not sufficient to induce an appreciable flow through the slots. In addition, when the dynamic pressure forces the valve off the seat, the flow is apparently more easily established and hence, the lower stability region is extended.

6.13 Suggestion for Practical Implementation of the Solution

The implementation of the final solution represented by either series B-C1-D1 or series C1-D1 should be a relatively

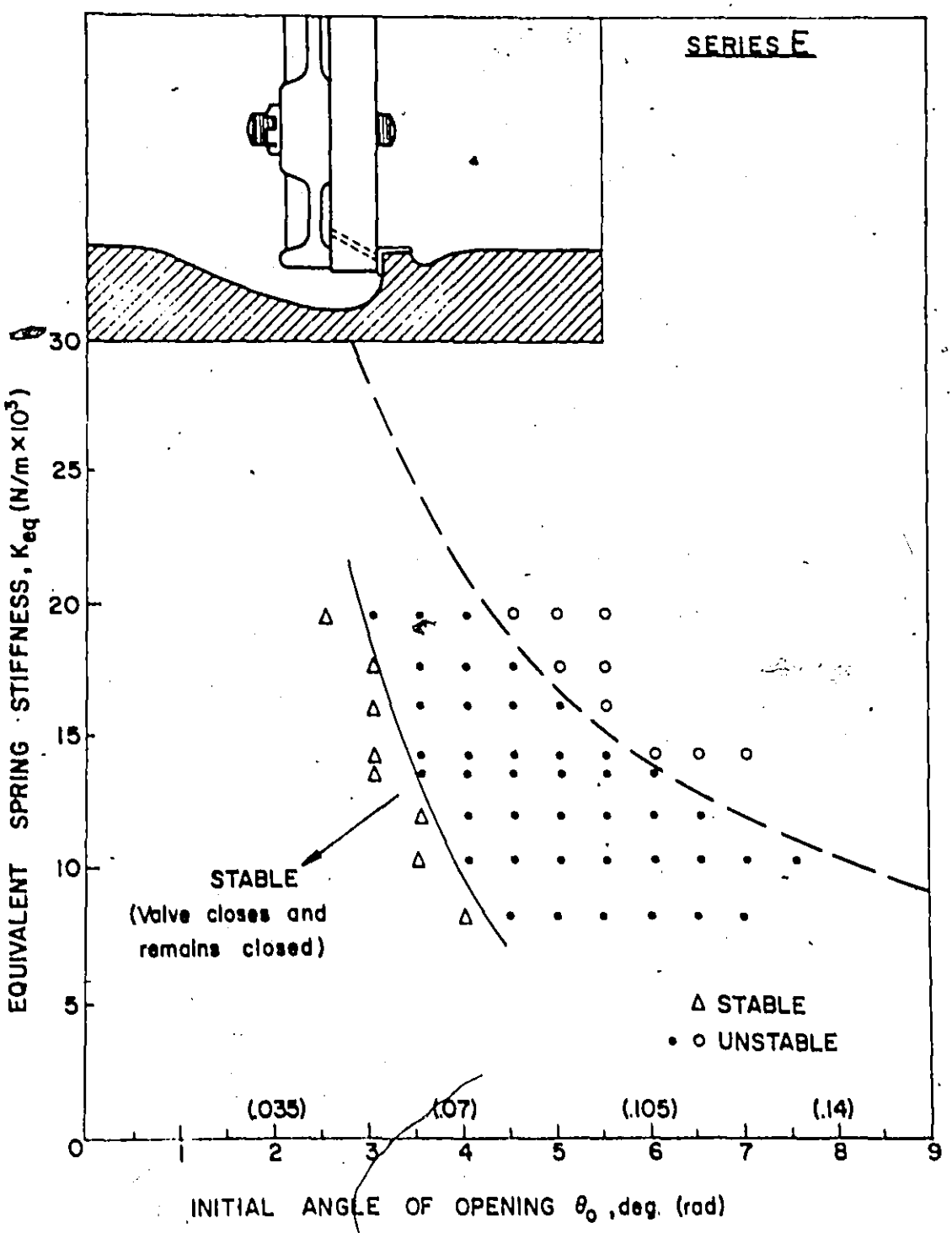

Figure 6.20. Series E Experiments: Design Modification and Stability Map.

simple and inexpensive exercise. Basically it involves the addition of two rings, (one to the valve seat, the other to the downstream face of the valve disc) and the removal of a portion of the downstream face of the disc. No alteration to the valve casing geometry is necessary but it may well be quite helpful in reducing the dynamic pressure when the valve swings through large angles as in closing during regular service. The proposed solution, for the 6 inch diameter prototype modelled in this thesis, is shown in Fig.6.21.

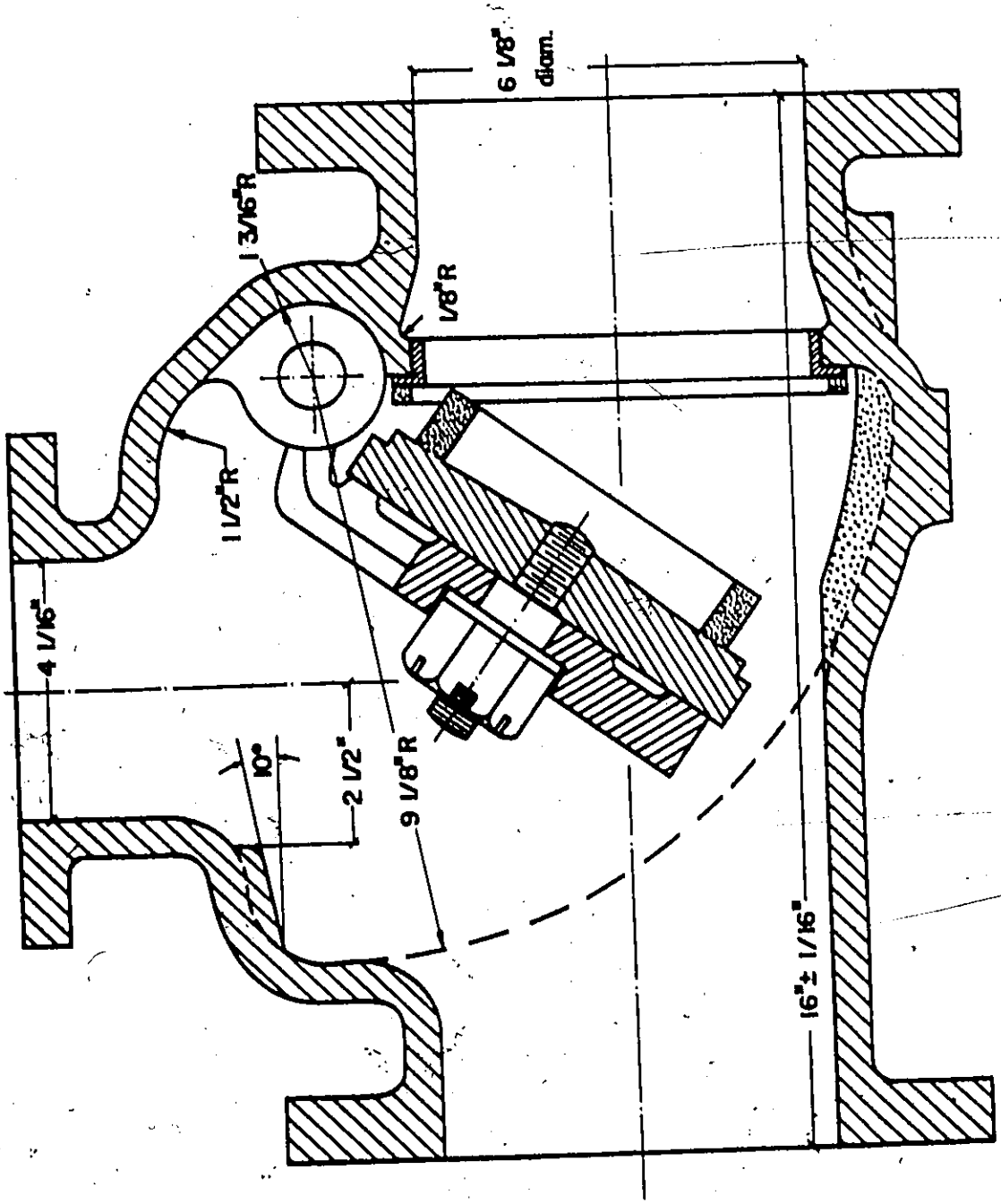

Figure 6.21. Suggested Vibration-Free Design of the Swing Check Valve with Spring Dumper.

CHAPTER 7

CONCLUSIONS

The dynamic behaviour of a hydraulic check valve which was found to vibrate violently upon rapid shut-down of the pump has been successfully modelled in two dimensions. In order to experimentally investigate the hydroelastic vibration of the valve its two-dimensional geometrically similar model and a water tunnel test facility were designed and built.

Using this model, a technique, more generally used for the visualization of steady flows, has been demonstrated to be adaptable to the study of unsteady flow, yielding valuable information.

As a result of both theoretical and experimental studies carried out on the transient behaviour of the valve model vibrating with small amplitude in air and in quiescent water, a number of important effects have been demonstrated. First, the effect of close confinement on the dynamic behaviour of a body vibrating in a heavy fluid such as water, has been shown to be a remarkable increase in its added mass factor which in turn dramatically lowers its fundamental frequency. This agrees well with the work of Todd [30] who showed that the vibration behaviour of a ship in open water is quite different from its behaviour in a shallow channel because of an apparent increase in its added mass and a corresponding decrease in its natural frequencies. Secondly, damping, which

Todd [30] asserts remained virtually unchanged for small oscillations of bodies in relatively unconfined surroundings, has been shown to increase quite substantially for a body, such as this valve, vibrating in a closely confined environment.

A clear understanding of the dynamic behaviour of the valve system has emerged from the results of this work which show that there is a sudden increase in the hydrodynamic closing load as the valve approaches its seat. The cause of the sudden increase in the closing load is the changing discharge characteristic of the valve, especially in the last few degrees before closure. As the valve slams onto its seat, waterhammer pressures are produced upstream and downstream of the valve. However, as the valve responds only to the pressure difference across it, it remains on its seat until the pressure difference reduces to a point where it either forces the valve open, or allows the spring restoring forces to pull it open. The hydrodynamic closing load is less during the opening part of the vibration cycle than it is at the same angle during the closing part. This hysteretic effect means that there is a net energy transfer from the fluid during each cycle and the vibration is perpetuated. The phenomenon is clearly hydroelastic in nature.

The author has contributed to the state-of-the-art technology of flow-induced structural vibrations, and fulfilled the stated purpose of this thesis by developing an understanding of the dynamic behaviour of the valve system, demonstrating

the mechanism by which the oscillations are induced and, more important from a purely practical design sense, developing changes in the basic valve design to eliminate the valve vibration.

Economical design of hydraulic structures presupposes accurate knowledge of the loadings which occur in practice and awareness of the possibility of flow-induced vibration. The work of this thesis emphasizes the advisability of more frequent use of models at the design stage to determine prototype behaviour of novel designs. It is not always possible to anticipate the hydroelastic problems which can develop. When they do occur, model studies to ascertain the nature of the phenomenon as well as the effects of modifications offer many advantages over the usual cut and try modifications to the prototype.

REFERENCES

1. Pearson, G. H., "Valve Design in Recent Years", The Chartered Mechanical Engineer, Vol. 87, May 1974.

2. British Valve Manufacturers Association, "Valves for the Control of Fluids", Pergamon Press, London, England, 1964.

3. Glickman, M. and Hehn, A. H., "Valves", Chemical Engineering, Deskbook Issue, April 14, 1969.

4. Livingston, A. C., and Wilson, J. N., "Effects of Valve Operation", Proc. Instn. Mech. Engrs., Vol. 180, Pt. 3E, 1965-66.

5. Pearson, G. H., "Valve Design: Manually Operated Patterns", Pitman Publishing Co., 1972.

6. Board, C. S., "Final Control Elements: Valves and Actuators", Rimbach Publications Division, Chilton Co., 1969.

7. "Final Control Elements: Control Valves of the Seventies", Proceedings of the 1st ISA Symposium on Control Elements, 1970.

8. Angus, R. W., "Air Chambers and Valves in Relation to Waterhammer", Trans. ASME, HYD-59-8, 1937.

9. Jaeger, C., "The Theory of Resonance in Hydropower Systems. Discussion of Incidents and Accidents Occurring in Pressure Systems", J. Basic Engineering, Dec. 1963.

10. Bisplinghoff, R. L., Ashley, H., and Halfman, R. L., "Aeroelasticity", Addison-Wesley Publication Co., 1955.

11. Bolotin, V. V., "Nonconservative Problems of the Theory of Elastic Stability", Pergamon Press, New York, 1963.

12. Den Hartog, J. P., "Mechanical Vibrations", McGraw-Hill Book Co., Inc., New York, 1947.

13. Bagleson, P. S., Noustopoulos, G. K., and Daily, J. W., "The Nature of Self-Excitation in the Flow-Induced Vibration of Flat Plates", J. Basic Engineering, Trans. ASME, Sept. 1964.

14. Protos, A., Goldschmidt, V. W., and Toebes, G. H., "Hydroelastic Forces on Bluff Cylinders", J. Basic Engineering, Trans. ASME, Sept. 1968.

15. Heller, S. R., and Abramson, H. N., "Hydroelasticity - A New Naval Science", Journal of the American Society of Naval Engineers, Vol. 71, No. 2, 1959.

16. Schmidgall, T., "Spillway Gate Vibrations on the Arkansas River Dams", J. Hyd. Division, Proc. ASCE, Jan. 1972.

17. Simmons, W. P., "Experiences with Flow-Induced Vibrations", J. Hydraulics Division, Proc. ASCE, HY4, 1965.

18. Campbell, F. B., "Vibration Problems in Hydraulic Structures", J. Hyd. Div., Proc. ASCE, Vol. 87, March 1961.

19. Abbott, H. F., Gibson, W. L., and McCaig, I. W., "Measurements of Auto-Oscillation in a Hydroelectric Supply Tunnel and Penstock System", J. Basic Engineering, Dec. 1963.

20. Hoskestad, G., and Olberts, D. R., "Influence of Trailing-Edge Geometry on Hydraulic-Turbine-Blade Vibration Resulting from Vortex Excitation", Journal of Engineering for Power, Trans. ASME, April 1960.

21. Greenway, M. E. and Wood, C. J., "The Effect of a Bevelled Trailing Edge on Vortex Shedding and Vibration", J. Fluid Mechanics, Vol. 61(2), 1973.

22. Lyssenko, P. R. and Chopajkin, G. A., "On Self-Excited Oscillations of Seals Concerning the Gates of Hydrotechnical Structures", IUTAM-IAHR Symposium on Flow-Induced Structural Vibrations, Karlsruhe, Germany, 1972.

23. Petrikat, K., "Vibration Tests on Weirs and Bottom Gates", Water Power, Feb.-May 1958.

24. Naudascher, E., and Locher, F. A., "Flow-Induced Forces on Protruding Walls", J. Hyd. Division, Proc. ASCE, HY2, 1974.

25. Gongwer, C. A., "A Study of Vanes Singing in Water", J. App. Mech., Vol. 19, 1952.

26. Weaver, D. S., "On Flow-Induced Vibrations in Hydraulic Structures and their Alleviation", Paper presented at the 2nd Symposium on Applications of Solid Mechanics, McMaster University, July 1974.

27. Lamb, H., "Hydrodynamics", Cambridge Univ. Press, England.

28. Moullin, E. B., and Browne, A. D., "On the Periods of a Free-Free Bar Immersed in Water", Cambridge Philosophical Society, 1927.

29. Blake, W. K., "The Radiation from Free-Free Beams in Air and in Water", J. Sound and Vibration, Vol. 33(4), 1974.

30. Todd, F. H., "Ship Hull Vibrations", Edward Arnold Publishers, London, 1961.

31. Wang, C., "Analysis of Vibration of Hollow-cone Valves", ASCE Journal of the Engineering Mechanics Division, EMG, 1973.

32. Weaver, D. S., "The Hydroelastic Stability of a Flat Plate", Ph.D Thesis, University of Waterloo, 1969.

33. IUTAM/IAHR Symposium on Flow-Induced Structural Vibrations, Karlsruhe, Germany, 1972, (Proceedings published by Springer-Verlag, 1974).

34. International Symposium on Vibration Problems in Industry, Keswick, England, 1973. (U.K. Atomic Energy Authority at Windscale, N.P.L.)

35. Logvinovich, G. V. and Savchenko, Yu. N., "A Study of Hydrodynamic Forces Attending Sinusoidal Vibrations of a Disk", Fluid Mechanics - Soviet Research, Vol. 2, No. 4, 1973.

36. Reynolds, O., Philosophical Transactions of the Royal Society, London, 1883.

37. Prandtl, L., and Tietjens, O. J., Fundamentals of Hydro and Aero Mechanics, Dover Publications Inc., New York, 1957.

38. Morris, R. E. and Haythornthwaite, B., "Water Flow Analogues for Gas Dynamics", Engineering, London, Vol. 190, 1960, pages 261-263.

39. McEachern, N. V., and Bowker, A. J., "Water Tunnel Flow Visualization Experiments in a 2" Square Duct", NRC, NAE Laboratory Memo AE-117, National Research Council of Canada, Ottawa, April 1960.

40. Winter, E. F., "Flow Visualization Techniques Applied to Combustion Problems", J. Royal Aeronautical Society, Vol. 62, 1958, pages 268-276.

41. Geller, E. W., Journal of Aeronautical Sciences, Vol. 22, 1955, pages 869-870.

42. Clutter, D. W., Smith, A. M. O. and Brazier, J. G., "Techniques of Flow Visualization using Water as the Working Medium", Report of Douglas Aircraft Co. No. ES29D75, 1959.

43. Clayton, B. R., and Massey, B. S., "Flow Visualization in Water: A Review of Techniques", J. Scientific Instruments, Vol. 44, 1967.

44. Schraub, F. A., Kline, A. J., Henry, J., Runstadler, P. W., and Littell, A., "Use of Hydrogen Bubbles for Quantitative Determination of Time-Dependent Velocity Fields in Low-Speed Water Flows", J. Basic Engineering, Vol. 87, 1965, pages 429-444.

45. Dobrodzicki, G. A., "Flow Visualization in the NAE Water Tunnel", NRC Aeronautical Report LR-557, Feb. 1972.

46. Dobrodzicki, G. A., Private Communication, April 1973.

47. Chesters, J. H., Halliday, I. M. D. and Howes, R. S., Some Aspects of Fluid Flow (London: Arnold), 1951, pages 176-193.

48. Wood, D. J., "Influence of Line Motion on Waterhammer Pressures", J. Hydraulics Division, Proc. ASCE, May 1969.

49. Duc, J., "Negative Pressure Phenomena in Pump Pipelines", Paper presented at the International Symposium on Waterhammer in Pumped Storage Projects, Chicago, Illinois, Nov. 1965.

50. Weaver, D. S., Kouwen, N., and Mansour, W. M., "On the Hydroelastic Vibration of a Swing Check Valve", Symposium on Flow-Induced Structural Vibrations, Karlsruhe, Germany, 1972.

51. Hardwick, J. D., "Flow-Induced Vibration of Vertical-Lift Gate", J. Hydraulics Division, Proc. ASCE, HY5, May 1974.

52. Abelev, A. S., and Dolnikov, L. L., "Experimental Investigations of Self-Excited Vibrations of Submerged Vertical-Lift Hydraulic Gates", IUTAM-IAHR Symposium on Flow-Induced Structural Vibrations, Karlsruhe, Germany, 1972.

53. Naudascher, E., "Vibration of Gates During Overflow and Underflow", Journal of the Hydraulics Division, Proc. ASCE, Vol. 87, March 1961

54. Simmons, W. P., "Experiences with Flow-Induced Vibrations", J. Hydraulics Division, Proc. ASCE, HY4, 1965.

55. Price, J. T., "Flow-Induced Vibrations - Experiences of TVA with Hydraulic and other Structures", Civil Engineering ASCE, April 1965.

56. Douma, J. H., "Field Experiences with Hydraulic Structures", IUTAM/IAHR Symposium on Flow Induced Structural Vibrations, Karlsruhe, Germany, 1972.

APPENDIX A

EXPERIMENTAL RESULTS

SPRING STIFFNESS ($lb_f/in.$)	INITIAL ANGLE OF SETTING θ_o (degrees)	SERIES	FREQUENCY OF VIBRATION f (Hertz)	MAXIMUM DISP. FROM SEAT θ_{max} (degrees)
K_s=50.5	5°	A	2.81	4.4°
		B	N V	-
K_{eq}=47.0		C	N V	-
		C1	N V	-
K_T=0.076		B-C1	N V	-
		B-C2	N V	-
		B-D	N V	-
	6°	E	2.44	6.7°
		A	2.42	6.6°
		B	N V	-
		C	2.88	2.8°
		C1	N V	-
		B-C1	N V	-
		B-C2	N V	-
		B-D	N V	-
K_s=64.5	4°	E	3.08	3.4°
		A	3.1	3.2°
K_{eq}=58.8		B	N V	-
		C	N M*	-
K_T=0.096		C1	N V	-
		B-C1	N V	-
		B-C2	N V	-
		B-D	N V	-
	4.5°	E	2.94	4.3°
		A	2.82	4.6°
		B	N V	-
		C	N V	-
		C1	N V	-
		B-C1	N V	-
		B-C2	N V	-
		B-D	N V	-
	5°	E	2.62	5.5°
		A	2.71	5.5°
		B	N V	-
		C	2.95	2.9°
		C1	N V	-
		B-C1	V D*	-
		B-C2	V D*	-
		B-D	N V	-
		E	2.46	6.2°
		A	2.32	6.5°
		B	N V	-
		C	N M*	-
		C1	N V	-
		B-C1	2.98	2.1°
		B-C2	2.94	1.7°
		B-D	N V	-

SPRING STIFFNESS ($lb_f/in.$)	INITIAL ANGLE OF SETTING θ_o (degrees)	SERIES	FREQUENCY OF VIBRATION f (Hertz)	MAXIMUM DISP. FROM SEAT θ_{max} (degrees)
	6°	E	2.26	7.1°
		A	2.23	7.4°
		B	N V	-
		C	2.68	4.4°
		C1	2.81	1.8°
		B-C1	2.72	2.9°
		B-C2	2.70	2.3°
		B-D	N V	-
	6.5°	E	N M*	-
		A	2.03	7.9°
		B	N V	-
		C	N M*	-
		C1	2.63	3.0°
		B-C1	2.44	3.3°
		B-C2	2.39	2.8°
		B-D	V D*	-
	7°	E	N M*	-
		A	N M*	-
		B	N M*	-
		C	N M*	-
		C1	2.41	3.8°
		B-C1	2.28	4.0°
		B-C2	2.18	3.4°
		B-D	2.51	3.9°
K_s=76.0 K_{eq}=68.2 K_T=0.1137	4°	E	3.10	3.6°
		A	3.02	3.7°
		B	N V	-
		C	N V	-
		C1	N V	-
		B-C1	N V	-
		B-C2	N V	-
		B-D	N V	-
	4.5°	E	2.83	4.8°
		A	2.73	4.8°
		B	N V	-
		C	N V	-
		C1	N V	-
		B-C1	N V	-
		B-C2	N D*	-
		B-D	N V	-
	5°	E	2.6	5.6°
		A	2.5	5.8°
		B	N V	-
		C	2.82	3.2°
		C1	N V	-
		B-C1	3.03	2.0°
		B-C2		
		B-D	N V	-

	5.5°	E	2.24	6.8°
		A	2.22	6.7°
		B	N V	-
		C	2.77	2.3°
		C1	2.76	2.3°
		B-C1	2.70	2.8°
		B-C2		
		B-D	V D*	-

SPRING STIFFNESS ($lb_f/in.$)	INITIAL ANGLE OF SETTING θ_o (degrees)	SERIES	FREQUENCY OF VIBRATION f (Hertz)	MAXIMUM DISP. FROM SEAT θ_{max} (degrees)
	6°	B	2.09	7.2°
		A	2.14	7.73°
		B	N M*	-
		C	2.54	3.1°
		C1	2.38	3.1°
		B-C1	2.41	3.2°
		B-C2	2.42	2.8°
		B-D	2.76	3.1°
	6.5°	B	N M*	-
		A	N M*	-
		B	N M*	-
		C	2.39	4.2°
		C1	2.33	3.8°
		B-C1	2.23	3.9°
		B-C2	N M*	-
		B-D	N M*	-
	4°	B	3.08	3.7°
		A	2.92	3.74°
		B	N V	-
		C	N V	-
		C1	N V	-
		B-C1	N V	-
		B-C2	N V	-
		B-D	N V	-
	4.5°	B	N M*	-
		A	N M*	-
		B	N V	-
		C	N M*	-
		C1	N V	-
		B-C1	3.13	1.6°
		B-C2		
K_s=80.5		B-D	N V	-
K_{oq}=71.9	5°	B	2.51	6.0°
K_r=0.1204		A	2.57	5.9°
		B	N V	-
		C	N M*	-
		C1	2.88	2.0°
		B-C1	2.85	2.2°
		B-C2		
		B-D	N V	-
	5.5°	B	2.24	6.7°
		A	N M*	-
		B	N M*	-
		C	N M*	-
		C1	2.69	2.5°
		B-C1	2.48	2.8°
		B-C2		
		B-D	2.86	2.1°

	6°	E A B C C1 B-C1 B-C2 B-D	N M* 2.1 N M* N M* 2.44 2.24 N M*	- 7.8° - - 3.8° 3.6° -

SPRING STIFFNESS (lb_f/in.)	INITIAL ANGLE OF SETTING θ_o (degrees)	SERIES	FREQUENCY OF VIBRATION f (Hertz)	MAXIMUM DISP. FROM SEAT θ_{max} (degrees
		E	2.94	4.3°
		A	2.90	4.2°
		B	N V	-
	4°	C	3.21	2.2°
		C1	N V	-
		B-C1	3.18	1.2°
		B-C2		
		B-D	N V	-
		E	2.63	5.3°
		A	2.70	5.0°
		B	N V	-
	4.5°	C	N M*	-
		C1	3.05	2.0°
		B-C1	2.93	2.1°
K_s=92.0		B-D	N V	-
		E	2.37	6.1°
K_{eq}=80.9		A	2.36	6.2°
		B	N M*	-
K_r=0.1376		C	2.64	3.8°
	5°	C1	2.70	2.9°
		B-C1	2.63	2.6°
		B-C2		
		B-D	2.90	1.7°
		E	2.18	6.9°
		A	1.82	6.9°
		B	N M*	-
	5.5°	C	N M*	-
		C1	2.54	3.3°
		B-C1	2.28	3.2°
		B-C2		
		B-D	2.72	3.4°
		E	2.06	7.5°
		A	1.99	7.9°
		B	N M*	-
	6°	C	2.3	5.8°
		C1	2.33	4.0°
		B-C1	N V	-
		B-C2	N M*	-
		B-D	2.49	4.3°
		E	N M*	-
		A	N M*	-
		B	N V	-
	6.5°	C	N M*	-
		C1	2.12	4.8°
		B-C1	N V	-
		B-C2	N V	-
		B-D	2.36	4.8°

SPRING STIFFNESS (lb_f/in.)	INITIAL ANGLE OF SETTING θ_o (degrees)	SERIES	FREQUENCY OF VIBRATION f (Hertz)	MAXIMUM DISP. FROM SET θ_{max} (degrees)
K_s=106.0 K_{eq}=91.5 K_r=0.1586	3.5°	E	3.26	2.9°
		A	N M*	-
		B	N V	-
		C	N V	-
		C1	N V	-
		B-C1	N V	-
		B-C2	N M*	-
		B-D	N V	-
	4°	E	2.82	4.4°
		A	2.82	4.3°
		B	N V	-
		C	3.04	2.4°
		C1	N V	-
		B-C1	3.06	1.5°
		B-C2		
		B-D	N V	-
	4.5°	E	2.6	5.0°
		A	N M*	-
		B	N M*	-
		C	N M*	-
		C1	2.85	2.3°
		B-C1	2.76	2.1°
		B-C2		
		B-D	2.92	1.2°
	5°	E	N M*	-
		A	2.29	5.9°
		B	N M*	-
		C	N M*	-
		C1	N M*	-
		B-C1	N M*	-
		B-C2	N M*	-
		B-D	N M*	-
K_s=117.5 K_{eq}=99.9 K_r=0.1758	3°	E	V D*	-
		A	3.28	1.9°
		B	N V	-
		C	N V	-
		C1	N V	-
		B-C1	N V	-
		B-C2	N V	-
		B-D	N V	-
	3.5°	E	3.28	3.1°
		A	N M*	-
		B	N M*	-
		C		
		C1	N V	-
		B-C1	3.45	1.0°
		B-C2	N M*	-
		B-D	N V	-

SPRING STIFFNESS ($lb_f/in.$)	INITIAL ANGLE OF SETTING θ_o (degrees)	SERIES	FREQUENCY OF VIBRATION f (Hertz)	MAXIMUM DISP. FROM SEAT θ_{max} (degrees)
	4°	E	2.8	4.2°
		A	2.64	4.5°
		B	N M*	-
		C	2.98	2.5°
		C1	3.03	1.6°
		B-C1	2.98	1.5°
		B-C2		
		B-D	N V	-
	4.5°	E	2.56	4.8°
		A	N M*	-
		B	N M*	-
		C	N M*	-
		C1	2.79	2.5°
		B-C1	2.57	2.1°
		B-C2		
		B-D	2.88	2.2°
	5°	E	N M*	-
		A	2.17	6.7°
		B	N M*	-
		C	2.38	3.7°
		C1	2.45	3.2°
		B-C1	2.23	2.4°
		B-C2		
		B-D	2.7	2.9°
K_g=129.0 K_{eq}=108.1 K_r=0.1930	3°	E	V D*	-
		A	3.22	2.4°
		B	N V	-
		C	N V	-
		C1	N V	-
		B-C1	N V	-
		B-C2	N V	-
		B-D	N V	-
	3.5°	E	3.18	3.3°
		A	N M*	-
		B	N V	-
		C	N M*	-
		C1	N V	-
		B-C1	3.30	1.1°
		B-C2		
		B-D	N V	-
	4°	E	2.76	4.4°
		A	2.62	4.6°
		B	N M*	-
		C	2.87	2.7°
		C1	2.98	2.0°
		B-C1	2.85	1.7°
		B-C2		
		B-D	3.03	1.4°

SPRING STIFFNESS ($lb_f/in.$)	INITIAL ANGLE OF SETTING θ_o (degrees)	SERIES	FREQUENCY OF VIBRATION f (Hertz)	MAXIMUM DISP. FROM SEAT θ_{max} (degrees)
	4.5°	E	2.45	5.0°
		A	N M*	-
		B	N M*	-
		C	N M*	-
		C1	2.73	2.7°
		B-C1	2.44	2.3°
		B-C2		
		B-D	2.84	2.3°
	5°	E	N M*	-
		A	2.13	6.8°
		B	N M*	-
		C	2.26	3.9°
		C1	N M*	-
		B-C1	N M*	-
		B-C2	N M*	-
		B-D	N M*	-
	3°	E	3.57	2.1°
		A	3.31	2.5°
		B	N V	-
		C	N V	-
		C1	N V	-
		B-C1	N V	-
		B-C2	N M*	-
		B-D	N V	-
K_s=133.5	3.5°	E	3.12	3.6°
		A	N M*	-
K_{eq}=111.3		B	N V	-
		C	N M*	-
K_r=0.1992		C1	3.06	-1.5°
		B-C1	3.11	1.3°
		B-C2		
		B-D	N V	-
	4°	E	2.73	4.4°
		A	2.57	4.6°
		B	N M*	-
		C	2.85	2.5°
		C1	2.91	2.0°
		B-C1	2.78	2.0°
		B-C2		
		B-D	2.91	1.3°
	4.5°	E	2.44	5.3°
		A	N M*	-
		B	N M*	-
		C	N M*	-
		C1	2.62	2.6°
		B-C1	2.30	2.4°
		B-C2		
		B-D	2.76	2.7°

SPRING STIFFNESS ($lb_f/in.$)	INITIAL ANGLE OF SETTING θ_o (degrees)	SERIES	FREQUENCY OF VIBRATION f (Hertz)	MAXIMUM DISP. FROM SEAT θ_{max} (degrees)
K_s=133.5	5°	E	N M*	-
		A	2.07	6.9°
		B	N M*	-
		C	2.15	3.9°
		C1	N V	-
		B-C1	N V	-
		B-C2	N V	-
		B-D	N M*	-

Guide to Interpretation of Results in Appendix A.

N V indicates "No Vibration".

N M* indicates "Vibration observed but no measurements taken".

V D* indicates "Vibration damped", (generally after 3 or 4 cycles).

$K_r = (K_s L^2/K_\theta)$

APPENDIX B

(a) Design Data for the Model

Length of the pivot shaft	= 21 inches
Diameter of the pivot shaft	= 7/8 inch
Distance between pin positions on pivot shaft	= 6 7/8 inches
Weight of perspex disc, bolt and nut	= 3.50 lb_f
Length of spring arm	= 14 inches
Cross-sectional area of spring arm	= 1.50 in^2 (2"x3/4")
Weight of spring arm	= 5.95 lb_f
Weight of pivot shaft	= 3.58 lb_f

(b) Determination of K_θ

The torsional stiffness K_θ of the pivot shaft was calculated from

$$K_\theta = \frac{T}{\theta} = \frac{GJ_s}{L_1}$$

where G is the shear modulus of the shaft material,

T is the torque necessary to twist the shaft through angle θ,

L_1 is the distance between the points of application of the force,

and $J_s = \frac{\pi d^4}{32}$ is the polar moment of inertia of the shaft.

Thus

$$K_\theta = \frac{\pi G d^4}{32 L_1} = \frac{\pi \times 11.5 \times (0.875)^4 \times 10^6}{32 \times 6.875}$$

$$= (9.6262 \times 10^4) \text{ lb}_f\text{-in/radian}$$

(c) Calculation of K_{eq}

K_{eq} is the effective spring constant for the valve system, and is made up of the series combination of K_θ and $K_s L^2$. Thus,

$$\frac{1}{K_{eq}} = \frac{1}{K_s L^2} + \frac{1}{K_\theta}$$

i.e., $$K_{eq} = \left(\frac{K_s K_\theta L^2}{K_\theta + K_s L^2}\right)$$

(d) Conversion from British to International Units

1 psi = 6.9 kPa = 6.9 kN/m^2.

1 inch = 2.54 cm = 0.0254 m.

1 lb_f/in = 175.13 N/m = 0.17513 kN/m.

1 ft^3/min = 0.0004719474 m^3/sec.

1 lb_f = 4.45 N.

1 lb_f-ft = 1.35582 N-m.

1 ft/sec = 0.3048 m/sec.